UNIVERSIDAD NACIONAL AUTÓNOMA DE MÉXICO

Posgrado en Ciencia e Ingeniería de Materiales

Instituto de Investigaciones en Materiales

THE VISCOELASTICITY OF CRUDE OIL AND LINEAR ALKANES

(La viscoelasticidad de crudo y alcanos lineales)

T e s i s

que para obtener el grado de

Doctor en Ciencia e Ingeniería

de Materiales

presenta:

Roberto Cipriano Dante Lavista

UNAM
POSGRADO
Ciencia e Ingeniería
de Materiales

Director de Tesis

Dr. Enrique Geffroy Aguilar

México, 2006

To Georgette Denisse and Birgit

The Viscoelasticity of Crude Oil and Linear Alkanes
(La viscoelasticidad de crudo y alcanos lineales)

Part I

Introduction to crude oil properties and to the rheological models utilized in the experimental part

Part II

Experimental part, model and theory development

ABSTRACT

The comprehension of crude oil rheology has a practical use, connected with flow properties of crude oils in reservoirs and when transported through pipelines. The interest onto this topic is increased due to exploitation of crude oils with high viscosity, and the correlated exploitation of vacuum residua for power plant combustion.

The rheological modeling of crude oils has been to date a difficult task due mainly to the complexity and variability of these fluids depending on the origin, feedstocks, etc. Thus, finding a experimental model capable of describing qualitative and quantitatively the viscoelastic properties of crude oils is the subject and the purpose of this work, as well as interpreting the Arrhenius factor in terms of disorder-order transitions, occurring in the crude oil sample and associated to specific relaxation times.

A method to bypass this obstacle consists in developing simpler fluid systems, based on well known compounds such as linear alkanes, capable of modeling the main rheological characteristics of some classes of petroleum such as Mexican oil types. This quest implies finding suitable experimental physico-chemical models that can describe both systems.

Linear alkanes provide a simplified physical model of crude oils, with the advantage to have completely known and defined properties. The utilization of a specific shear thinning model for suspensions, coupled with both Oldroyd contravariant derivative and Adam-Gibbs theory for cooperative transformations, makes possible to find a linkage between macroscopic rheological properties and microscopic transformations, such as changes of conformations of alkanes' oligomers, induced by flow stresses.

The Weissenberg number, obtained through the Adam-Gibbs-like theory and based on the characteristic time of the cooperative phenomena involved in crude oil

flows, adequately scales viscosity curves of both oils and alkanes of long chains (17 and 20 carbon atoms); moreover, the model is flexible and of general validity.

Therefore, this work presents both a mathematical model for crude oil rheology, and a physical one through the application of the Adam-Gibbs theory explaining the Arrhenius factor determined for crude oil. This framework is considered to be the base for further studies focused onto the rheology of oil-in-water suspensions, which has as fundaments the comprehension of oil rhelogy *in primis*. In case of water-in-oil emulsions, i. e., where the continuous phase is oil, the equations developed throughout the text will be useful to manage the complex rheology of this non-Newtonian fluid and to create adequate models to describe their flow behavior.

RESUMEN

La comprensión de la reología del petróleo crudo tiene un uso práctico, relacionado con las propiedades de flujo de los crudos en medios porosos así como cuando se éste se transporta a través de tuberías. El interés sobre este tema se ha aumentado principalmente debido a la explotación de petróleos crudos de alta viscosidad y al uso de residuos de vacío para su combustión en centrales termoeléctricas. El modelado de las propiedades reológicas de petróleos crudos ha sido hasta ahora una tarea difícil principalmente por la complejidad y variabilidad de estos fluidos según el origen, los yacimientos, etc. La elaboración de un modelo que describa cualitativa y cuantitativamente las propiedades viscoelásticas de petróleos crudos es el tema y el objetivo de este trabajo, así como la interpretación del factor de Arrhenius en términos de transiciones orden-desorden en la muestra de crudo, asociadas a tiempos de relajamiento específicos.

Un método para evitar ese obstáculo consiste en el desarrollo de sistemas fluidos más simples, basados en compuestos conocidos como los alcanos lineales, capaces de modelar las características reológicas principales de algunas clases de petróleos como los mexicanos. Esta búsqueda implica el descubrimiento de modelos físicoquímicos experimentales convenientes que pueden describir ambos sistemas. Los alcanos lineales proveen un modelo físico muy simplificado de los crudos, pero con la ventaja de ser completamente conocidos y tener propiedades bien definidas. La utilización de un modelo específico de adelgazante (shear thinning) para suspensiones, conectada tanto con la derivada contravariante de Oldroyd, así como con la teoría de Adam-Gibbs para transformaciones cooperativas, hace posible encontrar una conexión entre propiedades reológicas macroscópicas y transformaciones microscópicas, como los cambios de conformaciones de oligomeros como los alcanos de cadena corta, inducidos por esfuerzos de flujo.

El número de Weissenberg, obtenido a través de la teoría de Adam-Gibbs y basado en el tiempo característico de los fenómenos cooperativos implicados en flujos de petróleo crudo, escala adecuadamente las curvas de viscosidad de petróleo y alcanos de cadenas largas (17 y 20 átomos de carbono); además, el modelo es flexible y de validez general.

Por lo tanto, conseguimos un modelo matemático para la reología de petróleo crudo, así como una interpretación física basada en la aplicación de la teoría de Adam - Gibbs para el factor de Arrhenius determinado para el crudo. Se piensa que este marco es la base para estudios adicionales enfocados a la reología de suspensiones de petróleo en agua, que tiene como fundamentos la comprensión de la reología de petróleo *in primis*. En caso de emulsiones de agua en petróleo, es decir donde la fase continua es el petróleo, las ecuaciones desarrolladas a lo largo del texto de esta tesis serán útiles para manejar la compleja reología de este fluido no newtoniano y crear modelos adecuados para describir su comportamiento de flujo.

INTRODUCTION

Crude oil is a suspension or emulsion[*] of several polymers, oligomers and organic as inorganic components, thus a non-Newtonian behavior with normal stresses and shear thinning is expected. Moreover, crude-oil samples have compositions that depend on the feedstock, on the sampling method, on the time of sampling, and on many other variables; therefore, they exhibit a high variability, which imposes high restraints to draw good conclusions as means of characterizing and understanding the dynamics of the complex rheological and physical phenomena of such materials. In contrast to crude oil, rheological measurements for samples of linear aliphatic com pounds, such as linear alkanes with chain sizes from C7 to C20, are completely reproducible.

In fact, linear alkanes alone or in mixtures have well defined properties. Several attempts have been made to generate "synthetic crudes" in order to have good controlled system. However, previous attempts have produced samples that are as particular and complex as the samples of natural crude; the only advantage being that there is an exactly known method of preparation and composition for the synthetic sample. The approach to the rheology of crude oil, for the aforementioned reasons, has been often directed to engineering uses, searching phenomenological equations. Nevertheless, some theoretical and simulation studies of steady shear flows have been carried out on alkanes due to their simple physical and chemical characteristics.

The hypothesis of this work assumes that the rheology of crude oil is dominated by the aliphatic fraction, mainly alkanes and alkylic long branches –for its viscous properties– while the elastic properties are due to the colloidal nature of petroleum. The colloidal nature of crude oils is due mainly to the asphaltenes and waxes suspended in the aliphatic matrix. Furthermore, crude oil and mixtures of alkanes present measurable

[*] Throughout the text the terms "emulsion" and "suspension" are used with a certain latitude, because most crude oils have high viscosities at low temperatures that they can be considered solid materials Therefore, we can speak also of suspension of crude oil in water.

normal stresses. These rheological characteristics can be correlated to changes of both alkane and alkylic branch conformations.

In order to consider this relevant rheological property, models based on Oldroyd derivatives are used as suitable tools to describe the viscoelasticity of both systems. Also a prescription of a constitutive equation for the viscoelasticity is a viable option without having to rely on molecular characteristics that are extremely difficult, if not impossible, to manage in the case of oils. Furthermore, Oldroyd derivatives allow us to use Maxwell-type models for this work.

Nevertheless, in this work the necessary molecular mechanisms are considered thoroughly via the activation energies often observed in oils and high alkanes subjected to shear flows. In this work, it is shown that the Adam Gibbs theory, adapted for alkanes, can provide an interpretation of the activation energies found in crude oils viscosity functions. This activation energy interpretation enables us to correlate most macroscopic properties (viscosity) to microscopic properties, e. g., the changes of conformations in long and flexible molecules such as alkanes and alkylic chains.

Therefore, phase transitions of alkanes can explain the appearance of the Arrhenius factor observed in crude oils, which is an important result, considering the current lack of understanding and of attention given to the problem of waxes deposition in pipelines.

The latter attempts of using alkanes with linear chains were enticed by the need to have simple systems, even when these hydrocarbons are used, in mixtures, to obtain rheological functions. Their values are comparable to those of crude oil samples, as well as behavior and trends, if dimensionless variables are used, such as the Weissenberg number.

That is, what is important in using these aliphatic alternatives is that difference between crude oil and the aliphatic mixtures should be essentially more *quantitative*

than *qualitative*. If the rheological behavior of aliphatic compounds can simulate partially the behavior of crude oils, also with an elevated content of asphaltenes, then the former can be used for the preparation of emulsions with water, obtaining completely reproducible and knowable systems, which can be used to obtain better general conclusions, as well as being a data set useful for further detailed analyses. The importance of such emulsions is directly linked to the energy industry. Heavy crude oils flows and burns difficultly; their utilization in power plants can be made possible in large scale, only if these characteristics are improved. The preparation of these oil-in-water emulsions is a way to improve altogether these characteristics. The construction of rheology models for crude oils is the first step towards the development a nd study of oil-in-water emulsions. These emulsions have to satisfy many characteristics at the same time to be widely utilized: low viscosity, low yield stress, both thermal and time stability, high heating power and low production of small particles. Huge research and development efforts are needed to achieve these goals altogether. I believe that the work presented in this manuscript is one of the efforts needed.

This manuscript is divided into two parts; in the first part, called Part I, which is essentially introductory, some information is provided on petroleum and fundamental rheology concepts. The rheometer characteristics are presented; moreover, the fundaments of the utilized rheological models are discussed. The second part, called Part II is focused on the specific work carried out, and the chapters are organized as scientific papers, and can be read in an independent manner from each other. Finally, a general conclusion resumes the main achievements obtained.

Chapter 1.

Oil and asphaltenes

1.1. Introduction

Crude petroleum is a mixture of compounds, each with different boiling temperatures, which can be separated into a variety of generic fractions by distillation and by fractionation [1]; for instance, in Fig. 1.1 the complexity of petroleum composition or "petroleum continuum" is made evident. However, petroleum from different sources exhibits different characteristics, and the behavioral characteristics are often difficult to define with a high degree of precision. As can be anticipated, there is a wide variation of properties of petroleum, with proportions of different constituents varying widely [1-3] (see Table 1.1).

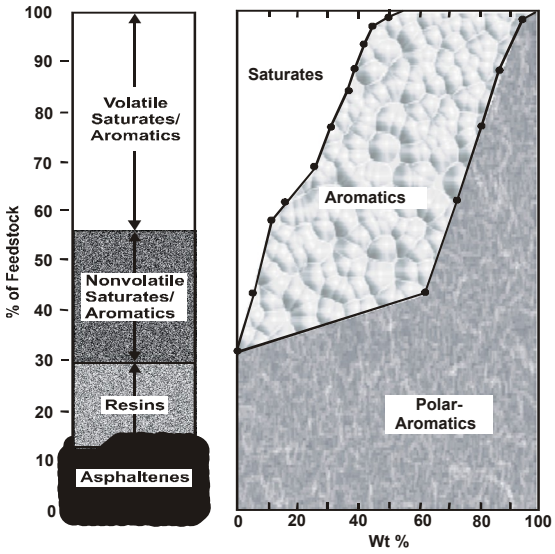

Figure 1.1. The continuum of petroleum. The variety of petroleum composition is shown schematically, making emphasis on volatile and non-volatile components.

Thus, some crude oils have higher proportions of the lower temperature boiling constituents, whereas others (such as bitumen, also referred to as natural asphalt) have

higher proportions of the higher boiling constituents (often called the “asphaltic components” or “residuum”). It is the higher boiling constituents that often lead to problems during recovery and refining operations.

Table 1.1. Types of Asphaltene Occurring in Different Feedstocks

Substance	Asphaltenes W%	Resins W%	Oils W%
Petroleum	< 0.1-12	3-22	67-97
Heavy oil	11-45	14-39	24-64
Residues[a]	11-29	29-39	32-60

[a] Asphaltene occurrence in bitumen is similar to that found in residues.

In fact, distillation and fractionation methods provide a better sense of the overall composition of petroleum and behavioral characteristics. Petroleum can be considered to be a delicately balanced system insofar as different fractions being compatible, provided that no significant disturbances or changes are made to the system. The four most important changes are: (1) the alteration of the natural occurrences of the different fractions; (2) the chemical or physical alteration of the constituents as might occur during refining, especially changes that might be brought up by thermal processes; and (3) alteration of the polar group distribution as might occur during oxidation (i.e., asphalt manufacture); or (4) the elimination of polar functions during processing. In addition, the sudden exposure of petroleum to air, as might occur during the initial stages of recovery operations, or the release of dissolved gases when a reservoir is first penetrated can also cause alterations to the system .

Scientific knowledge of a “good dispersion” is a valuable asset for understanding the behavior of petroleum during refining and recovery operations. Especially, it is most helpful for understanding the behavior of heavy oil and bitumen,

which have greater proportions of the higher molecular weight constituents than conventional petroleum. Because of this (in part or in total), more problems exist in recovery and refining operations with heavy oils.

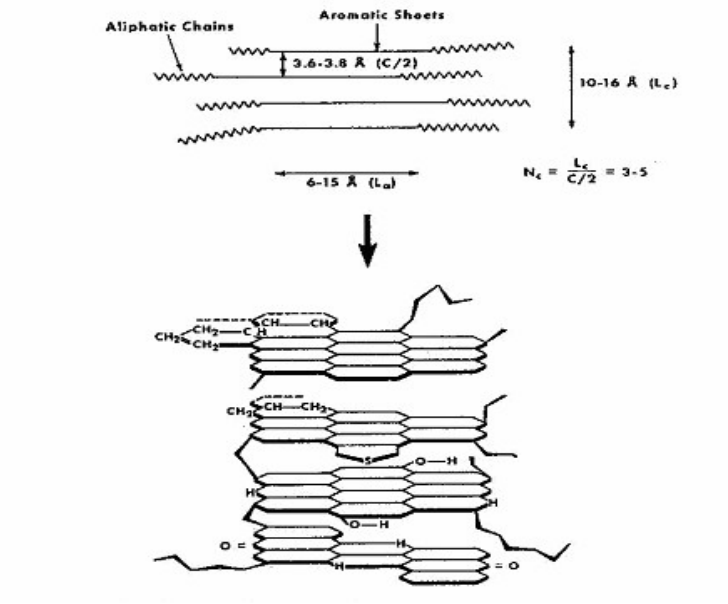

Figure 1.2. The asphaltene micelle has been proposed as being composed of a "stack" associated by *s* bond or *p-p* interaction.

1.2. Molecular Models

The macromolecular structure of asphaltenes has also been subjected to investigation insofar as the means by which molecules can form a micelle; a structural condition of importance to geochemists and to process chemists. X-ray analyses and molecular weight determinations have been among the most frequently used methods chosen to investigate the macro-molecular structure of asphaltenes [4]. X-ray methods are well documented in its use for carbon and graphite, and yields information about dimension of the unit cell such as inter-lamellar distance ($c/2$), layer diameter (L_a), height of unit cell (L_c) and the number of lamellae (N_c) contributing to the micelle (see Fig. 1.2).

The concept of asphaltene models that incorporate smaller polynuclear aromatic systems keeps tabs with those types of systems that occur in nature. Indeed, smaller polynuclear aromatic (and pseudo-aromatic) systems are capable of producing high

yields of thermal coke either because of the heteroatom contents or because of the presence of pendant alkyl moieties that have the capability of forming the internuclear cross-links that lead to coke. In this latter case, it is likely that the indigent alkyl chains can interact in this manner, or shorter alkyl chains, formed by thermolysis, can play the role of cross linking agents.

Early postulates of asphaltene structure centered on a variety of polymer structures based on aromatic systems [5, 6]. More recent information has related to the structural parameters and carbon skeleton of petroleum fractions, and asphaltenes structures have been derived from spectroscopic studies of asphaltenes isolated from various petroleum and bitumen [7-15].

The data from these studies support the hypothesis that asphaltenes, viewed structurally, contain condensed polynuclear aromatic ring systems bearing alkyl side chains. These systems with heteroelements (i. e., nitrogen, oxygen and sulfur) scattered throughout in various, including heterocyclic, locations. With increasing molecular weight of the asphaltene fraction, both aromaticity and the proportion of heteroelements increase [3, 16, 17].

These findings led to the concept of large polynuclear aromatic systems, and efforts were made to describe the total structures of asphaltenes in accordance with magnetic resonance data and results of spectroscopic and analytical techniques [8, 10, 11, 18, 19].

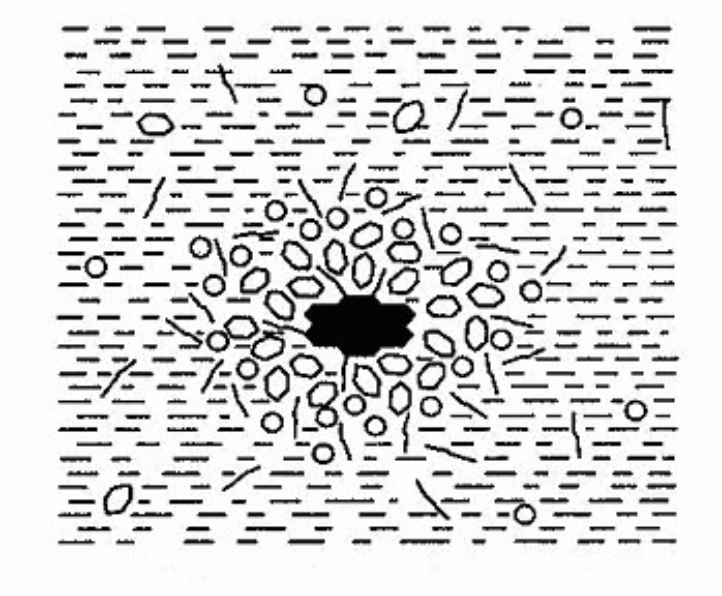

Figure 1.3. An early model of the physical structure of petroleum showed the asphaltenes dispersed and peptized by resin species.

However, the number of rings in such systems is open to question, apparently varying from as low as 6 to 15 or more. The concept of hydrogen -bonding interactions as one of the means of association between the asphaltenes and r esins has, however, led to reconsideration of assumed clusters as part of the micelle [20 -22]. Indeed, it appears that when both resins and asphaltenes are present, hydrogen bonding may be one of the mechanisms by which resin-asphaltene interactions are achieved. In some instances, it appears that resin-asphaltene interactions may be preferred over asphaltene-asphaltene interactions (Fig. 1.3).

1.3 Petroleum features and stability

Petroleum is a delicately balanced system insofar as the different fractions are compatible, provided that no significant disturbances or changes are made to the system. Such changes are the alteration of the natural occurrences of the different

fractions; the chemical or physical alteration of the constituents as might occur during recovery and refining, especially changes that might be brought on by thermal processes and alteration of the polar group distribution as might occur during processing. When such disturbances occur, the higher molecular weight constituents are most seriously affected. This can lead to incompatibility [23], which is variously referred to as loss of dispersion, precipitation, and sludge formation.

Thus, dispersion of the higher molecular weight constituents becomes an issue that needs attention. One way to understand this issue is to be aware of the chemical and physical character of dispersions; hence, the attending issue of incompatibility can be understood and even predicted.

1.4 References

[1] Speight JG. In *The Chemistry and Technology of Petroleum, 2nd ed*. Marcel Dekker, New York, 1991.

[2] Gruse WA & Stevens DR. In *The Chemical Technology of Petroleum*, Mc Graw-Hill; New York, 1960.

[3] Koots JA & Speight JG. *Fuel* 1975, *54*, 179.

[4] Helm RV, Latham DR, Ferrin CR & Ball JS. *Chem. Eng. Data. Ser.* 1957, **2**, 95.

[5] Murphy BJ. *Inst. Pet*. 1945, **31**, 475.

[6] Yen TF & Erdman JG. *Prepr. Am. Chem. Soc. Div. Pet. Chem*. 1962, **7**, 99.

[7] Yen TF. *Prepr. Am. Chem. Soc. Div. Pet. Chem*. 1972, *17*, F102.

[8] Haley GA. *Anal. Chem*. 1972, **44**, 580.

[9] Speight JG. *Appl. Spectrosc. Rev*. 1972, **5**, 211.

[10] Speight JG. *Appl. Spectrosc. Rev*. 1994, **29**, 269.

[11] Dickinson EM. *Fuel* 1980, **59**, 290.

[12] Bandurski Moschopedis E. *Energy Sources* 1982, **6**, 47.

[13] Sadeghi KM, Sadeghi MA, Wu WH & Yen TF. *Fuel* 1989, **68**, 782.

[14] Ali LH, Al-Ghannam KA & Al-Rawi JM. *Fuel* 1990, **69**, 519.

[15] Yen TF. *Fuel* 1970, **49**, 134.

[16] Yen TF. *Prepr. Am. Chem. Soc. Div. Fuel Chem*. 1971, **15**, 57.

[17] Sawatsky H, Boyd ML & Montgomery DS. *J. Inst. Pet.* 1967, **53**, 162.

[18] Witherspoon PA & Winniford RS. In *Fundamental Aspects of Petroleum Geochemistry*. Nagy B., Colombo U. Eds. Elsevier, New York, 1967.

[19] Yen TF, Erdman JG & Pollack SS. *Anal. Chem*. 1961, **33**, 1587.

[20] Speight JG & Pancirov RJ. *Liq. Fuels Technol*. 1984, **2**, 287.

[21] Acevedo S, Mendez B, Rojas A, Larisse L & Rivas H. *Fuel* 1985, **64**, 1741.

[22] Penzes S & Speight JG. *Fuel* 1974, **53**, 192.

[23] Speight JG. In *Catalysis on the Energy Scene*, Kaliaguine S, Mahay A., Eds. Elsevier, Amsterdam, Netherlands, 1984.

Chapter 2.

Suspensions: basic principles

2.1. Definition and classification of suspensions

A suspension is a special kind of colloidal dispersions: one in which a solid is dispersed in a liquid continuous phase. The dispersed phase is sometimes referred to as the internal phase and the continuous phase as the external phase. Colloidal particles (or droplets and bubbles) are usually defined as species, different from the continuous medium, having at least one length dimension between 1 and 1000 nm.

Two different broad types of colloidal dispersions have been distinguished since Graham proposed the term "colloid" in 1861. Originally, colloids were subdivided into lyophobic and lyophilic colloids. Lyophilic colloids are formed spontaneously when the two phases are brought together, because the dispersion is thermodynamically more stable than the original separated states. The term lyophilic is less frequently used in modern practice because many of the dispersions that once considered as lyophilic are now recognized as single-phase systems in which large molecules are dissolved. Lyophobic colloids, which include all petroleum suspensions, are not formed spontaneously on contact of the phases because they are thermodynamically unstable compared with separated states. These dispersions can be formed with mechanical energy input via some form of agitation, such as that provided by a propeller-style mixer, a colloid mill, or an ultrasound generator. The resulting suspension may well have considerable stability as a metastable dispersion. One may also describe surface properties in terms of its hydrophilic or hydrophobic character. For example, smeetite clay particles, whose surfaces are strongly hydrophilic, can form quite stable

suspensions in water: an example of a hydrophobic dispersion of hydrophilic particles [1].

2.2. Importance of suspension

Suspensions have long been of great practical interest because of their widespread occurrence in everyday life. Suspensions have important properties that may be desirable in a natural formulated product or undesirable, such an unwanted suspension in an industrial process. Some important kinds of familiar suspensions include those occurring in foods (batters, pudding, sauces), pharmaceuticals (cough syrup, laxatives), household products (inks, paints, "liquid" waxes), and the environment (suspended lake and river sediments, sewage).

Suspensions are also quite important and widespread in the petroleum industry. In fact, suspensions may be encountered throughout each stage of petroleum processing (in reservoirs, drilling fluids, production fluids, process plant streams, and tailing ponds) as shown in the following list:

- migrating fines during secondary and enhanced oil recovery
- dispersions of asphaltenes in crude oils
- produced (well-head) solids in oil recovery
- drilling fluid (mud) suspensions
- well stimulation and fracturing suspensions
- well cementing slurry
- oil-sand-slurry in the hot water flotation process
- oil-sands tailing ponds
- oil field surface facility sludges

The various suspensions occurring in the petroleum industry may be desirable or undesirable. For example the classic oil well drilling fluids (drilling mud) are desirable

suspensions. Here, a stable suspension is formulated and used to lubricate the cutting bit and to carry up cuttings to the surface. Conversely, certain secondary and enhanced (tertiary) oil recovery processes, if not carefully designed, may cause in situ mobilization or swelling of clay in reservoir, leading to drastic permeability reduction; in this case, mobilized clays form an undesirable suspension.

Suspensions may contain not just solid particles and water but also emulsified oils and even dispersed gas bubbles. In oil-sands mining and associated process operations, bitumen are disengaged from the sand matrix in suspensions in large tumblers. Bitumen is then separated from the suspension by a flotation process with the flotation medium being a suspension of fine particles that also contains emulsified oils (bitumen) and dispersed air bubbles.

In the petroleum industry, applications and problems of suspensions have in common the same basic principles of colloid science that govern the nature, stability, and properties of suspensions. The widespread importance of suspensions in general and scientific interest in their formation, stability, and properties generated a wealth of published literature on the subject.

2.3. Rheology of suspensions

The rheological properties of a suspension are very important. High viscosity may be the reason that a suspension is troublesome, a resistance to flow that must be dealt with, or a desirable property for which a suspension is formulated [2]. The simplest description applies to Newtonian behavior in laminar flow. The coefficient of viscosity, η, is given in terms of the shear stress, τ, and shear rate, $\dot{\gamma}$, by:

$$\tau = \eta\dot{\gamma} \quad , \tag{2.1}$$

where η has units of *pressure·time*. Many colloidal dispersions, including concentrated suspensions, do not obey the Newtonian equation. For non-Newtonian fluids the coefficient of viscosity is not a constant but is itself a function of the shear rate; thus:

$$\tau = \eta(\dot{\gamma})\dot{\gamma} \, .$$

(2.2)

Table 2.1. Approximate values of shear rate appropriate to various processes.

Process	**Approximate shear rate** (s^{-1})
Very slow stirring	0.01-0.1
Reservoir flow in oil recovery	1-5
Mixing	10-100
Pumping	100-1000
Coating	10000
Oilwell drilling fluid at the bit nozzle	10000-100000

Non-Newtonian fluids manifest a behavior characterized by significant normal stresses that, besides the viscosity function, are associated to other relevant physical properties such as $N_{1,}$ the first normal stresses function; N_2, the second normal stress function; Ψ_{12}, the first normal stress coefficient; and Ψ_{23}, the second normal stress coefficient:

$$N_1 = \tau_{11} - \tau_{22} \quad ,$$

(2.3)

$$N_2 = \tau_{22} - \tau_{33} \quad ,$$

(2.4)

$$\psi_{12} = \frac{N_1}{\dot{\gamma}^2} \quad ,$$

(2.5)

$$\psi_{23} = \frac{N_2}{\dot{\gamma}^2} \ . \tag{2.6}$$

It is common for industrial pumping and processing equipment to use shear rates that fall in the intermediate shear regime from about 10 to 1000 s^{-1} as illustrated in Table 2.1. A convenient way to summarize the flow properties of fluids is by plotting flow curves of shear stress versus shear-rate. These curves can be categorized into several rheological classifications; see for *e. g*., Fig. 2.1. Suspensions are frequently pseudoplastic: as shear rate increases viscosity decreases. This is also termed shear-thinning.

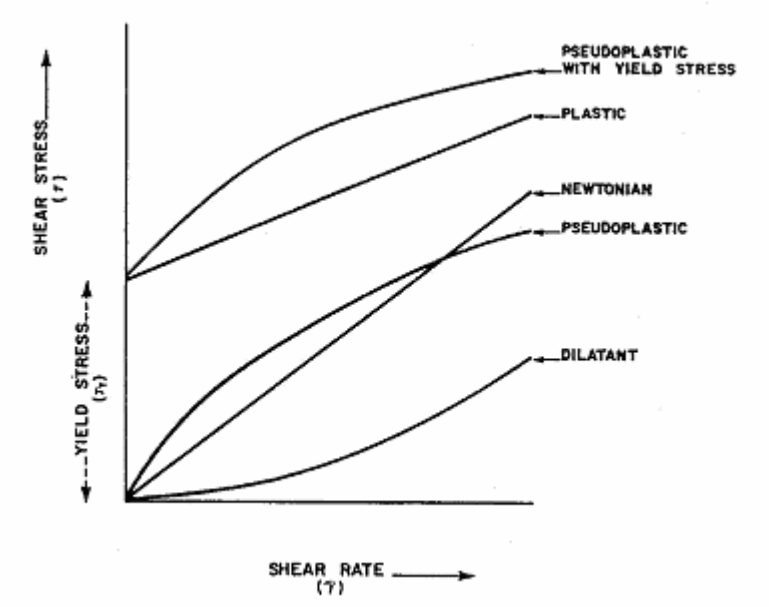

Figure 2.1. Illustration of the characteristic fluid types and their corresponding curve.

A suspension may also exhibit a yield stress, that is, the shear rate (flow) remains zero until a threshold shear stress is reached, referred to as the yield stress (τ_y) and then flow begins. Some descriptions appropriate to different yield stresses are given in Table 2.2. Pseudoplastic flow, which is time-dependent, is termed thixotropic; that is, at a constant applied shear rate viscosity decreases, and in a flow curve hysteresis occurs.

It is also not unusual for suspensions that are pseudoplastic at low to moderate solids concentrations to become dilatant (shear thickening) at high solids concentrations. In this case there is also a critical shear rate for the onset of shear thickening.

Table 2.2. Some descriptions appropriate to different yield stresses.

Yield Stress (Pa)	**Description**
<10	Easy to pour
10-30	Thick, pours easy. Use unconventional liquid design
30-40	Thick, hard to pour, form peaks. Difficult to transfer under pump suction
40-100	Flows poorly; will cleave to walls under gravity. Need push into pump suction
>100	Can build with it; will cleave to top of jar. Requires positive flow pump

Whorlow [3] and others described very useful experimental techniques. Very often, measurements are made with a suspension sample placed in the annulus between two concentric cylinders. The shear stress is calculated from the measured torque required to maintain a given rotational velocity of one cylinder with respect to the other. There are other geometries as cone-plate or plate–plate geometries that, in some cases, can be suitable for studies of some kinds of suspensions, but, in any case, knowing the geometry, the effective shear rate can be calculated from the rotational velocity. Less useful are the various kinds of simplified measuring devices found in many industrial plants and even in their technica1 support laboratories. Such devices may not be capable of determining shear stresses for known shear rates or may not be capable of operation at shear rates that are appropriate to the process under consideration.

Instruments that are capable of dynamic viscosity measurements provide much more useful information.

In an attempt to conduct rheological measurements on suspensions, a number of changes may occur in the sample chamber, making the measurements irreproducible and not representative of the original suspension. Prevalent among these changes is the sedimentation, or even centrifugal segregation, of solids, causing a non-uniform distribution within the measuring chamber. In the extreme sedimentation can cause complete removal of solids from the region in which measurements are made

It is frequently desirable to be able to describe the viscosity of a suspension in term of the viscosity of the liquid continuous phase (η_o) and the amount or suspended material. A very large number of equations have been advanced for estimating suspension (or emulsion, etc.) viscosities. Most of these are empirical extensions of Einstein's equation for a dilute "suspension of spheres":

$$\eta = \eta_o(1 + 2.5\phi) \quad , \tag{2.7}$$

where η_o is the medium viscosity and ϕ, is the dispersed phase volume fraction (ϕ <<1).

Examples of two empirical equations are the Oliver-Ward equation for spheres

$$\eta = \eta_o(1 + a\phi + a^2\phi^2 + a^3\phi^3 + ...) \ , \tag{2.8}$$

where η_o is an empirical constant, and the Thomas equation for suspensions

$$\eta = \eta_o(1 + 2.5\phi + 10.5\phi^2 + 0.00273\exp[16.6\phi]) \ . \tag{2.9}$$

These equations apply to Newtonian behavior, or at least to the Newtonian region of a flow curve, and they usually require that particles not be too large and have no strong electrostatic interactions.

Other modifications have been made for application to suspensions of anisometric (unsymmetrical) particles such as clays. In this case intrinsic viscosity [η], given by

$$[\eta] = \lim_{\phi \to 0} \lim_{\dot{\gamma} \to 0} (\eta / \eta_o - 1) / \phi \quad , \tag{2.10}$$

which is 2.5 for a dilute suspension of uncharged spheres, but takes different values, more difficult to predict for charged particles. A useful such modification to Einstein's equation for dilute suspensions of ellipsoidal particles is given by the Simha's Equation, which is approximately

$$[\eta] = \eta_o (1 + a\phi / 1.47\, b) \quad , \tag{2.11}$$

where a is the major particle dimension and b the minor particle dimension. Suspensions can show various rheological or viscosity behaviors, which are due to stabilizing agents in the suspension. However, typically particle-particle interactions are sufficient to cause the suspension viscosity to increase because of electrostatic interactions.

But regardless of the excellent tools available for dilute or semidilute suspensions, it is more difficult to deal with dense or concentrated suspensions and find a unifying procedure or model. The latter suspensions frequently exhibit shear thinning and shear thickening behaviors, as well as yield stress and normal stresses. It is now generally accepted that the non-Newtonian behavior of dense suspensions is due to changes in their microstructure under shear [4].

It is known that, through micrographic studies of suspensions, an initially random suspension under shear may become a two-dimensional hexagonal structure [5], among other possibilities. This result supports the work of Hoffman (1972) [6], in which he obtained light diffraction patterns for suspensions undergoing shear. From these diffraction patterns he deduced that at low to moderate shear rates, for which the rheology was shear-thinning type, the particles arranged into hexagonal packed sheets that slid over one another. At higher shear rates, with the onset of shear thickening, the diffraction patterns did not indicate any organized mesoscopic structure.

The microstructure of suspensions of hard spheres can be analytically described by the pair-distribution function, $g(r)$. It describes the probability of finding a particle at position r relative to relative to the position of a reference particle. Random suspensions exhibit only a radial distribution with exclusion of size particle. For suspensions of fore-aft asymmetric particles its $g(r)$ function obtained through micrographic study of suspensions under shear flow, indicates that particles spend more time in their approach than separating form each other. Phan-Thien (1995) [7] and Phan-Thien *et al*. (1999) [8] considered concentrated suspensions to be composed of doublets of neighboring particles.

Phenomenological equations that take into account ϕ_m, the maximum packing fraction of dispersed particles, also depends on the shear flow conditions, and can predict some of the dense suspension rheological properties such as the shear thinning behavior. It is noteworthy to emphasize that in these models, ϕ_m is a measure of the microstructure and changes of ϕ_m reflect change of its microstructure.

One model proposed by Wildemuth and Williams (1984) [9] derive a relationship where ϕ_m is a function of shear stress and monotonically increases from ϕ_{m_0} at shear stress $\tau = 0$, to ϕ_{m_∞} as $\tau \to \infty$:

$$\phi_m = \left[\frac{1}{\phi_{m_0}} - \left(\frac{1}{\phi_{m_0}} - \frac{1}{\phi_{m_\infty}} \right) \left(\frac{1}{1 + A\tau^{-n}} \right) \right]^{-1} .$$

(2.12)

When substituted into an appropriate viscosity versus ϕ/ϕ_m relationship, the result is a model that predicts the viscosity as a function of particle concentration and shear rate, predicting as well a shear thinning and yield stress behavior.

2.4. Viscoelastic behavior

Concentrated suspensions commonly display viscoelastic behavior. The most important viscoelastic properties can be measured with oscillatory shear tests. Compared with steady shear measurements the oscillatory tests are made under small deformations, at which the suspension structure is only slightly perturbed. Hence, oscillatory tests are suitable for correlating rheological behavior with structural data and inter-particle potentials.

Viscoelastic materials are characterized by a combination of elastic and viscous properties. Thus, the shear stress is not only dependent on the rate of shearing but also on the strain as well. In the simplest case, the viscoelastic behavior is governed by

$$\tau = G\gamma + \eta\dot{\gamma} \quad , \tag{2.13}$$

where G is the shear modulus of the system. The four commonly used techniques to extract information on the viscoelastic behavior of suspensions are creep-compliance measurements, stress relaxation measurement, shear-wave velocity measurements, and sinusoidal oscillatory testing. In general, transient measurements are aimed at two types of measurements, namely, stress relaxation, which is to measure the time-dependence of the shear stress for a constant small strain, and creep measurements, which measures the time-dependence of the strain for a constant stress.

The most widely used technique is the sinusoidal oscillatory or forced oscillation measurements. Oscillatory measurements consist of subjecting the medium under study to a continuously oscillating strain over a range of frequencies and measuring the peak value of the stress and the phase difference between the stress and the strain.

$$\delta = \omega t_d \quad . \tag{2.14}$$

Here ω is the frequency of the applied stress, while t_d is the time interval between two equivalent points of the strain and stress sinusoids, such as two adjacent minima.

Normally, the amplitude of the applied strain γ_0 is small enough to ensure the system is in the linear viscoelastic region. The applied strain or the strain can be expressed in complex form by

$$\gamma = \gamma_0 e^{i(\omega t+\delta)} \quad , \tag{2.15}$$

$$\dot{\gamma} = i\omega\gamma_0 e^{i(\omega t+\delta)} \quad . \tag{2.16}$$

In the linear viscoelastic region the following equations are used:

$$G^* = G' + iG'' \quad , \tag{2.17}$$

$$\eta^* = \frac{G^*}{i\omega} = \eta' - i\eta'' \quad , \tag{2.18}$$

$$\eta' = \frac{G''}{\omega} \quad , \tag{2.19}$$

$$\eta'' = \frac{G'}{\omega} \quad . \tag{2.20}$$

Here G^* is the complex shear modulus, G' the storage modulus, G'' the loss modulus, η^* the complex viscosity, η' the dynamic viscosity and η'' the out of phase component of η^*.

In general for any viscoelastic material, the observed increase in the storage modulus with increasing frequency can be understood through its relaxation time λ. At low frequencies, the characteristic experimental time scale $t_E = 1/\omega$ is longer than λ, and the perturbed structure of the material is able to relax during an oscillation period. This results in mainly a viscous response (small storage modulus), and for a suspension it implies that is able to dissipate most of the energy input. With increasing, t_E approaches λ, resulting in a viscoelastic behavior where the suspension has both a viscous and elastic response.

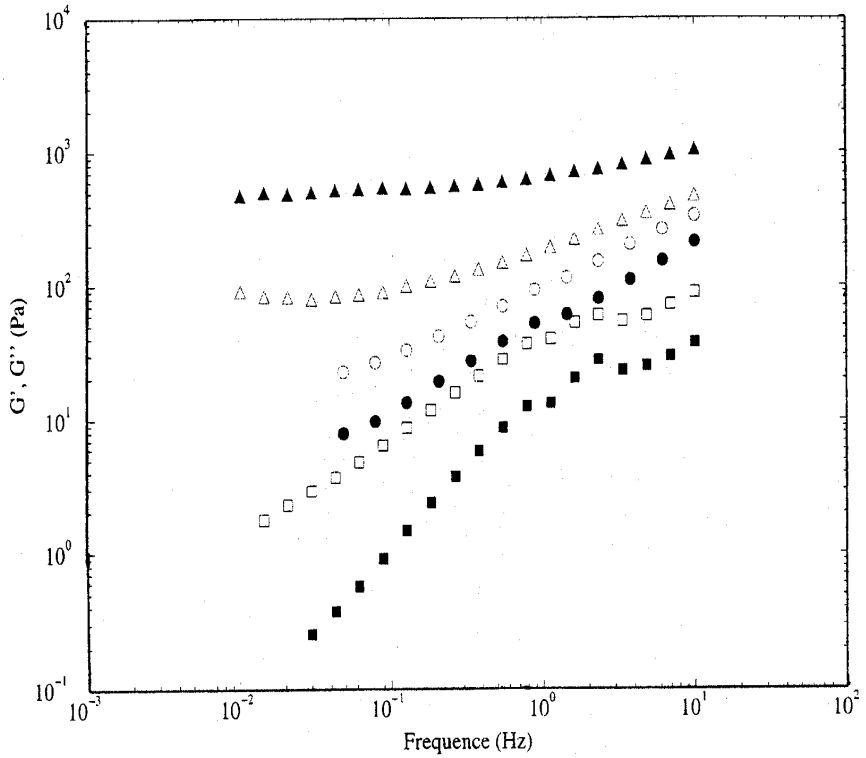

Figure 2.2. Variation of the loss modulus and storage modulus *vs*. the frequency for emulsions of water in crude oil *G'* for Φ=0.558 ■ , *G''* for *Φ* = 0.558 □ , *G'* for *Φ* = 0.61 ● , *G''* for *Φ* = 0.61 ○ , *G'* for *Φ* = 0.69 ▲ , and *G''* for *Φ* = 0.69 Δ [10].

When the frequency is increased further, t_E becomes smaller than λ, the perturbed suspension is unable to relax during an oscillation period, and the suspension display an elastic response. In this region, the storage modulus is larger than the loss modulus and the shear modulus tends to be constant, which is observed in high solid content suspension samples. $G'' > G'$ represents a viscous-dominated behavior, while $G'' < G'$ corresponds to an elastic one. For small particles, the particles' size effect becomes noticeable. In all the cases, the shear moduli depict a gradual change from a viscous behavior to a more elastic behavior with increasing solid fraction volume. Figure 2.2 shows this effect for a water-in-oil emulsion, where the high frequency elastic behavior can be verified as well as the arising elastic character with suspended phase volume increment [10].

The viscoelastic responses of flocculated systems are strongly dependent on the suspension structure. The suspension starts to show an elastic response at a critical solid volume fraction of ϕ_{ct} = 0.05 - 0.07, at which particles form a continuous three dimensional network. The magnitude of the elastic response for flocculated suspensions above ϕ_{ct} depends on several parameters, such as the suspension structure, interparticle's attraction forces and particle's size, shape and volume fraction. Buscall *et al*. [11] found that the volume fraction dependence of the storage modulus follows a power-law behavior,

$$G' \approx \phi^m \quad , \tag{2.21}$$

with the power of m = 2 - 5.

2.5. References

[1] Schramm LL. Chapter 1, Suspensions: Basic Principles, Schramm L.L., Editor, *Suspensions: Fundamentals and Applications in the Petroleum Industry*, American Chemical Society Books, Advances in Chemistry Series, Washington D.C., 1966.

[2] Liu S & Masliya JH. Chapter 3, Rheology of suspensions, *Suspensions: Fundamentals and Applications in the Petroleum Iindustry*, Schramm L.L., Editor, American Chemical Society Books, Advances in Chemistry Series, Washington D.C., 1966.

[3] Whorlow RW. In *Rheological Techniques, 2nd Edition*, Ellis Horwood, New York, 1992.

[4] Stickel JJ & Powell RL. *Annu. Rev. Fluid Mech*. 2005, **37**, 129.

[5] Völtz C, Nitschke M, Heynmann L & Rehberg I. *Phys. Rev. E*, 2002, **65**(5), 051402.

[6] Hoffmann RL. *J. Rheol*. 1992, **36**(5), 947.

[7] Phan-Thien N, Graham AL, Altobelli SA, Abbott JR & Mondy LA. *Ind. Eng. Chem. Res*. 1995, **34**(10), 3187.

[8] Phan-Thien N, Fan XJ & Zheng R. *Rheol. Acta* 1999, **38**(4), 297.

[9] Wildemuth CR & Williams MC. *Rheol. Acta* 1984, **23**(6), 627.

[10] Aomari N, Gaudu R., Cabioc'h F & Omari A. *Colloids and Surfaces A: Physicochem. Eng. Aspects* 1998, **139**, 13.

[11] Buscall HA, Mill PDA & Yates GE. *Colloids Surf.* 1986, **18**, 341.

Chapter 3.

Rheometry and rheological model

3.1.Experimental equipment

The rheology of the systems proposed in this study is carried out by ARES Rheometric Scientific: ARES stands for Advanced Rheometric Expansion System (see the equipment in Figure 3.1) and is a modular rheometer designed to cope with the changing needs of Materials Research and Process Development laboratories. It is designed to meet widely diverse testing requirements. ARES is a unit comprising an actuator, a torque and/or normal force transducer, and environmental system, and is applicable for testing almost any material-thermoplastics, thermosets, elastomers, or fluids.

Figure 3.1. ARES equipment by Rheometrics Inc.

3.2. ARES-Technology

ARES is a controlled strain rheometer for evaluating viscoelastic properties such as steady shear viscosity, normal force, shear modulus, complex viscosity, storage modulus, loss modulus, and damping. Controlled-strain rheometers employ an actuator to apply a deforming strain to the sample and a separate transducer to measure the resultant stress developed within the sample. This system provides a wider frequency range at high sensitivity, and achieves smaller dynamic strains than does a controlled stress rheometer. An ARES rheometer also performs steady, transient, and dynamic shear measurements using parallel plate, cone plate, Couette, torsion rectangular, and other fixtures.

3.3 Cone-plate geometry

Each geometry has a strain, a shear stress and a normal stress constants. In the case of cone-plate geometry the strain constant is given by

$$K_{\gamma} = \frac{1}{\beta} \quad , \tag{3.1}$$

where β is the angle, in radians, between cone and plate. The shear stress constant is given by

$$K_{\tau} = \frac{3000\ (G_C)}{2\pi R^3} \quad . \tag{3.2}$$

And the normal stress constant is given by

$$K_z = \frac{200(G_C)}{\pi R^2} \quad . \tag{3.3}$$

Therefore, the shear rate, shear stress and the first normal stress difference are calculated using the following equations

$$\dot{\gamma} = K_{\gamma}\dot{\theta} \quad , \tag{3.4}$$

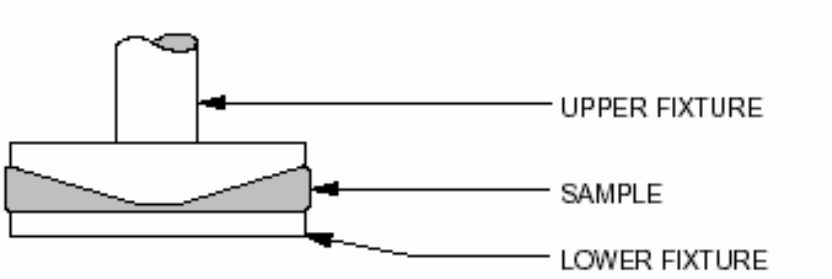

Figure 3.2. Cone-plate geometry with sample loaded.

$$\tau = K_{\tau}M \quad , \tag{3.5}$$

$$N_1 = K_z F_z \quad ; \tag{3.6}$$

where $\dot{\theta}$ is the applied angular velocity, M the measured torque and F_z the normal force. For this experimental work, the angle for the cone-plate is 0.04 radians, and a plate radius of 50 mm (Fig. 3.2). Moreover, shown in Table 3.1 are the values of the experimental setup parameters.

Table 3.1. Definitions and symbols for constants and parameters for cone-plate geometry

Symbol	Definition	Value or unit
G_c	Gravitational constant	980.7 cm s^{-2}
R	Radius of plate	50 mm
β	Cone angle	0.04 rad
K_z	Normal stress constant	3.75 dyne $g^{-1}cm^3$
K_γ	Shear constant	25 rad^{-1}
N_1	First normal stress difference	Dyne cm^{-2}
F_z	Normal force	g

3.4. A general rheological model for shear thinning fluids

On the basis of the observed behavior of a fluid subjected to a constant shear stress or a constant shear rate, the material response is classified into Newtonian and non–

Newtonian. Pseudoplastic fluids are called shear-thinning fluids because their viscosity decreases with increasing shear rate. Increasing shear rates can break down very rapidly the internal structure of a sheared fluid, and irreversibility and time-dependency of parameters is promptly manifested. Examples of fluids that exhibit shear thinning are: polymer melts and solutions such as rubbers, cellulose acetate and napalm, suspension such as paints, paper pulp, and detergent slurries, and dilute suspensions of inert solids.

Most of the equations that describe the relationship between the shear stress and shear rate are empirical. The two-parameter Power Law equation (*i. e.*, $\tau = k\dot{\gamma}^{n}$) is the most frequently used empirical equation for pseudoplastic fluids (Bird *et al*., 1960) [1]. However, this formula can fail both at low shear rates, in the first Newtonian region, and at significantly higher shear rates, when the fluid approaches the second Newtonian behavior. The Hershel-Bulkley formula represents stresses as

$$\tau = \tau_0 + k\dot{\gamma}^{n}, \tag{3.7}$$

considering a yield stress in addition to the Power Law term (Bird *et al*., 1960 [1]; Boger and Halmos, 1981 [2]); this Power Law model depends on three parameters. The Ellis model is a four-parameters model. It is the next step to complexity to describe pseudoplastic fluids and is given by the following formula (Bird *et al*., 1960 [1]):

$$\tau = \eta_\infty \dot{\gamma}^{n} + \frac{\dot{\gamma}(\eta_0 - \eta_\infty)}{1 + \left(\frac{\tau}{\tau_m}\right)^{\alpha - 1}}, \tag{3.8}$$

with parameters η_0, η_∞, τ_m, and α. Reiner (1960) [3] reported the same formula with the value of $\alpha = 3$. Another empirical model showing the approximate Newtonian behavior at both low and high shear is Eyring's Power Law given by

$$\tau = A\dot{\gamma} + \frac{1}{B}\sinh^{-1}\left(\frac{-1}{C}\dot{\gamma} g\right), \tag{3.9}$$

where A, B and C are constants. Seely (1964) [4] found that the following equation predicts the Newtonian behavior observed at high shear rates but not at low shear rates, fitting well the experimental behavior of polybutadiene solutions

$$\tau = A\dot{\gamma} + B\dot{\gamma}\, e^{-\dot{\gamma}\tau} \quad , \tag{3.10}$$

with A and B are constants. Sisko (1958) [5] developed the following equation for shear thinning fluids:

$$\tau = a\dot{\gamma} + b\dot{\gamma}^{c} \ , \tag{3.11}$$

where a, b and c are constants.

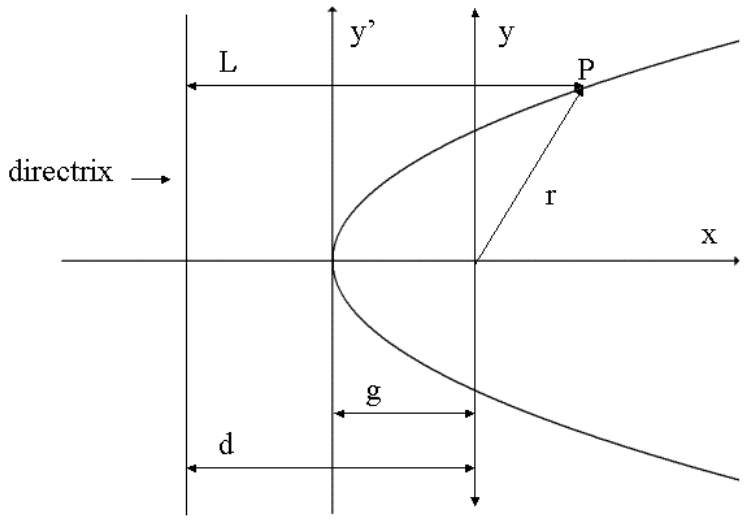

Figure 3.3. Geometrical interpretation of the model.

There are many other empirical formulas that describe pseudoplastic behavior. However, most, if not all of them, describe shear stress *vs* shear rate behavior within a limited range. Their application is justified by the elaborate mathematics that is otherwise required to solve even the simplest problems; using most of the empirical equations is difficult and rarely justified.

A general model for shear thinning fluids is hereby developed, with the purpose of achieving a model with few parameters, starting from geometrical observations related to the shapes of stress-shear rate curves, of the same type of Fig. 2.1. The

mathematical formula which relates the original coordinates for the shape shown in Fig. 3.3 has the following form:

$$x^2 + y^2 = \lambda^2 (d + x)^2 , \tag{3.12}$$

the locus point for which the value $r/L=\lambda$ is constant. By transforming the axes to *y'* and *x'*

$$x' = x + g, \tag{3.13a}$$

$$y' = y, \tag{3.13b}$$

by substituting Eqs. 3.13a and 3.13b into Eq. 3.12

$$(x' - g)^2 + y'^2 = \lambda^2 (d + x' - g)^2 , \tag{3.14}$$

at $y' = 0$, $x' = 0$ this yields

$$d - g = g / \lambda, \tag{3.15}$$

and substituting Eq. 3.15 into Eq. 3.14:

$$(x' - g)^2 + y'^2 = \lambda^2 \left(x' + \frac{g}{\lambda} \right)^2 . \tag{3.16}$$

Rearranging Eq. 3.16 and dividing by $(1 - \lambda^2)$:

$$x'^2 - \frac{2g(1+\lambda)}{(1-\lambda^2)} x' + \frac{y'^2}{(1-\lambda^2)} = 0. \tag{3.17}$$

Adding and subtracting $[g / (1-\lambda)]^2$ to the above equation:

$$\left(x' - \frac{g}{1-\lambda} \right)^2 + \frac{y^2}{(1-\lambda^2)} = \left(\frac{g}{1-\lambda} \right)^2 , \tag{3.18}$$

or

$$\frac{\left(x' - \frac{g}{1-\lambda} \right)^2}{\left(\frac{g}{1-\lambda} \right)^2} + \frac{y^2}{g^2 \frac{(1+\lambda)}{(1+\lambda)}} = 1. \tag{3.19}$$

Let:

$$\frac{g}{1-\lambda} = \mathrm{A} \tag{3.20a}$$

$$g^2 \frac{(1\lambda)}{(1+\lambda)} = B^2 \quad . \tag{3.20b}$$

If $x' = \dot{\gamma}$ and $y = \tau$, therefore, Eq. 3.19 acquires the following form:

$$\frac{(\dot{\gamma} + \delta A)^2}{A^2} - \delta\left(\frac{\tau}{B}\right)^2 = 1. \tag{3.21}$$

Generalizing the formula to cover all the ranges listed below, it is obtained:

$$\left[\frac{(\dot{\gamma} + \delta A)}{A}\right]^n - \delta\left(\frac{\tau}{B}\right)^n = 1. \tag{3.22}$$

The model equation, which depends on three parameters *A, B*, and *n,* may be used to match laboratory experiments by nonlinear regression techniques. Many useful relations are included in this model as special cases. For instance:

1. It can be reduced to a Newtonian fluid with or without yields stress, when $n = 1$. The resulting formulas are:

$$\tau = \frac{B}{A}\dot{\gamma} \quad \text{for } \delta = 1 \tag{3.23}$$

$$\tau = 2B - \frac{B}{A}\dot{\gamma} \quad \text{for } \delta = -1$$

(3.24)

2. The hyperbolic case can be when $n = 2$ and $\delta = 1$
3. The elliptic case occurs when $n = 2$ and $\delta = -1$

The model contains the index *n* which allows the model to cover a wide range of operating conditions and produces a model with power-law characteristics.

For the hyperbolic case, the general formula for the shear stress as a function of the shear rate has the following form:

$$\tau = B\left[\left(\frac{\dot{\gamma} + A}{A}\right)^{n} - 1\right]^{(1/n)}. \tag{3.25}$$

For the elliptic case, the general formula for the shear stress as function of the shear rate has the following form:

$$\tau = B\left[1 - \left(\frac{\dot{\gamma} - A}{A}\right)^{n}\right]^{(1/n)}, \tag{3.26}$$

which is the equation developed by Al-Zahrani (1997) [6]. This equation is used throughout this work, considering also that Al-Zahrani (1998) [7] demonstrated its good flexibility and adaptability for suspensions, emulsions and crude oils.

3.5. References

[1] Bird RB, Steward WE & Lightfoot EW. In *Transport Phenomena*. Wiley, New York, NY, 1960.

[2] Boger DV & Halmos AL. *AIChE J.* (Am. Inst. Chem. Eng.) 1981, **Module C 2.2**, 8.

[3] Reiner M. In *Deformation, Strain, and Flow*. Interscience, New York. NY, 1960.

[4] Seely G.R. *AIChE J*. (Am. Inst. Chem. Eng.), 1964, **10**, 56.

[5] Sisko AW. *Ind. Eng. Chem*. 1958, 1789.

[6] Al-Zahrani SM. *Journal of Petroleum Science and Engineering*. 1997, **17,** 211.

[7] Al-Zahrani SM & Al-Fariss TF. *Chemical Engineering and Processing*. 1998, **37**, 433.

Chapter 4.

Viscoelastic models

4.1. Maxwell model based on distributions of relaxation times

Viscoelastic materials are characterized by a combination of elastic and viscous properties, and in the simplest case the viscoelastic behavior is governed by Eqns. 2.12 .

The four commonly used techniques to extract information on the viscoelastic behavior of suspensions are also described briefly in Chapter 2. The Maxwell viscoelastic model satisfies with the requirements to manifest viscous and elastic behaviors typically present in dispersions [1-3]:

$$\tau_{ij} + \lambda \frac{\partial\, \tau_{ij}}{\partial\, t} = \eta_0 D_{ij} \quad , \tag{4.1}$$

For the Maxwell model, the storage and loss moduli are given by:

$$G'(\omega) = \frac{G\omega^2\lambda^2}{1+\omega^2\lambda^2} \ , \tag{4.2}$$

$$G''(\omega) = \frac{G\omega\lambda}{1+\omega^2\lambda^2} \, . \tag{4.3}$$

This model has only one relaxation time λ, but crude-oil and several other mixtures or dispersions have several relaxation times; or generally, a distribution of relaxation times as the simplified version shown in Fig. 4.1. For a multiple relaxation-time Maxwellian model

$$G'(\omega) = \int_{-\infty}^{\infty} \frac{\omega^2\lambda^2 H(\lambda)}{1+\omega^2\lambda^2} d\ln\lambda \, , \tag{4.4}$$

$$G''(\omega) = \int_{-\infty}^{\infty} \frac{\omega\lambda H(\lambda)}{1+\omega^2\lambda^2} d\ln\lambda \ . \tag{4.5}$$

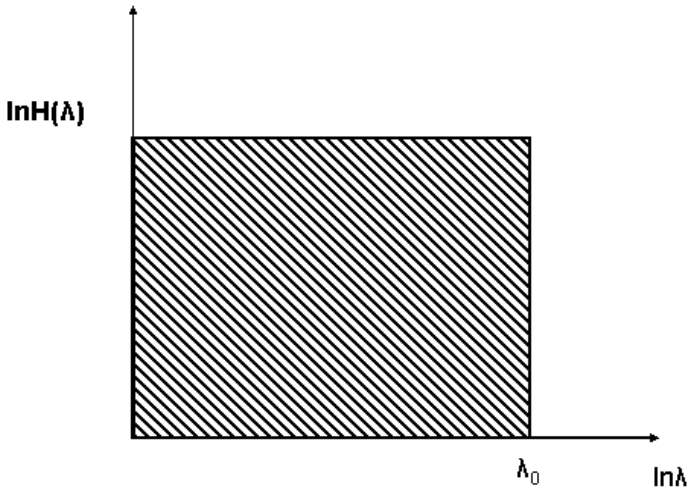

Figure 4.1. Simplified relaxation spectrum.

For a material with the relaxation spectrum of Fig. 4.1, the storage and loss moduli are:

$$G'(\omega) = \frac{G_0}{2}\ln(1+\omega^2\lambda^2) \ , \tag{4.6}$$

$$G''(\omega) = G_0 \tan^{-1}(\omega\lambda) \ . \tag{4.7}$$

4.2. Viscoelastic fluids and other viscoelastic models

Perhaps it is best to begin at the end, with an admission of failure. There is no constitutive equation capable of predicting all of the material functions that characterize the full variety of simple flows which are useful for studying and modeling polymeric fluids. There are several constitutive equations capable of predicting the behavior of some of the material functions, even with great accuracy, requiring only a small number of free constants −or adjustable parameters− to do so. However, some of the "best" constitutive equations are complicated mathematically. If they are used in conjunction with the dynamic equations, the resulting mathematical model is so complex that an analytical solution is generally impossible to obtain. We must be able to examine a flow process and judge which elements

of the kinematics are truly essential to model its behavior. Then we must select an appropriate constitutive capable of describing the dominant type of kinematics of that flow field. The resulting solution of the dynamic equations, for the velocities and stresses, must be interpreted in light of the known weaknesses of the constitutive equation used. Finally, experience −the comparison of prediction and observation− must be the judge for success.

In contrast to the purely viscous models, viscoelastic models must characterize two essential features of real viscoelastic fluids: the development of normal stresses in shearing flows, and transient phenomena of the type characterized by stress growth functions η^+, Ψ^+, etc., but including "classical" stress relaxation phenomena as well.

Since we have used the word "classical", let us begin with the classical viscoelastic Maxwell model, expressed in Eqn. 4.1, where λ and η_0 are constants.

This model is useless to our goals, except as a conceptual link to more adequate constitutive equations. It is useless because:

1- it predicts Newtonian behavior in shear,

2- it does not predict the existence of normal stresses,

3- its transient behavior is monotonic in stress growth, contrary to the experience at all but the lower shear rates [3].

Furthermore, it is not correct mathematically. It is possible to show that the ordinary time derivative of a tensor is not a tensor!

We have to specify the state of stress in a continuously deforming continuous medium, we must also account in some way for the deformation of the material when we transform from a *material coordinate system* to the laboratory coordinate system. The difficulty lies in the fact that there is no *unique* mathematical way to do this.

In any physically meaningful mathematical statement certain basic principle must be observed. Some of the principles are so familiar that we rarely think of them. For

example, we can only add terms if they are dimensionally consistent. Neither can we add terms which have different mathematical character; so, we cannot add a scalar and a vector, nor a tensor and a pseudo-tensor. Thus, if we wish to incorporate a time derivative of stress in a constitutive equation, we must find a way of writing a time derivative which preserves the physical idea of time rate of change while preserving the symmetry properties of the physical quantity and the required mathematical character for its representation [3-6].

The general configuration derivative is so expressed (where $\dot{\underline{\underline{\tau}}}$ is the total time derivative of the stress tensor) by:

$$\overset{\diamond}{\underline{\tau}} = \left(1-\frac{\varepsilon}{2}\right)\overset{\nabla}{\underline{\tau}} + \frac{\varepsilon}{2}\overset{\Delta}{\underline{\tau}} \quad , \tag{4.8}$$

$$\overset{\nabla}{\underline{\underline{\tau}}} = \dot{\underline{\underline{\tau}}} - \left(\underline{\underline{L}}\cdot\underline{\underline{\tau}} + \underline{\underline{\tau}}\cdot\underline{\underline{L}}^{T}\right) , \tag{4.9}$$

$$\overset{\Delta}{\underline{\underline{\tau}}} = \dot{\underline{\underline{\tau}}} + \left(\underline{\underline{L}}^{T}\cdot\underline{\underline{\tau}} + \underline{\underline{\tau}}\cdot\underline{\underline{L}}\right) \quad . \tag{4.10}$$

$\underline{\underline{L}}$: *Velocity gradient tensor*

For:

- $\varepsilon = 0$ the convective contravariant derivative (contravariant Oldroyd derivative) is obtained,
- $\varepsilon = 1$ implies the corrotational derivative (Jaumann derivative), and for
- $\varepsilon = 2$ prescribes the convective covariant derivative (covariant Oldroyd derivative).

From Equation 4.8, and using the Oldroyd and Jaumann derivatives −with the appropriate parameter ε− the modified Maxwell model is obtained, that is,

$$\underline{\tau} + \lambda\overset{\diamond}{\underline{\tau}} = \eta_0\underline{D} \tag{4.11}$$

$\underline{D}$: *Rate − of − deformation tensor*

One recommended compromise is the White-Metzner modification [2] of the Maxwell model, utilizing Oldroyd derivative in the contravariant form ($\varepsilon = 0$) that consists in taking both λ and η to be function of the second invariant of the flow field [3], and the usual assumption is to relate λ to η through a "modulus" G, so that:

$$\lambda = \frac{\eta(II_D)}{G}, \tag{4.12}$$

The unspecified function $\eta(II_D)$ can be selected from experimental data and a realistic shear-viscosity behavior can be modeled.

4.3. References

[1] Bird RB, Stewart WE & Lightfoot EN, In *Transport Phenomena*, John Wiley & Sons, Inc., New York, 1960.

[2] White JL & Metzner AB. *Journal of applied Polymer Science*. 1963, **7**, 1867.

[3] Middleman S. In *The Flow of High Polymers*, Interscience Publishers, a Division of John Wiley & Sons, Inc., New York, 1968.

[4] Chen I-J & Bogue DC. *Trans. Soc. Rheol*. 1972, **16**, 59.

[5] Huppler JD, Ashare E & Holmes LA. *Trans. Soc. Rheol*. 1967,**11**,159.

[6] Bird RB, Hassager O & Abdel-Khalik SI. *AIChE J*. (Am. Inst. Chem. Eng.) 1974, **20**, 1041.

Chapter 5.

Shear thinning and viscoelastic models for Mexican crude oil and comparison with alkanes *

From the paper published by R. C. Dante, A.E. Chávez and E. Geffroy,

Fuel 2006, **85**, 559)

Abstract

The viscoelastic knowledge of crude oil is limited by the complexity and variability of the raw material. Viscoelastic models of Maxwell type describe a large variety of Mexican crude oils when an Oldroyd contravariant derivative is considered. Moreover, a Weissenberg number is defined by the product of the shear rate and the characteristic time of the considered system. This dimensionless number allows for scaling of viscosities of both crude oil, at different temperatures, and mixtures of *n*-eicosane/*n*-heptadecane. Thus, blends of linear alkanes can simulate the viscous behavior of crude oils after adequate scaling and can be used to predict crude oil rheological properties with the advantage to be completely known and reproducible systems.

5.1. Introduction

Crude petroleum is a mixture of compounds, each with different boiling temperatures that can be separated into a variety of generic fractions by distillation and by fractionation [1, 2]. However, petroleum from different sources exhibits different characteristics, and the behavioral characteristics are often difficult to define with a high degree of precision. There is a wide variation of properties of petroleum, with proportions of different constituents varying largely [1-4]. Thus, some crude oils have

* This Chapter is based on the paper published in the journal *Fuel*, but has been complemented with new experimental data and a more detailed analysis, including reflections and suggestions by members of Exam Committee.

higher proportions of the lower boiling constituents, whereas others (such as bitumen, also referred to as natural asphalt) have greater proportions of the higher boiling constituents (often called the “asphaltic components” or “residuum”). However, from a rheological point of view, crude oils can be classified in the general field of suspensions, since they show shear thinning behavior in steady shear strain conditions as well as normal stresses [5]. This very complex behavior depends partially on a Newtonian contribution of non colloidal particles combined with a non-Newtonian contribution due to the colloidal particles [6]. There are two approaches to understand and achieve a general scope of rheological properties of crude oil: (i) the former consists in reproducing crude oils artificially by mixing several typical compounds of oils in a well known proportions [7-9]; (ii) the latter, in finding a class of chemically well defined compounds which can describe at least the main oil characteristics with the introduction of an adequate scaling of variables.

The second approach may allow also an extensive set of modeling possibilities. Blends of linear aliphatic compounds manifest a similar behavior to that of oils, but with different absolute values of the rheological parameters. In both cases, it may be inferred that the main rheological features are dominated by the preponderant aliphatic or paraffinic phase [7, 10]. The present chapter is an attempt to unify in a whole rheological model frame the two systems: crude oil and alkanes mixtures, in order to use the latter to simulate and forecast the principal rheological characteristics of the former, thinking overall on the wide technological uses of such predictions as the asphaltenic oil fluidization for transportation through pipelines to power plants and their final combustion atomization.

5.2 Materials, equipments, experiments and methodology

5.2.1 Materials and equipment

The specimens of waxy crude oil came from the same sample of Cantarell reservoirs in south-east Mexico, and they were tested at different temperatures (293-333K) without addition of any kind of substances. The linear alkanes used have a number of carbon atoms of C17 and C20. The mixtures of alkanes were prepared mixing them by mechanical agitation above their melting points up to the formation of solutions. The rheological tests were carried out by a strain controlled rheometer ARES (Advanced Rheometric Expansion System). The same cone-plate geometry was used for all tests with an angle of 0.04 radians and a plate radius of 50 mm. This rheometer measures the normal force applied by the sample, which is used to estimate the first difference of normal stresses N_1, and to calculate the first coefficient of normal stresses ψ_1. A delay of 400 seconds was applied before every measurement in order to ensure that the steady state has been achieved.

5.2.2. General rheological model for shear thinning fluids

The model adopted for the crude oil shear thinning behavior is the same described in detail in Chapter 3 and proposed by Al-Zahrani for waxy oils [11, 12]: a four parameters equation of *power-law* type,

$$\left[\frac{(\dot{\gamma} + \delta A)}{A}\right]^n - \delta\left(\frac{\tau}{B}\right)^n = 1 \ , \qquad (5.1)$$

where τ is the shear stress, $\dot{\gamma}$ is the shear rate, A has dimensions of shear rate and B of stress, the ratio B/A is the viscosity at shear rates tending to infinity when the shape parameter $\delta = 1$, and n is an exponent correlated to the extent of shear thinning. Based on Eq. 5.1, the fluid viscosity $\eta(\dot{\gamma})$ is given by

$$\eta(\dot{\gamma}) = \frac{B}{\delta^{1/n}}\left[\left(\frac{1}{A} + \frac{\delta}{\dot{\gamma}}\right)^{n} - \frac{1}{\dot{\gamma}^{n}}\right]^{\frac{1}{n}} . \tag{5.2}$$

For $\delta = 1$ the hyperbolic case, Eq. 5.2 reduces to a three parameters equation:

$$\eta(\dot{\gamma}) = B\left[\left(\frac{\dot{\gamma} + A}{\dot{\gamma}A}\right)^{n} - \frac{1}{\dot{\gamma}^{n}}\right]^{\frac{1}{n}} . \tag{5.3}$$

Expressing the dependence upon the second invariant of the shear rate tensor in Eq. 5.3, the following general equation is obtained:

$$\eta(II_D) = \frac{B}{\dot{\gamma}}\left[\left(\frac{\dot{\gamma} + A}{A}\right)^{n} - 1\right]^{\frac{1}{n}} = \frac{\sqrt{2}B}{\sqrt{II_D}}\left[\left(\frac{\sqrt{II_D} + \sqrt{2}A}{\sqrt{2}A}\right)^{n} - 1\right]^{\frac{1}{n}}; \tag{5.4}$$

where the second invariant of the shear rate tensor is $II_D = 2\ \dot{\gamma}^2$. The advantage of the model is that it can describe the shear thinning behavior of both crude oils and a wide variety of suspensions [11].

5.2.3. Viscoelastic model

Viscoelastic materials are characterized by a combination of elastic and viscous properties. Thus, a simple power-law model is not suitable for predicting the behavior of such complex fluids. The next level of complexity may be reached by using the Maxwell model, that also considers elastic properties. Furthermore, the Maxwell standard model can be enriched by the introduction of the Oldroyd contravariant derivative, as described in Chapter 4, in order to model a nonzero first coefficient of normal stresses, and to be able to describe the transient and the steady state functions of both the viscosity and the first coefficient of normal stresses ψ_1 [13]

$$\tau_{ij} + \lambda(II_D)\frac{\partial_{ol}\tau_{ij}}{\partial_{ol}t} = \eta(II_D)D_{ij} , \tag{5.5}$$

$$\frac{\partial_{ol}\tau_{ij}}{\partial_{ol}t} = \frac{\partial \tau_{ij}}{\partial t} + u_k \frac{\partial \tau_{ij}}{\partial x_k} - \tau_{kj}\frac{\partial u_i}{\partial x_k} - \tau_{ik}\frac{\partial u_j}{\partial x_k} \ , \tag{5.6}$$

where in Eq. 5.6 the viscosity η and the relaxation time λ are functions of the second invariant of the rate-of-deformation tensor II_D; while, τ_{ij} are the components of the stress tensor. In Eq. 5.6, the Oldroyd contravariant derivative is shown, where u_k, u_i and u_j are the fluid velocity components. Applying the White-Metzner approximation [14], i.e., using in place of $\eta(II_D)$ of Eq. 5.5, the result obtained in Eq. 5.4, the *transient* viscosity η^+ and the *transient* first coefficient of normal stresses ψ_1^+ functions are therefore properly expressed respectively by

$$\eta^+(II_D) = \eta(II_D)\left[1 - \exp\left(-\frac{t}{\lambda(II_D)}\right)\right] \ , \tag{5.7}$$

and

$$\psi_1{}^+ = 2\frac{\eta^2(II_D)}{G}\left[1 - \left(1 + \frac{t}{\lambda(II_D)}\right)\exp\left(-\frac{t}{\lambda(II_D)}\right)\right] \ . \tag{5.8}$$

In the latter equation, G is the elastic modulus. Finally, the *steady* state first coefficient of normal stresses, ψ_1, results to be proportional only to the square of the viscosity function

$$\psi_1 = 2\frac{\eta^2(II_D)}{G}; \quad t \to \infty \ . \tag{5.9}$$

5.2.4. Dimensionless viscosity and shear rate

The scaling of viscosity and shear rate allows us to include different systems in the same general model and therefore to explain complex systems starting from a more simple, well-characterized analogous systems. Scaling often implies looking for functions of the type $k\eta$ and $k'\dot{\gamma}$, with units for [k] = $mass^{-1}$·$length$· $time$ or simply $viscosity^{-1}$ dimensions and k' given in *time* units. On the other hand, both k and k' can

be a combination of several variables so that $k\eta$ and $k'\dot{\gamma}$ represent the balance of the two main characteristic forces, expressed mathematically by

$$k'\dot{\gamma} = f(W_{viscous}, E_{activation}). \quad (5.10)$$

For instance, the two main characteristic energies for oils are the work done by the viscous forces $W_{viscous}$ and the energy barriers necessary to overcome the local structure of aggregates and molecules, named as $E_{activation}$. The energy of activation is essentially associated to the existence of an internal "*micro-meso*" structure, besides that of the purely atomistic nature, with time-scales dependent on the mesoscopic changes of structure. In this work, these barriers correspond to the energy implicated in the reorientation of large molecules, such as alkanes, along the flow direction by means of the shear stress applied [15-17]. The dimensionless number proposed in Eq. 5.10 as a function of $W_{viscous}$ and $E_{activation}$ can be interpreted also as a Weissenberg number, remembering that *k'* is given in time-units

$$k'\dot{\gamma} = We(E_{activation}, W_{viscous}) . \quad (5.11)$$

In this interpretation, *k'* is the characteristic time of the phenomena being scaled [17-19].

5.3. Experimental results

5.3.1. Crude oil results

The results for crude oil at different temperatures are shown in Fig. 5.1. For each plot and at different temperatures, all limiting viscosity values start at about 10^5 Poise (10^4 Pa·s), for a shear rate of 10^{-4} s^{-1}. In a general way, within the temperature range of 293-333K, there exists first, a shear thinning linear region followed by a Newtonian region. The shear thinning region expands itself with increasing temperature, with final viscosities varying from about 10^3 Poise (10^2 Pa·s), at 293K, down to 10^1 Poise (1 Pa·s) at 333 K. At this transition point –from a shear thinning to steady viscosity– both a

critical viscosity η_c (crossing viscosity) and a critical shear rate $\dot{\gamma}_c$ (crossing shear rate) can be defined as the viscosity and shear rate corresponding to the crossing point of the straight lines extrapolated from the shear thinning region and from the subsequent plateau, respectively. For each system, both the crossing viscosity and crossing shear rate are reported in Table 5.1. The crossing shear rates increase from 0.025 s^{-1} at 293 K up to 0.593 s^{-1} at 333 K, while the crossing viscosities decrease from 1069 Poise (106.9 Pa·s) at 293K to 30 Poise (3.0 Pa·s) at 333 K. In Section 5.4, these critical viscosities and shear rates are used to build all dimensionless variables used. However, the behavior at shear rates higher than 100 s^{-1} was not observable, due to torque values causing a transducer overload. At temperatures higher than 333 K, the dependence of viscosity on temperature is not so marked, even within the second Newtonian region.

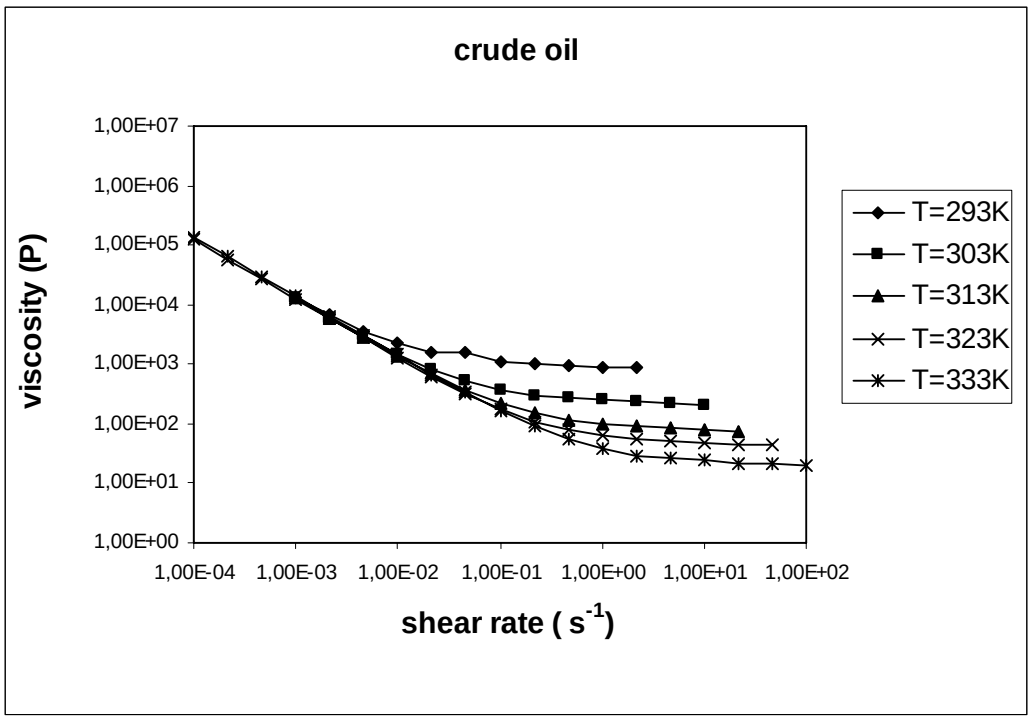

Figure 5.1. Steady shear rate viscosities at different temperatures, for Crude Oil. There is no zero-shear rate viscosity observed for this sample from the field of Cantarell in the Gulf of Mexico.

The crossing viscosities and shear rates manifest a linear logarithmic dependence on the inverse of temperature, as shown in Fig. 5.2, which means that an Arrhenius factor is implicated in both the increment of the crossing shear rate and decrement of the crossing viscosity.

Table 5.1. Crude oil crossing shear rates and viscosities determined by intersection of the two linear regions.

$\dot{\gamma}_c(s^{-1})$	η_c(Poise)	T(K)
0.025	*1069.1*	*293*
0.059	*319.2*	*303*
0.141	*127.1*	*313*
0.228	*64.0*	*323*
0.593	*30.0*	*333*

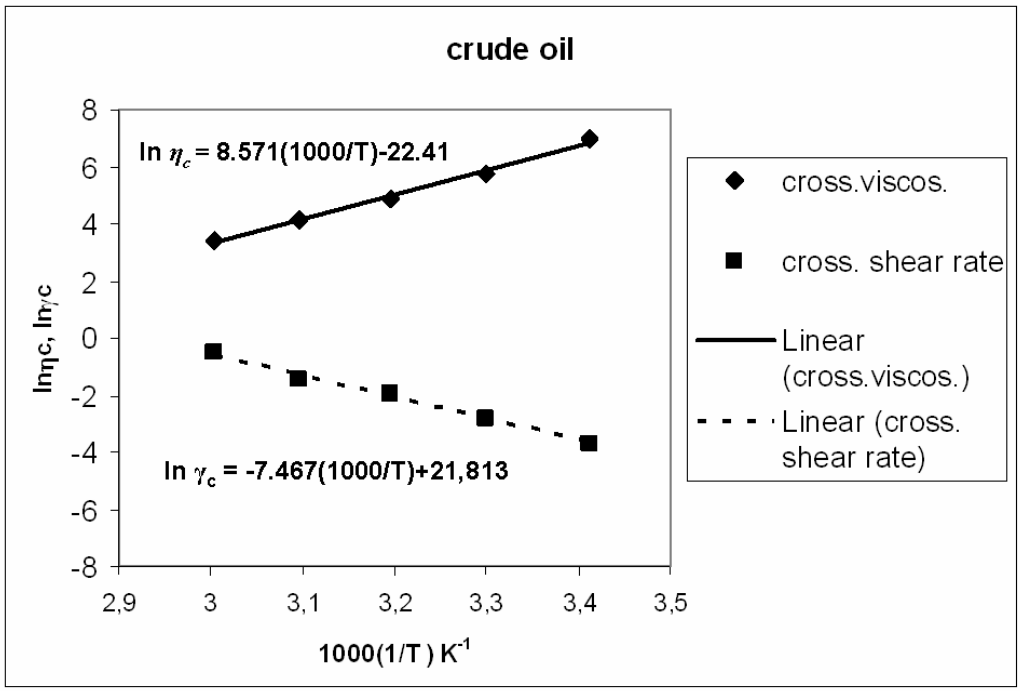

Figure 5.2. Relationship between $ln\ \dot{\gamma}_c$ (lower line) and $\ln \eta_c$ (upper line) with the inverse of temperature ($1/T$).

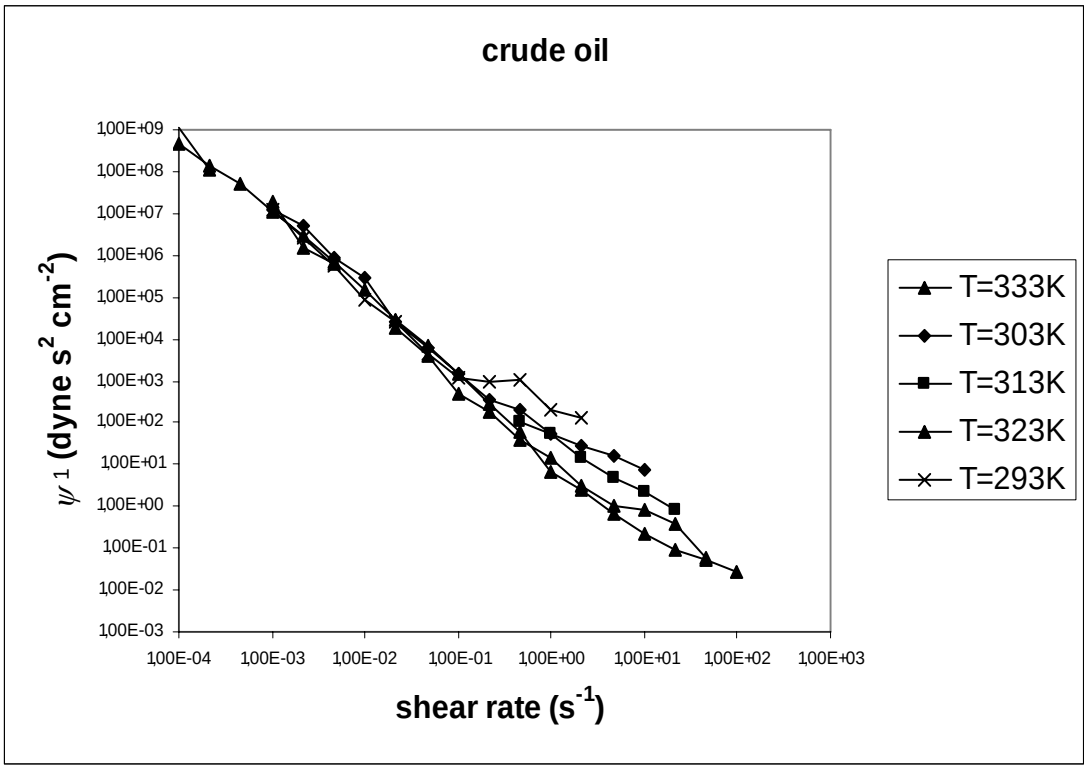

Figure 5.3. First normal stresses coefficient ψ_1 of crude oil at different temperatures.

The first coefficient of normal stresses ψ_1 also shows a shear thinning trend (see Fig. 5.3): the values of ψ_1 start from about 10^9 dyne·s^2·cm^{-2} (10^8 Pa·s^2) and reach about 10^{-2} dyne·s^2·cm^{-2} (10^{-3} Pa·s^2). The shear thinning region is larger at higher temperature (333K), while at lower temperatures it tends to be smoothed with a softer decay; herewith, the behavior is quite different from viscosity. The transient viscosity is shown for a shear rate of 1 s^{-1} and at 293 K, as an example of transient behavior; in which it is noteworthy that a small initial overshoot is observed, with a lower value of the steady viscosity (Fig. 5.4). The overshoot tends to disappear either by increasing the temperature of the sample or by incrementing the shear rate. The transient first coefficient of normal stresses exhibits a marked overshoot, which disappear with increasing either temperature or shear rate.

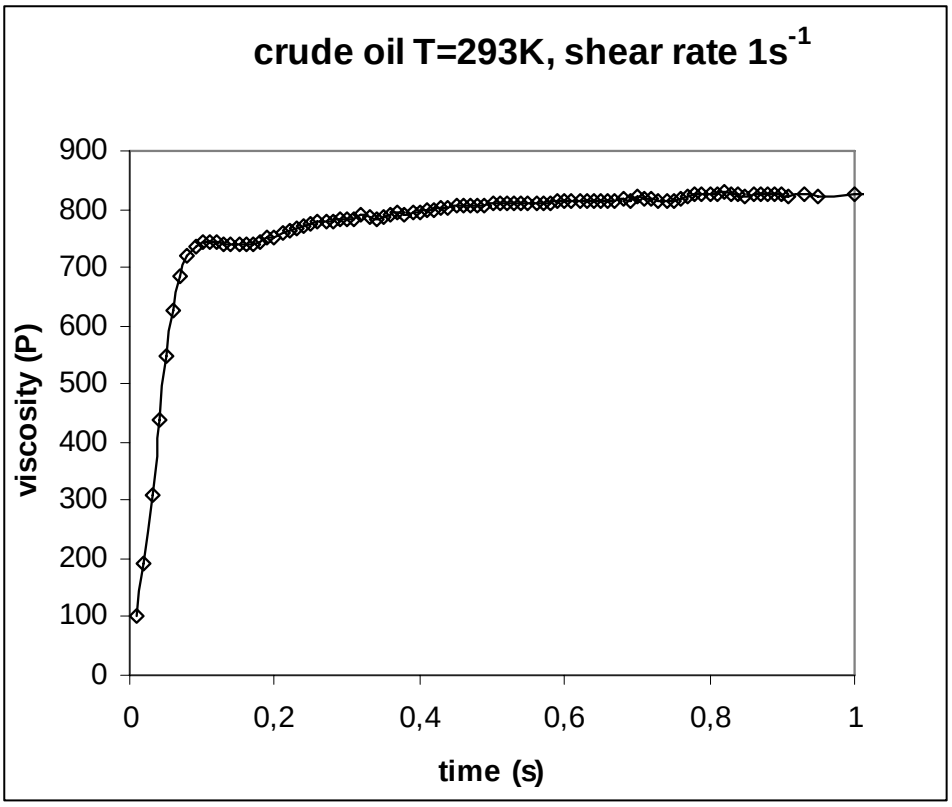

Figure 5.4. Transient test at shear rate of $1s^{-1}$ and T = 293K for crude oil.

5.3.2 Linear alkanes results

The mixture of *n*-heptadecane (C17) and *n*-eicosane (C20), with an eicosane molar fraction of 0.16, was tested within the temperature range of 298-325 K. Below 298 K, large solid phases are present. No more significant phase changes are observed at temperatures higher than 325 K. The viscosities start with values next to 10^3 Poise (10^2 Pa·s) at a shear rate of 10^{-3} s^{-1}. At low shear rates (10^{-3} s^{-1}- 1 s^{-1}), the mixture viscosities have the same trend of shear thinning and very close values (Fig. 5.5). It seems that temperature does not affect phenomena corresponding to large relaxation times. However, at higher shear rates, in the Newtonian region, the viscosities decreases slightly with temperature increments, but in a less pronounced manner than crude oil. The critical shear rates are 20.0 s^{-1} at 298 K, 23.6 s^{-1} at 305 K, and 44.5 s^{-1} at 325 K.

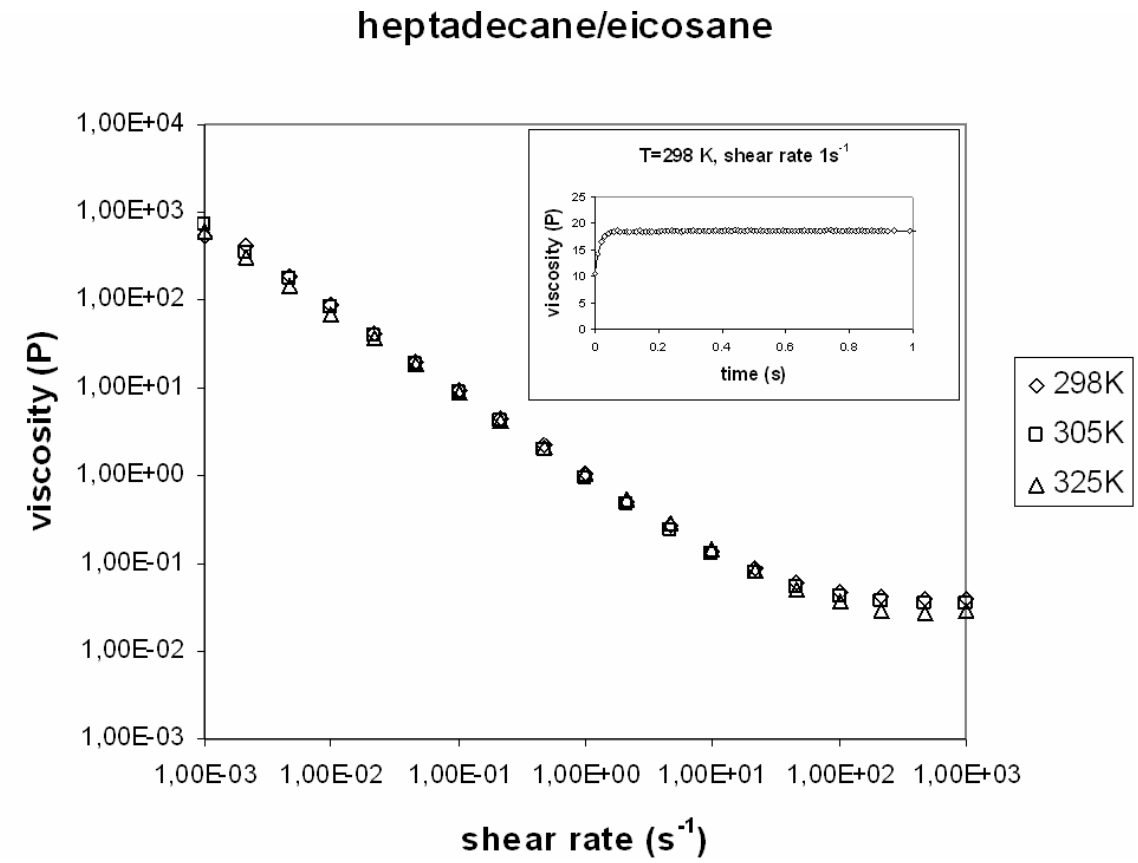

Figure 5.5. Viscosity of heptadecane/ eicosane mixture at different temperatures. In the inserted box at top right, the transient viscosity at the shear rate of $1s^{-1}$ is shown.

Given that all values –and curves– plotted in Fig. 5.5 are very close among themselves, it is difficult to perceive the present small differences. The corresponding crossing viscosities are $5.2 \cdot 10^{-2}$ Poise ($5.2 \cdot 10^{-3}$ Pa·s) at 298 K, $4.5 \cdot 10^{-2}$ ($4.5 \cdot 10^{-3}$ Pa·s) Poise at 305 K, and $3.7 \cdot 10^{-2}$ Poise ($3.7 \cdot 10^{-3}$ Pa·s) at 325 K.

In the inserted plot in Fig. 5.5, the transient viscosity at the shear rate of $1s^{-1}$ is shown. In this case, no overshoot is observed as in crude oil; moreover, the steady state is reached quicker than in the case of crude oil. However, at lower shear rates the overshoot is clearly observable but tends to disappear either with increasing temperature or shear rate.

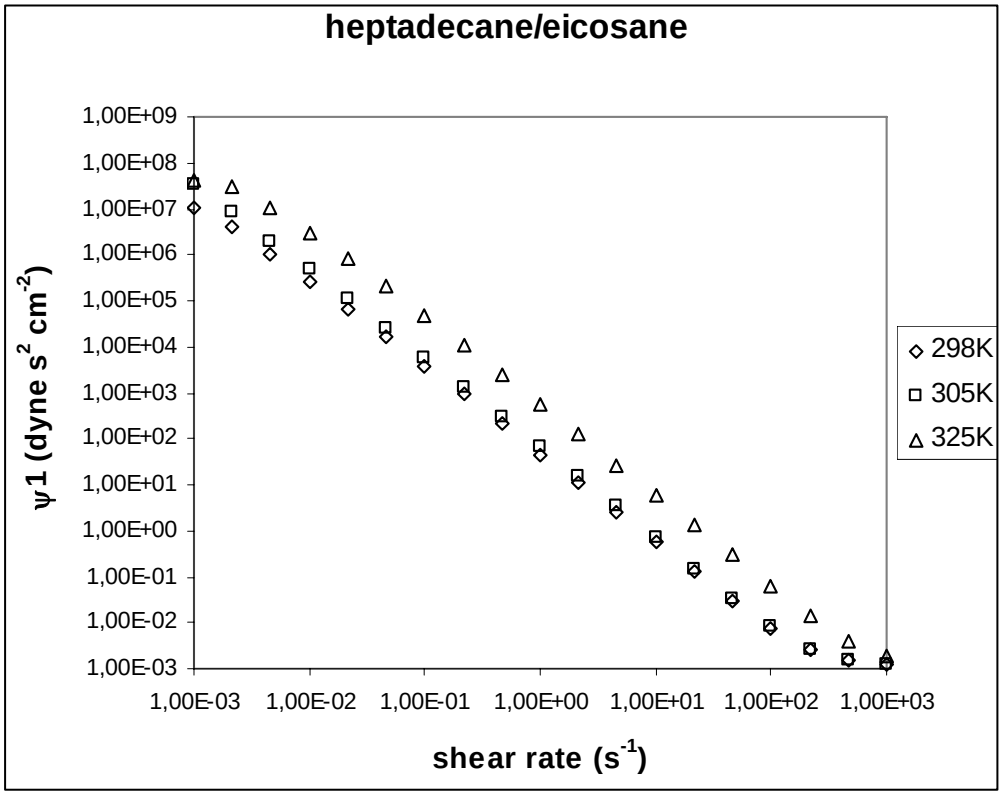

Figure 5.6. First coefficient of normal stresses for heptadecane/eicosane mixture at different temperatures.

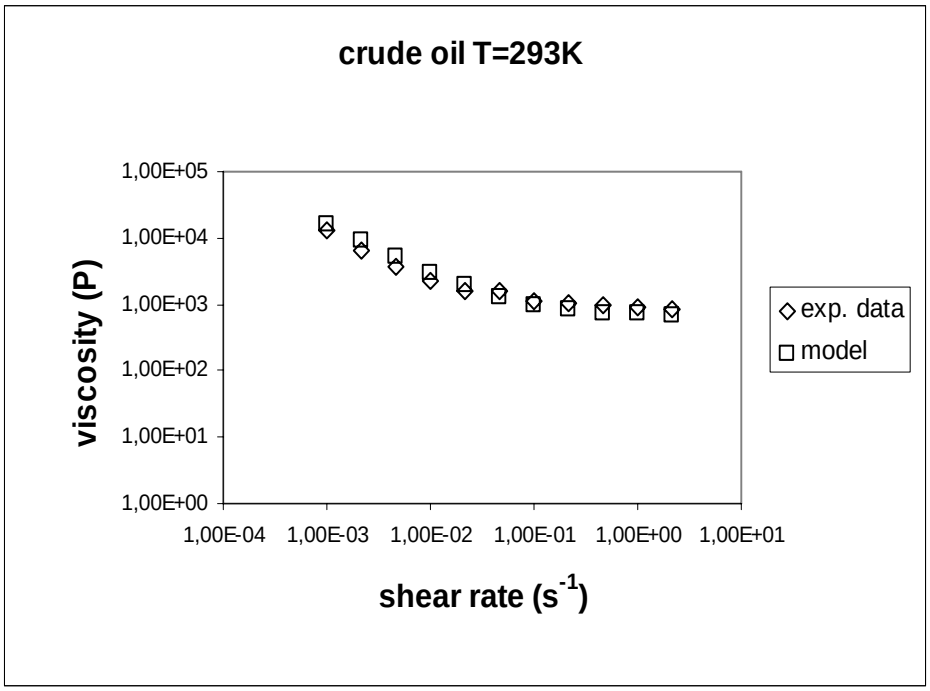

Figure 5.7. Comparison between the experimental data of the viscosity curve of crude oil at 293 K and the model predictions.

The first coefficient of normal stresses for the mixture is shown in Fig. 5.6. Values of ψ_1 around 10^7 dyne·s^2·cm^{-2} (10^6 Pa·s^2) for the test at 298 K and around 10^8 dyne·s^2·cm^{-2} for the test at 325 K, are observed at a shear rate of 10^{-3} s^{-1}. It is noteworthy to point out that at very low shear rate a region of constant ψ_1 may be observed, this region not been observable for the viscosity.

5.4. Model implementation and scaling

The model described in Subsection 5.2.2 is applied to crude oil samples subjected to steady shear flows, with comparisons between experimental data and model predictions shown in Figures 5.7 and 5.8, for tests performed at 293K. The estimated values of the parameters of Eq. 5.3 are: $A = 3.98 \cdot 10^{-2}$ s^{-1}, $B = 27$ dyne·cm^{-2} (2.7 Pa), and n is 4.2. For the case of polymer solutions, the exponent $1/n$ can be correlated with the molecular weight of the suspended polymer, and values of $1/n$ around 0.25 ($n = 4$) are associated with large molecular weights [11]. The experimental values of viscosity are about a 25% greater than predictions by the rheological model, while at higher frequency the situation is inverted and experimental measurements are lower than predictions by about 11 to 20%. As can be observed in Fig. 5.8, at low shear rates the experimental shear stress is lower than model predictions; and the maximum discrepancy is of about 40%. Such discrepancy is less accentuated in plots of the logarithmic viscosity, although it is still observable (see Fig. 5.7).

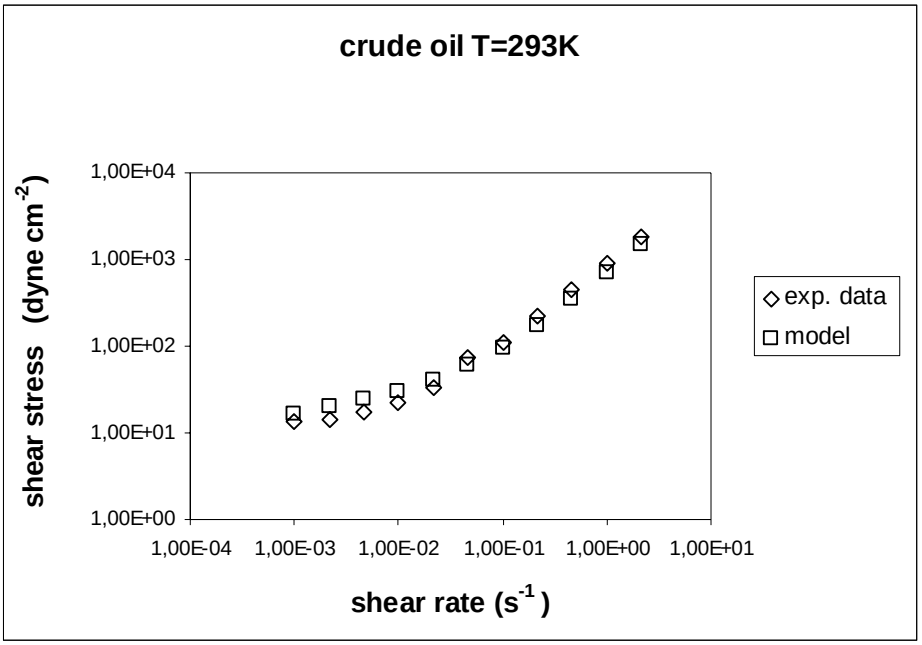

Figure 5.8. Comparison between the experimental data of shear stress at 293K of crude oil and the model predictions.

The scaling proposed in Eq. 5.11 is built considering that temperature may be an important factor, because crude oil samples show rheological properties that change enough, in a well-defined manner, with temperature at high shear rates (see Figs. 5.1 and 5.2). The Arrhenius factor obtained from the correlation of samples' data (see Fig. 5.2) suggests a simple balance of energies between the viscous work and the activation energy such as that indicated by Eq. 5.10, which, for these crude oil samples, can be reduced empirically to the following ratios for shear rate and viscosity respectively:

$$\dot{\gamma}' = \frac{\dot{\gamma}}{\dot{\gamma}_c}, \tag{5.12a}$$

and

$$\eta' = \frac{\eta}{\eta_c}. \tag{5.12b}$$

The new dimensionless variables $\dot{\gamma}'$ and η' in a logarithmic scale will represent a shift of axes and Eq. 5.3 will take the following form:

$$\eta'(II'_D) = \frac{B'}{\dot{\gamma}'}\left[\left(\frac{\dot{\gamma}'+A'}{A'}\right)^n - 1\right]^{\frac{1}{n}} = \frac{\sqrt{2}B'}{\sqrt{II'_D}}\left[\left(\frac{\sqrt{II'_D}+\sqrt{2}A'}{\sqrt{2}A'}\right)^n - 1\right]^{\frac{1}{n}}; \qquad (5.13a)$$

with

$$B' = \frac{B}{\dot{\gamma}_c \eta_c}\ , \qquad (5.13b)$$

$$A' = \frac{A}{\dot{\gamma}_c}\ , \qquad (5.13c)$$

where II'_D is the dimensionless second invariant of the shear rate tensor, $II'_D = = 2\ \dot{\gamma}'^2$. The dimensionless viscosities of samples reported in Fig. 5.1 are presented in Fig. 5.9. All curves converge to one, meaning that a particular set of dimensionless values for *A'*, *B'* and *n* describe the behavior of crude oil within the considered range of temperatures. The dimensionless viscosity of the heptadecane/eicosane mixture manifests a similar behavior (see Fig. 5.10), indicating that the shear thinning model can describe also viscous behaviors of this aliphatic mixture. At 305 K, the estimated values of the parameters of Eq. 5.3 for the alkanes' mixture are: A = 37.51 s^{-1}, B = 1.12 dyne·cm^{-2} (0.112 Pa), and n is 18. The value of A is greater than the value of B, which is the opposite situation of the case of crude oil that, at 303 K, should have values of A and B of $9.4 \cdot 10^{-2}$ s^{-1} and 19.0 dyne·cm^{-2} (1.90 Pa), respectively. This is due to the fact that the viscosity at shear rates tending to infinity ($3.0 \cdot 10^{-2}$ Poise), defined by B/A, is very low in comparison to that of crude oil (678 Poise). As expected, the $1/n$ value is four-fold lower than that of crude oil, indicating a lower average molecular weight.

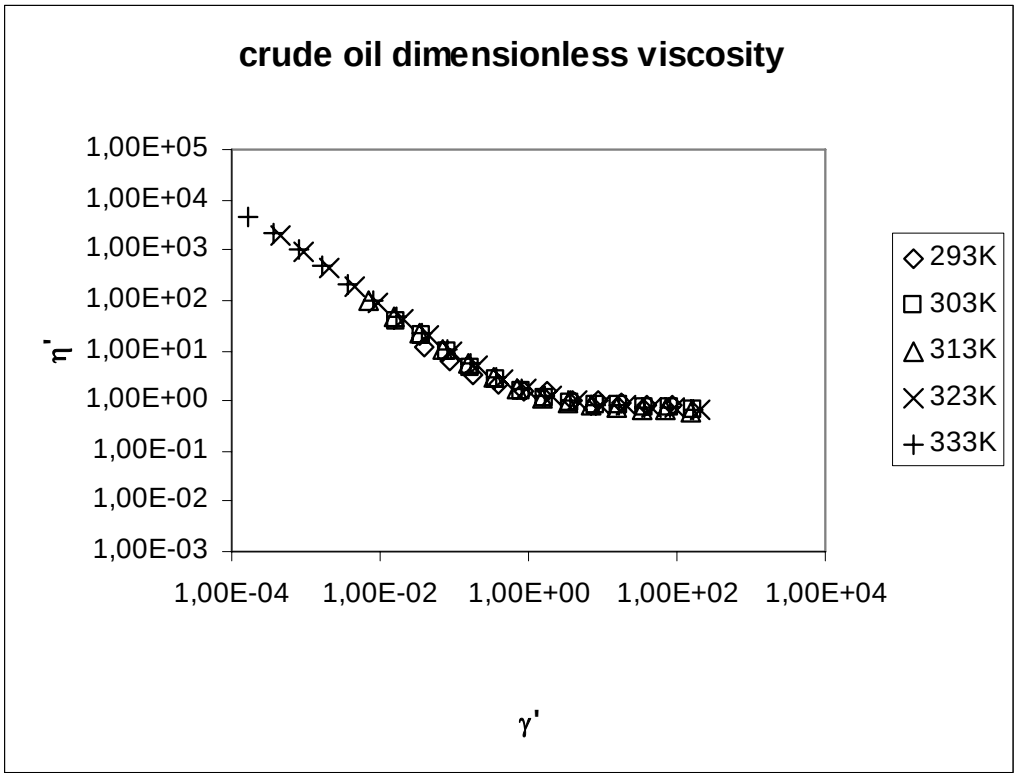

Figure 5.9. Dimensionless viscosities of crude oil at different temperatures.

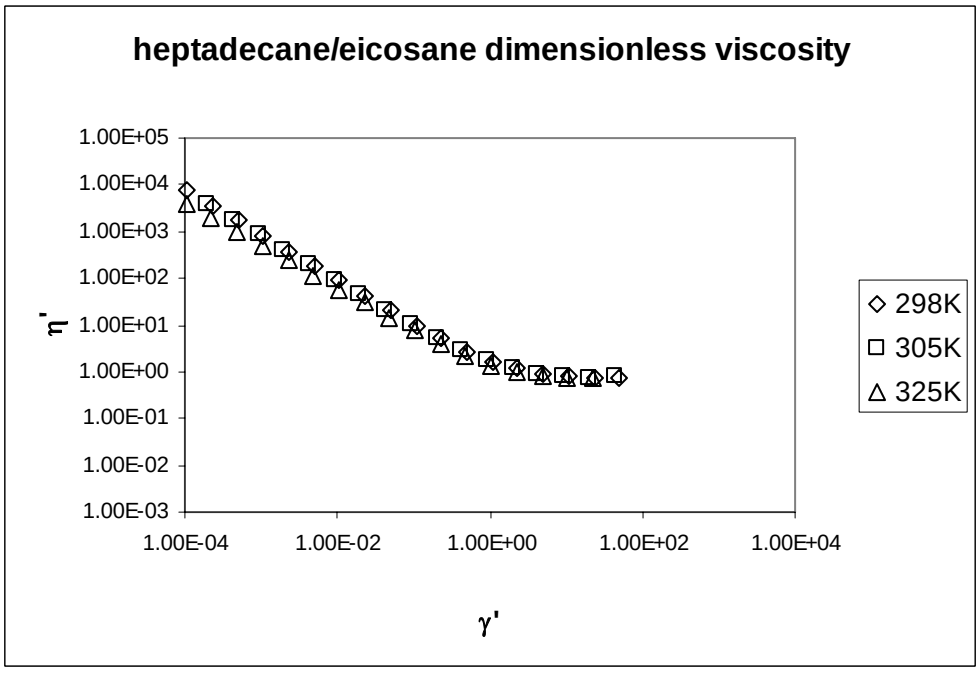

Figure 5.10. Dimensionless viscosities of the heptadeacane/eicosane mixture at different temperatures.

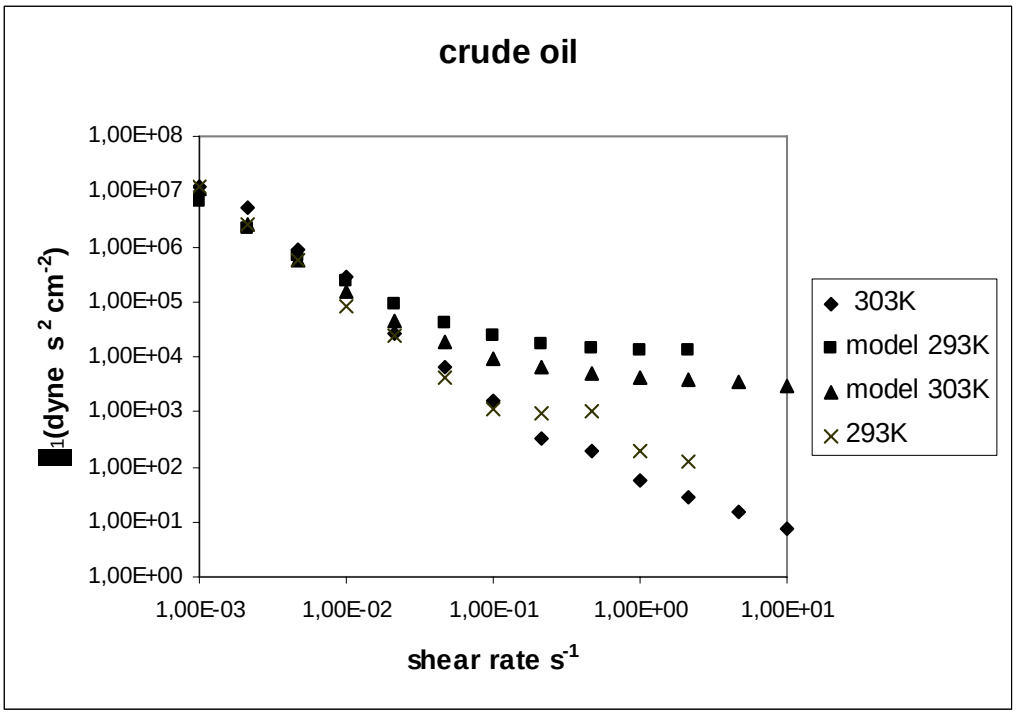

Figure 5.11. First coefficient of normal stresses of experiments at 293, 303K and the model predictions for the same temperatures.

The chosen Maxwellian viscoelastic model includes normal stresses, as indicated by Eq. 5.9, and the comparison among experimental results and model forecasts for the first normal stresses coefficient is reported in Figure 5.11 for crude oil: For this data set, the model fails with increasing shear rate, due to the variation of elastic modulus G, taken as a constant in the model. The same model applied for the mixture of heptadecane/eicosane reveals a better agreement, with the most noticeable discrepancy appearing for shear rates higher than 10 s^{-1} (see Fig. 5.12). This implies that for the alkane mixture, G is less affected by shear rate than the case of crude oil. Main features of the transient viscosity, corresponding to Eq. 5.7, are well prescribed also by this model. The comparison between model and the experimental transient viscosity is shown in Fig. 5.13 for a shear rate of 1 s^{-1} and a relaxation time, λ, of 0.067 s. The most significant difference corresponds to the initial overshoot of the experimental transient viscosity, not predicted by the model.

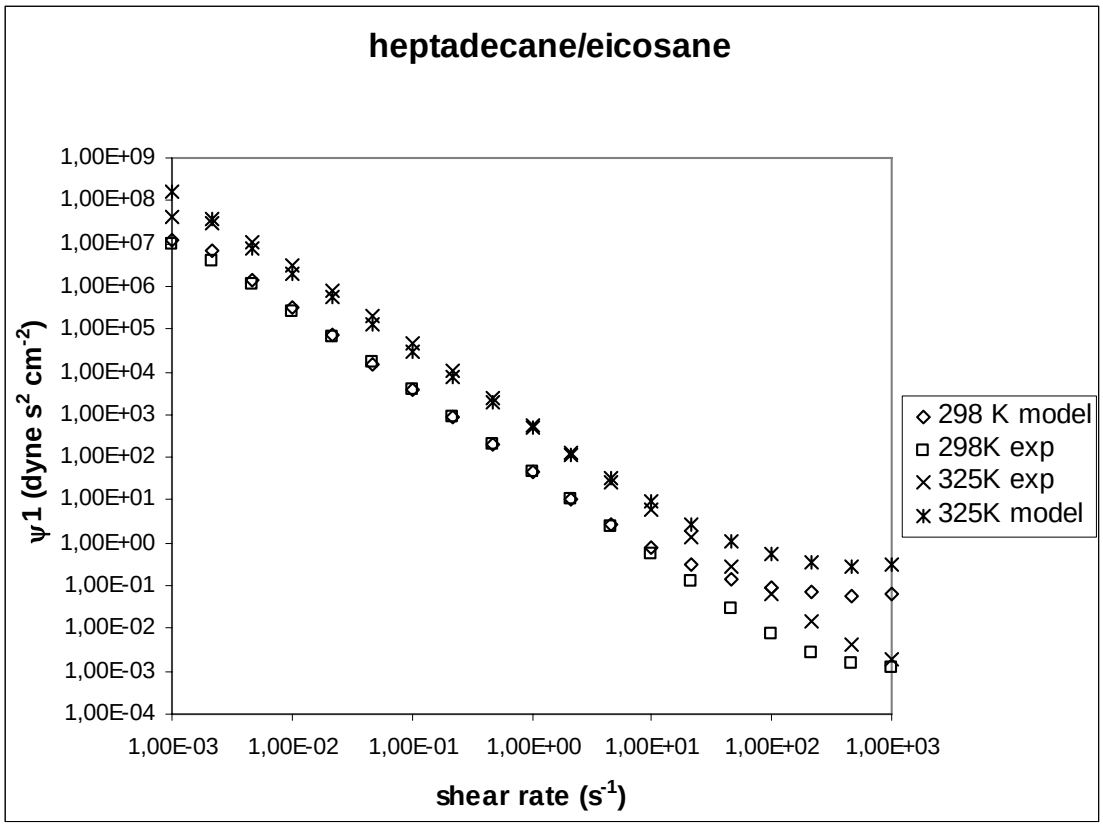

Figure 5.12. Comparison between the experimental first coefficient of normal stresses of the heptadecane/eicosane mixture and 303K and the model predictions for the same temperatures.

5.5. Discussion

It is desirable to express the observed transition phenomena in terms of dimensionless numbers. These dimensionless numbers are related to the dominant physical forces that determine the structure of the fluid. The observed transitions occur between two physical regimes, one dominated by one type of force, with the other dominated by a counterbalancing force field. For many suspension systems, dimensionless numbers represent a balance between two forces: on one hand, viscous friction force and on the other hand, attractive or Brownian forces. For suspensions of hard colloidal particles with dimensions smaller than 1 μm, competition between Brownian and hydrodynamic forces determine the flow behavior. Krieger [20] showed that the Peclet number, $Pe = \eta_s \dot{\gamma} a^3 / kT$ (η_s is the solvent viscosity, a is the particle or droplet radius, and k

the Boltzmann constant), is the appropriate scaling parameter for viscosity. For particles of larger radius (4.5 μm < a < 12 μm), Jansen *et al.* [15] proposed the depletion flow number Fl_d to scale the fluids' viscosity ($Fl_d = 4\pi\eta_s\dot{\gamma}a^2 a_m / kT\phi_m$, η_s is the solvent viscosity, a_m and ϕ_m are the micelle radius and the micelle volume fraction, respectively). In each case, there is an energy gap to overcome.

Our scaling, with the ratio $\dot{\gamma}' = \dot{\gamma}/\dot{\gamma}_c$ leads to a similar situation where a factor,

$$k' = \alpha \exp(\varepsilon / RT) = \frac{1}{\dot{\gamma}_c}, \tag{5.14}$$

scales the viscosity curves at different temperatures (with ε being the energy barrier, R is the gas constant, 8.314 J/mol K, and α is a constant with dimensions of *time*).

Based on values given by Table 5.1, for crude oil, the calculated value of k' is 40 s at 293 K and 1.68 s at 333 K. For the C17/C20 blend k' is $5.0 \cdot 10^{-2}$ s at 298 K and $2.2 \cdot 10^{-2}$ s at 325 K. The characteristic time k' of crude oil is larger than that of the alkanes' mixture at lower temperatures. This difference is reduced drastically by a small temperature increment. However, in the case of alkanes, there is not a large variation of k' with temperature as in the crude oil case. This is due to the activation energy that is greater for crude oil, but also to the factor α of Eq. 5.14. The values of α and ε can be extrapolated by linear regression of the logarithm of $\dot{\gamma}_c$ (e.g. see Fig. 5.2). The value of the ratio between k' of the crude oil and k' of the alkanes' mixture is $6.7 \cdot 10^{-5}$ for $T \to \infty$, and tends to ∞ for $T \to 0$. The value of $6.7 \cdot 10^{-5}$ corresponds to the ratio between the value of α of the crude oil and the value of α of the alkanes' mixture. This significant difference of α, which is the relaxation time at high temperature, $T \to \infty$, can be attributed to the presence in crude oil of a large variety of suspended particles which increase its elastic properties. However, at low temperature, $T \to 0$, where a solid phase should prevail, the situation is inverted, according to Eq. 5.14, and the blend has a

very lower relaxation time k' in comparison of crude oil. This is probably due to its capacity to organize itself in a crystalline phase. On the contrary, crude oil which is a heterogeneous mixture of substances with different chemical nature (from aliphatics to polyaromatics and asphaltenes) cannot solidify as a crystalline phase.

The parameter k' has dimensions of *time*, thus this characteristic time can be physically associated to the Weissenberg number mentioned in Section 5.2.4. Finally the Weissenberg number is given by

$$We = k'\dot{\gamma} = \alpha \exp(\varepsilon / RT)\dot{\gamma} = \frac{\dot{\gamma}}{\dot{\gamma}_c} = \dot{\gamma}'. \qquad (5.15)$$

The Weissenberg number expressed in Eq. 5.15 coincides with our scaling executed through Eq. 5.12a. The normalization of viscosity has been carried out with the crossing viscosity η_c which also obeys to an exponential dependence on the inverse of temperature.

The initial structure of the material (crude oil or alkanes' mixtures) is modified by the application of the shear stress, which deforms and orients microstructures (e.g. particles, large molecules, clusters, etc.) along the flow direction; these changes of structure imply the appearance of activation energies. The activation energies, ε, calculated from the linear correlation of the transitional viscosities at the critical shear rates, have values of 66.7 kJ/mol for crude oil and 24.4 kJ/mol for alkanes mixture, respectively. Considering that the same scaling and activation energies of the same magnitude order involves crude oil and alkanes, these activation energies could be related to changes in conformations of the alkanes' chains [21-23]. In the case of crude oil, the higher activation energy can be interpreted in the bigger average size of the aliphatic compounds compared with the average 17.5 carbon atoms of our alkanes' blend. The eventual contributions of dispersive energies like Van der Waals types should be low, reminding that they have values of the same magnitude of thermal

energy [24, 25]. These activation energies must be considered as a mean property (an appropriate average) of the whole set of crude oil components.

The aliphatic compounds in crude oil as well as alkanes in the blend are oriented by shear stress along the flow direction, implicating a rearrangement and deformation of the molecules or group of molecules, this rearrangement is probably one of the causes of shear thinning and normal stresses observed within Figures 5.1 – 5.6. On this point, it is noteworthy to say that in transient tests, viscosity of crude oil manifests some initial oscillations, which are usually caused by the reordering, along the flow direction, of particles, molecules and aggregates by means also of rotations due to shear flow, see Fig. 5.4. In the latter Figure, the initial shoulder (weak overshoot) is evidence of such reordering. The simple viscoelastic model prediction shows no initial overshoots; see Fig. 5.13. The combined effect of thermal energy (RT) and friction work ($\tau\dot{\gamma}$) leads to a displacement of the crossing point, defined by $\dot{\gamma}_c$ and η_c, rising test temperature, to higher shear rates, because, to overcome the energy barrier, we need higher shear rates to compensate the viscosity decrement due to thermal energy (Fig. 5.1). Consequently, at very low shear rates all viscosity curves in Fig. 5.1 tend to collapse onto a master curve, because under those conditions temperature effects are very weak, as there is mainly shear stress to overcome the activation energy barrier, which is about 20 - 30 times greater than the thermal energy [24, 25]. This behavior, at low shear rates, also suggests that the sample is in a solid-like state, and since most of the energy is used to disrupt this structure, no initial Newtonian zone is observed [26].

However, the same dimensionless parameters describe quite well crude oil and this mixture (see Figs. 5.9 and 5.10).

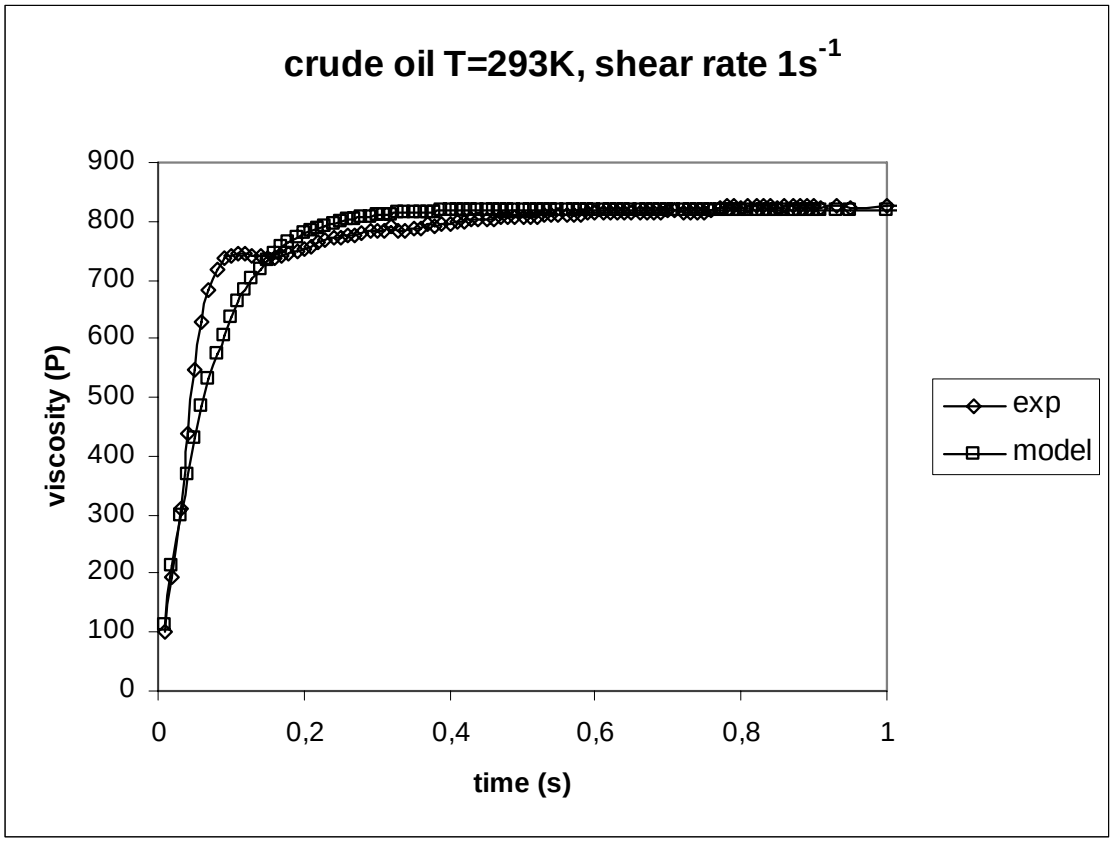

Figure 5.13. Comparison between experimental transitory viscosity of crude oil and the model predictions.

The first coefficient of the normal stresses for the case of crude oil reveals a relevant deviation from the proposed model, which begins at shear rates of about 10^{-2} s^{-1} (Fig. 5.11), The elastic modulus *G* is taken as constant in the model; a better agreement could certainly be found if *G* were given as a function of the shear rate. On the other hand, the experimental first coefficient of normal stresses ψ_1 for the C17/C20 mixture is in a good agreement with the model predictions (see Fig. 5.12), and it is possible to observe a deviation at shear rates higher than 10 s^{-1}, indicating that the elastic modulus remains almost constant up to such stresses. Based upon the presence of an initial overshoot in the experimental curve (Fig. 5.13), this observed discrepancy between the experimental and the model transient viscosities is due to rotational components not included in the model. The lower viscosity value of the overshoot in comparison with

steady state viscosity is probably due to the destruction of highly degradable structures, such as polymer networks, with slow reformation rates [27].

5.6. Conclusions

By means of the same dimensionless parameters *A'*, *B'* of the utilized model (Eqs. 5.1 – 5.4), the shear steady flow of both heptadecane/eicosane and waxy crude oil systems can be described.

The common aliphatic phase defines the main rheological viscous features. In brief, the continuous phase dominates the viscous properties. For the, non-Newtonian behavior, such as the existence of shear-thinning and normal stresses, it can be associated with rearrangement of molecules along the flow direction. The estimated activation energies, extrapolated from steady shear tests of both systems (crude oil, alkanes mixtures), are of the same magnitude order (66.7 kJ for crude oil, 24.4 kJ for heptadecane/eicosane mixture). The difference can be attributed to the fact that larger molecules or mesostructures are present in the crude oil sample than those occurring in the alkane blends, which have an average number of carbon atoms of 17.5. A greater number of carbon atoms implies greater activation energies to reorganize these macromolecular chains-structures. Nevertheless, other factors can influence the activation energy such as the presence of dispersed particles and large polyaromatic molecules. A Weissenberg number type (Eq. 5.15) is obtained by the product of the shear rate and the characteristic time constituted by the inverse of the rate constant of reordering of particles and molecules along the flow direction (Eq. 5.14). This dimensionless number, called $\dot{\gamma}'$ in graphics of Figures 5.9 and 5.10, leads towards a molecular dynamics interpretation of the main viscous properties than to a colloidal-particles-dynamics; e.g. our scaling number is quite different from numbers of Peclet number type [2]. However, the effects of colloidal particles of crude oil dominate

viscoelastic features. Finally, we can argue that appropriate mixtures of alkanes of high molecular weight can be used to simulate and reproduce steady shear flow characteristics of some classes of crude oil, such those presented in this paper; although, they have a variable composition and balance of aliphatic compounds, aromatics and asphaltenes. The latter achievement opens the possibility to find mathematical and physical models which can describe both systems in a certain range of the rheological variables. These mathematical and physical models can be used also to predict the viscous properties, for example, of oils' blends and oil-water emulsions, which have an important technological potential in the power generation field.

5.7. References

[1] Speight JG. In *The Chemistry and Technology of Petroleum*, 2nd Ed., Marcel Dekker; New York, 1991.

[2] Sjoblom J, Aske N, Auflem IH, Brandal Ø, Havre TE, Sæther Ø, Westvik A, Johnsen EE & Kallevik H. "Our current understanding of water-in-crude oil emulsions. Recent characterization techniques and high pressure performance", *Adv. Colloid Interface Sci*. 2003, **100-102**, 399.

[3] Gruse WA & Stevens DR. In *The Chemical Technology of Petroleum*, McGraw-Hill; New York, 1960.

[4] Koots JA & Speight JG. "Relation of petroleum resins to asphaltenes", *Fuel* 1975, **54** (3), 179.

[5] Onogi S, Matsumoto T & Warashina Y. "Rheological properties of dispersions of spherical particles in polymer solutions", *J. Rheology* 1973, **17**, 175.

[6] Sengun MZ & Probstein RF. "Bimodal model of suspension viscoelasticity", *J. Rheology* 1997, **41**(4), 811.

[7] Werner A, Behar F, de Hemptinne JC & Behar E. "Viscosity and phase behavior of petroleum fluids with high asphaltenes contents", *Fluid Phase Equilibria* 1998, **147**, 343.

[8] Al-Besharah JM, Salman OA & Akashah SA. "Viscosity of crude oil blends", *Ind. Eng. Chem. Res*. 1987, **26**, 2445.

[9] Schorling P-C, Kesse DG & Rahimian I. "Influence of the crude oil resin/asphaltene ratio on the stability of oil/water emulsions", *Colloids and Surfaces A* 1999, **152**, 95.

[10] El-Gamal IM & Gad EAM. “Low temperature rheological behavior of Umbarka waxy crude and influence of flow improver”, *Colloids and Surfaces A: Physicochem. Engineering Aspects* 1998, **131**, 181.

[11] Al-Zahrani SM. “A generalized rheological model for shear thinning fluids”, *Journal of Petroleum Science and Engineering* 1997, **17**, 211.

[12] Al-Zahrani SM & Al-Fariss TF. “A general model for the viscosity of waxy oils”, Chemical Engineering and Processing. 1998, **37**, 433.

[13] Oldroyd JG. “On the formulation of rheological equations of state”, *Proc. R. Soc. Lon*. 1950, **A 200**, 523.

[14] White JL & Metzner AB. “Development of constitutive equations for polymeric melts and solutions”, *Journal of applied Polymer Science* 1963, **7**, 1867.

[15] Jansen KMB, Pearson JRA & Mackley MR. “Viscosity of surfactant stabilized emulsions”, *J. Rheology* 2001, **45** (6), 1341.

[16] Pal R. “Scaling of relative viscosity of emulsions”, *J. Rheology* 1997, **41**, 141.

[17] Larson RG. In *Constitutive Equations for Polymer Melts and Solutions,* Butterworths, New York, 1988.

[18] Gupta M, Hieber CA & Wang KK. “Viscoelastic modeling of entrance flow using multimode Leonov model”, *Int. J. Numerical Methods Fluids* 1997, **24**, 493.

[19] White JL. In *Principles of Polymer Engineering Rheology*, Wiley-Interscience Publ., USA, 1990.

[20] Krieger IM. “Rheology of monodisperse lattices”, *Adv. Colloid Interface Sci*. 1972, **3**, 111.

[21] Asakura S & Oosawa F. “Interaction between particles suspended in solutions of macromolecules”, *J. Polym. Sci*. 1958, **33**, 183.

[22] Lee SH, Lee H & Pak H. "Molecular dynamics of liquid alkanes III. Thermodynamics, structural and dynamic properties of branched-chain alkanes", *Bull. Korean. Chem. Soc*. 1997, **18** (5), 501.

[23] Daivis PJ & Evans DJ & Morriss GP. "Computer simulation study of the comparative rheology of branched and linear alkanes". *J. Chem. Phys*. 1992, **97** (1), 616.

[24] Drummond CJ & Chan DYC. "Van der Waals Interactions, surface free energies and contact angles: dispersive polymers and liquids", *Langmuir* 1997, **13**, 3890.

[25] Hernández de la Torre G. "An approach to the intermolecular energy in pure liquids", *Revista Colombiana de Química* 1997, **26**(2), 35.

[26] Lapasin R., Visintin RFG, D'Antona P., Lockhart T. "Proprietà lineari e non lineari di greggi cerosi", *Atti VIII Convegno della Società Italiana di Reologia*, Sant'Angelo di Ischia, Italy, 2004.

[27] Rincón E, Chávez AE, Herrera R & Manero O. "Rheological modelling of complex fluids: A transient network model with microstates". *J. Non-Newtonian Fluid Mech*. 2005, **131,** 64.

Chapter 6.

Adam-Gibbs theory adapted to a unifying rheological model of crude oil and alkanes

Abstract

The knowledge of the viscous properties of crude oils is limited by the complexity and variability of the raw material. However, a Weissenberg number, defined by the product of the shear rate and the characteristic time of the considered system, allows us to scale viscosities of both crude oil and mixtures of alkanes, at different temperatures. The characteristic time has its origins in the reorientation of oligomeric chains of alkanes along the flow direction. This reorientation has associated an activation energy, which, according to a model inspired to the Adam-Gibbs theory, would allow us to associate this activation energy with changes in the configurational entropy.

6.1. Introduction

Crude oil is a complex mixture of several, equally complex, hydrocarbon components; it exhibits the typical rheology of a non-Newtonian fluid with shear thinning and normal stresses [1-10]. Through an Arrhenius factor, viscosity curves of crude oils can be scaled, and a general similarity and analogy may be found with much simpler *alkanes* of long hydrocarbon chains (17 – 20 carbon atoms). This was the main objective of Chapter 5. However, no physical relevant explanation was found for the Weissenberg number proposed besides the existence of an order – disorder transition, and that each state or phase transformation is coupled with an activation energy. Here it is proposed that the shear thinning observed is associated to a phase with a weak degree of order aligned with the flow direction, i. e., along the direction of strained polymer and oligomer chains. Usually, the relaxation time −obtained as the inverse of the shear rate at the onset

of zero shear rate viscosity– is used to scale viscosities in the shear thinning region [11]. In this work, the relaxation time is the inverse of the shear rate at the *onset of the end of the shear thinning* region, concerning to a transition from one ordered region, where oligomers' chains should be more packed and oriented, to a more disordered Newtonian region. From this point, there is the connection with the Adam-Gibbs theory which deals with the relaxation times involved in phase transitions, such as glass transition of polymers, from a more packed arrangement of chains with low configurational entropy to new arrangements with higher configurational entropy. The configurational entropy consists of all possible manners in which objects, such as oligomer chains, can be arranged and packed in the available space, strictly correlated with the conformations that oligomer chains can perform. The core of this Chapter is the use of the Adam-Gibbs theory [12] to correlate the Arrhenius factor, which is part of the characteristic time of the Weissenberg number, with the conformational changes observed in the aliphatic chains. In this Chapter, thermodynamics will provide the bridge between the macroscopic rheological behavior and the microscopic changes of conformation of molecules, specifically the case of crude oil samples of the Mexican reservoir of Cantarell and the blend of *n*-heptadecane (C17) and *n*-eicosane (C20) are here considered.

6.2.Adaptation of the Adam-Gibbs theory to the viscoelasticity of alkanes

The expression of an Arrhenius factor in order to describe the behavior of viscosity with temperature is present in several theories such as the Adam-Gibbs [12-13] theory and in several modified expressions of the WLF equation [14]; moreover it is present in phenomenological equations which relate viscosity and temperature [14]. The Adam-Gibbs theory was first used to describe the viscoelastic properties of polymers in the vicinity of the glass transition range [12]. Nevertheless, it is also working above 100 °C

of the transition temperature. These theories provide the suitable frameworks to express the presence of an activation energy when occurs a transformation, which involves several molecules or several unit segments either of a oligomer or a polymer. These models are ascribable to the equations 5.14 and 5.15, as exposed in the Chapter 5, about the activation energy found in steady viscous flow. On the contrary, bead-spring models work adequately for dilute solutions [15], but will fail in the complex case of crude oil or alkanes mixtures, where the components are strongly interacting.

The proposed adaptation of the Adam-Gibbs theory relates the temperature dependence of the relaxation processes to the temperature dependence of the size of a blob, which is defined as a volume large enough to allow cooperative rearrangement to take place, without affecting neighboring regions [12, 13]. This cooperatively rearranging region is large enough to allow a transition to a new configuration; hence, it is determined by the average size of chain conformations and by definition will equal the sample size at the temperature of solidification of the substance. In the case of suspensions under shear flow, the transition induced by shear stress will be from a disordered arrangement -typical of liquids- to a more ordered arrangement, which will be similar in a certain way to a liquid crystal order. This transition is reflected by the viscous shear thinning range up to reach the Newtonian behavior, with the limiting shear rate $\dot{\gamma}_c$, in which this transition is complete. Then another "disordered" region begins with the Newtonian region. The transition frequency of such a cooperative rearrangement is then calculated as a function of this subsystem size, to be:

$$f(T) = A_T^{'} \exp(-z^* \Delta\mu / RT); \tag{6.1}$$

where $\Delta\mu$ is the transition state activation energy, $A_T^{'}$ is the frequency factor, whose temperature dependence is usually weak and assumed to have a quasi-constant value [12], Each blob contains z^* unit segments of oligomers or polymer sample that is

described as an ensemble of quasi-independent cooperative regions, or subsystems. T is the absolute temperature, and R the universal gas constant.

The characteristic relaxation time will be:

$$k(T) = A_T \exp(z^* \Delta\mu / RT), \tag{6.2}$$

where A_T is the relaxation time at temperature T, which varies with temperature; e. g., when structure properties are varying or a phase transition occurs. The temperature dependence of z^* is determined by the macroscopic configurational entropy $S_c(T)$:

$$z^* = \frac{N_A s_c^*}{S_c(T)}; \tag{6.3}$$

where N_A is the Avogadro's number, s_c^* is the configurational entropy of the smallest number of rearranging molecular entities. Combining Equations 6.2 and 6.3, the following equation is obtained:

$$k(T) = A_T \exp\left(\frac{N_A s_c^* \Delta\mu}{S_c(T) RT}\right). \tag{6.4}$$

$S_c(T)$ can be extrapolated by means of the empirical equation for the heat capacity proposed by Van Miltenburg [16] for alkanes, and is given by:

$$S_c(T) = \int_{T_o}^{T} \frac{\Delta C_p}{T} dT = \frac{(n-1)}{C_0} \int_{T_o}^{T} \left(\frac{b}{T} + c\right) dT = \frac{(n-1)}{C_0} \left[b \ln \frac{T}{T_0} + c(T - T_0) \right]; \tag{6.5.a}$$

$$C_o = b(3-1) + c(3-1)T_0 = 2(b + cT_0). \tag{6.5.b}$$

In Eq. 6.5.b, the term ΔC_p is only the configurational term of heat capacity, depending on the number n of carbon atoms of the alkane chain, b and c are constants, C_o is the configurational heat capacity for a polymer segment of 3 carbon atoms, at the reference melting temperature T_0 of the considered alkane; b and c are constants and according to the equations developed by Van Miltenburg for linear alkanes, the values of

b and c are 13.990 J K^{-1} and 0.0543 J K^{-1} [16], respectively. The configurational entropy of the corresponding smallest unit, as usually done for polymers [12], was taken:

$$s_c = K_B \ln 2^3; \tag{6.6}$$

where K_B is the Boltzmann's constant, and the exponent 3 [12] corresponds to the small polymer segment considered, because it has been demonstrated that this choice shows better results for polymers. Thus z^* is:

$$z^* = \frac{N_A s_c}{S_c(T)} = \frac{R \ln 2^3}{\frac{(n-1)}{C_0}\left[b \ln \frac{T}{T_0} + c(T - T_0) \right]}. \tag{6.7}$$

Eq. 6.7 is valid only for $n \geq 3$; on the contrary, we have not the 3 conformations required by Eq. 6.6.

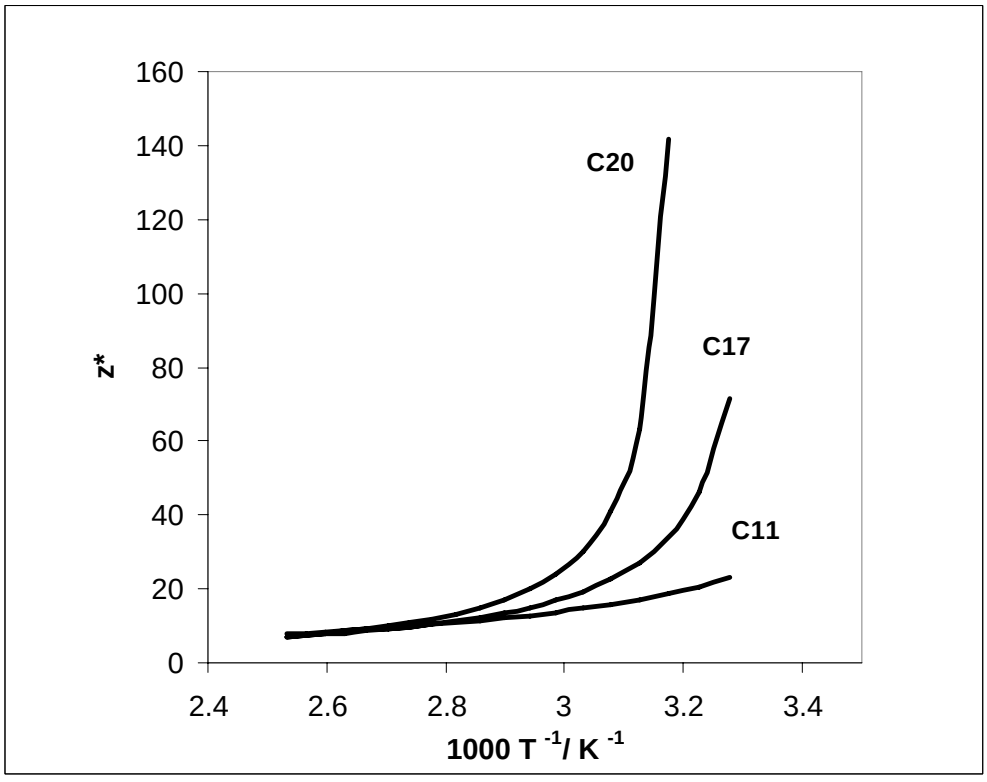

Figure 6.1. Dependence of z^* curves versus temperature for C11, C17 and C20.

In Figure 6.1, the variation of z^* with the inverse of the temperature T (1000/T) is shown, for C17, C20, and for *n*-undecane (C11) (in order to show the z^* trend with the

variation of carbon atoms), as calculated from the equation set Eqs. 6.1. – 6.7. It is possible to observe that z^* of C20 is higher than the others, and z^* of C17 is higher than that of C11. Approaching the melting temperature, which corresponds to the value of 310.6 K (1000/T = 3.2 K^{-1}) for C20, the z^* value increases asymptotically. However, at high temperatures (low $1/T$) their z^* values are very similar.

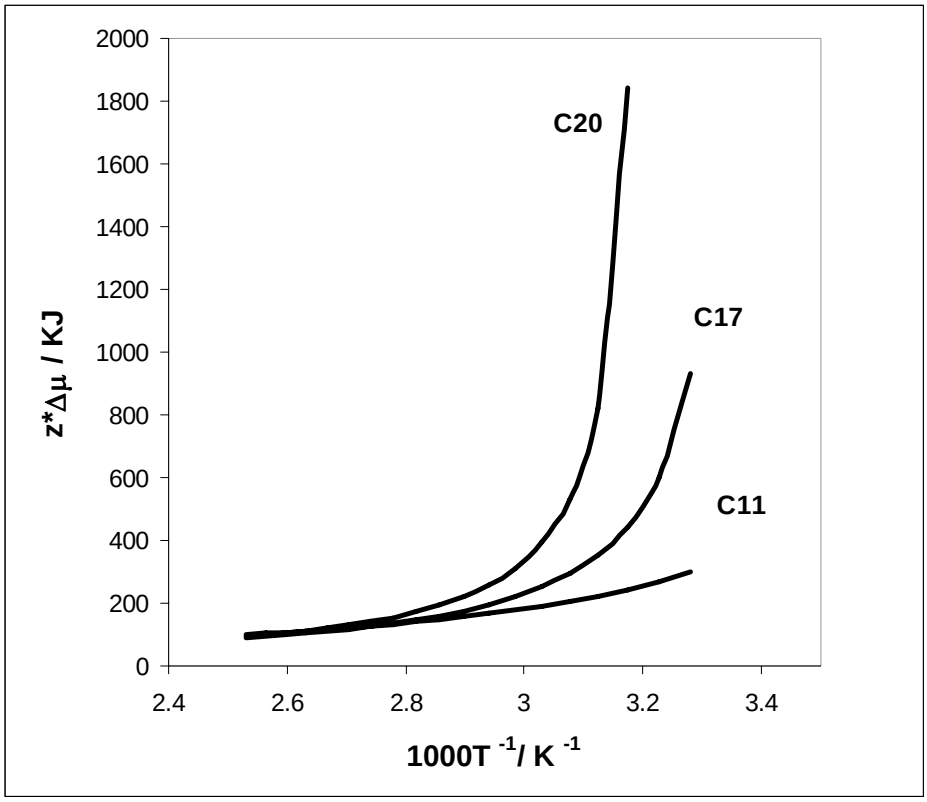

Figure 6.2. Activation energy vs. $1000T^{-1}$ for C11, C17 and C20. The three activation energies tend to be similar at high T.

Figure 6.2 presents the variation of the term $z^*\Delta\mu$, where the trend is similar to that of Fig. 6.1. Here $\Delta\mu$ was taken 13 kJ mol^{-1}[17], which corresponds to the approximated value of the rotational barrier around a C-C bond, from a stable conformation to another one (*GT* transitions). The same values of Fig. 6.2 are reported in Fig. 6.3, but in a logarithmic scale evidencing that C11 at high temperature exhibits a

higher $z^*\Delta\mu$ than C17 and C20, according to Eq. 6.7, and due to the high $S_c(T)$ of alkanes with long chains.

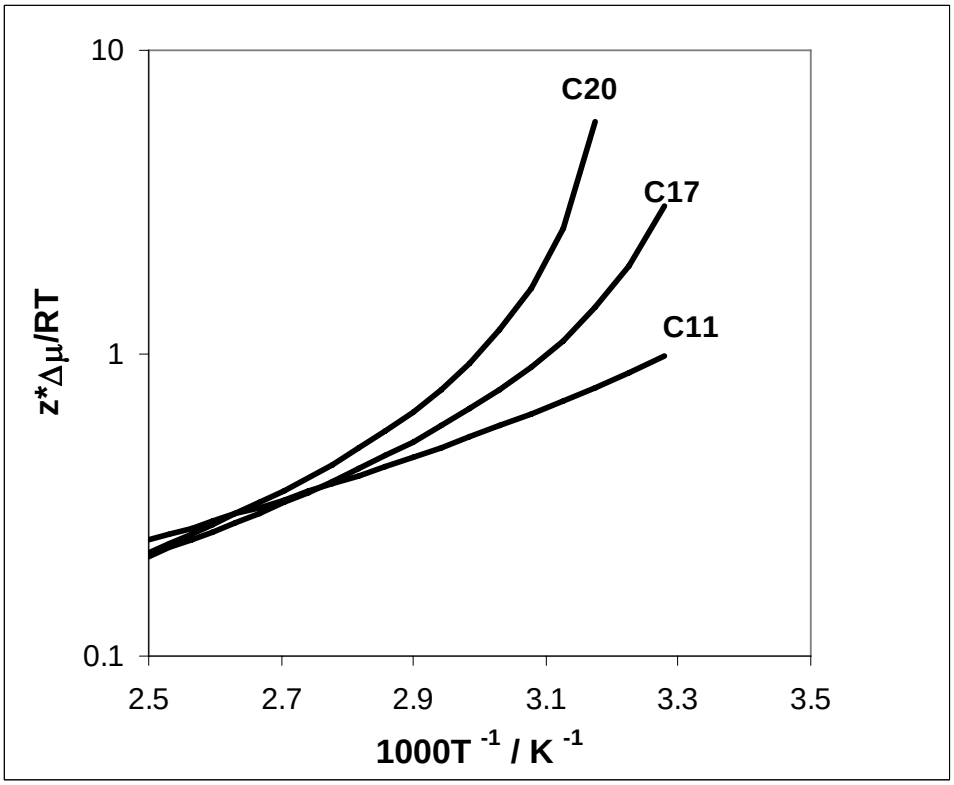

Figure 6.3. Arrhenius factor vs 1000 T^{-1} for C11, C17 and C20 in logarithmic scale. It is possible to observe that at high T, the Arrhenius factor of C11 is higher than those of C17 and C20.

6.3. Adam-Gibbs-like theory applied to crude oil and blends of alkanes

In the case of crude oil, where a distribution of alkanes with different numbers of carbon atoms n is present, the calculation of z* of the mixture is defined as the average $\langle z^* \rangle$ corresponding to the given distribution (molar fraction) of alkanes $X(n)$:

$$\langle z^* \rangle = \sum_{n=1}^{n_{\max}} z^*(n) X(n) \approx \int_1^{\infty} z^*(n-1) X(n-1) dn \,, \tag{6.8.a}$$

$$\int_1^{\infty} X(n-1) dn = 1 \,, \tag{6.8.b}$$

where, in Eqs. 6.8.a and 6.8.b, $X(n\text{-}1)$ substitutes $X(n)$ to simplify the calculations, and $z^*(n)$ is the z* of the alkane with n carbon atoms. Assuming now a Poisson distribution of alkanes in the complex mixture of real oil, the following expression can be used:

$$X(n-1) = \lambda^2 (n-1) \exp\left[-\lambda(n-1)\right], \tag{6.9}$$

which satisfies Eqs. 6.8.a and 6.8.b, and λ is the frequency factor [18]. It is easy to show that the average $\langle z^* \rangle$ is given by:

$$\langle z^* \rangle = \int_1^\infty X(n-1) \frac{N_A s_c^*}{S_c(T)} dn = \int_1^\infty \frac{\lambda^2 (n-1) \exp\left[-\lambda(n-1)\right] R \ln 2^3}{\frac{(n-1)}{\xi_o}\left[b \ln \frac{T}{\theta_0} + c\left(T - \theta_0\right)\right]} dn$$
$$= \frac{\lambda R \ln 2^3}{\frac{b}{\xi_0} \ln \frac{T}{\theta_0} + \frac{c}{\xi_0}\left(T - \theta_0\right)} \tag{6.10}$$

Equation 6.10 implies that $\langle z^* \rangle$ depends on three parameters, λ, ξ_o and θ_o. The factor λ corresponds to the exponential frequency factor of Eq. 6.9; the inverse of λ being $N - 1$, the maximum n - 1 of the proposed Poisson distribution (Eq. 6.9):

$$N - 1 = \frac{1}{\lambda}. \tag{6.11.a}$$

Thus Equation 6.10 can be re-written in a form similar enough to Eq. 6.7 but with the explicit linkage between the average z*, $\langle z^* \rangle$, with maximum n-1, N-1.

$$\langle z^* \rangle = \frac{R \ln 2^3}{\frac{(N-1)}{\xi_0}\left[b \ln \frac{T}{\theta_0} + c\left(T - \theta_0\right)\right]}. \tag{6.11.b}$$

The parameter ξ_0 correspond to C_0 (Eq. 6.5.b) calculated for the temperature θ_0. Otherwise, θ_0 is a parameter substituting the melting temperature.

In Equation 6.10, the physical significance of melting temperature of a pure compound can not be associated to θ_0, and is given by the substitution of n - 1 with N - 1 in the following equation [19]:

$$T_{0n} = 1635.5 + 2971(n-1)^{0.1428} - 4460(n-2)^{0.05842} - 236.7(n-3)^{0.3554} - 0.01762(n-4)^{2.727} + 16.11\left\{\frac{(n-1)n(n+1)}{6}\left[\frac{\Gamma(n+1)}{2\Gamma(n-1)}\right]^{-1}\right\}^{1.047}, \quad (6.12)$$

where T_{0n} is the melting of the pure alkane with n carbon atoms. Equation 6.12 [19] predicts the values of the melting temperatures of normal alkanes with n carbon atoms in the range of 8 to 25.

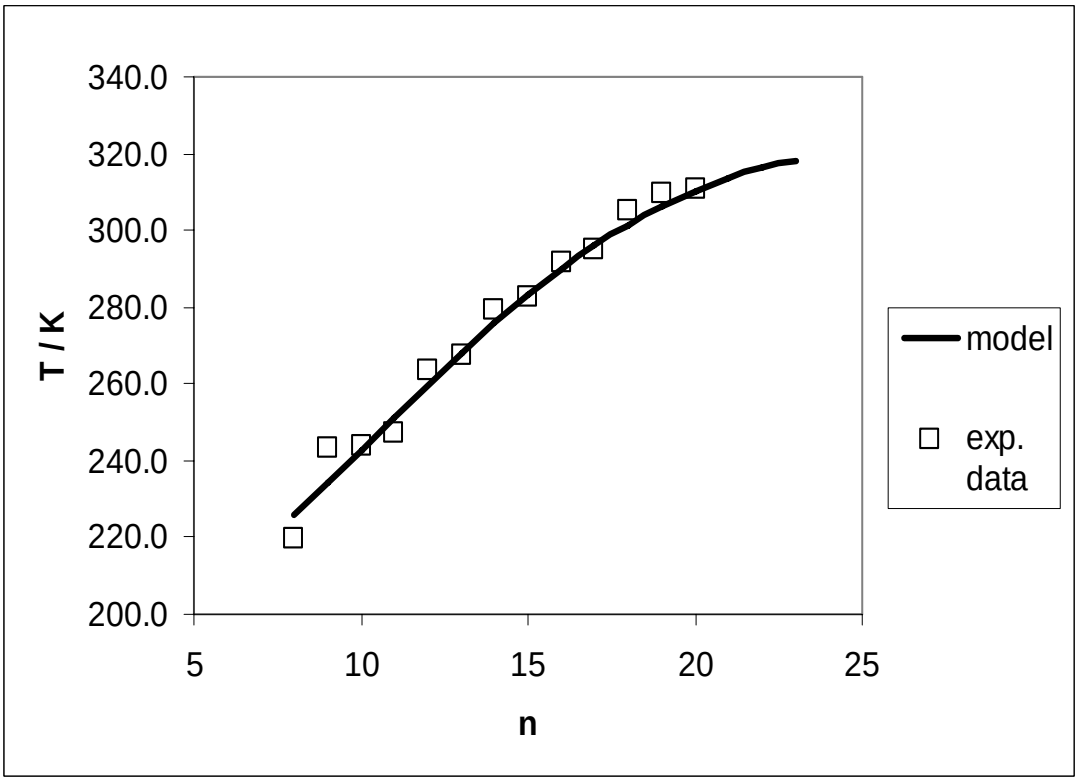

Figure 6.4. Melting temperatures of n-alkanes. Solid curve: model prediction. Boxes: experimental values [16, 19].

In Fig. 6.4, it is shown the predictive capacity of this Equation. The gamma function Γ is used to avoid the use of the factorial function, because, if calculated by Eq. 6.11.a, n or N - 1 are not generally integer values. Moreover, Eq. 6.12 is derived from the model proposed by Burch and Whitehead [19], which is a suitable model to predict the melting points of both pure linear and branched alkanes.

If a physical meaning can be attributed to the temperature θ_0 , although it is here proposed as the melting temperature of alkanes with *N* carbon atoms, it can not correspond to the melting temperature of a pure compound, but more probably to a transition temperature of a mixture of several compounds, with a behavior due to the prevailing excess alkane. Probably, this excess alkane contributes significantly to the interlocking lattice of wax crystals of the crude.

It is noteworthy to point out that the average number of the cooperative regions $\langle z^* \rangle$ does not depend on the average of *n* - 1, $\langle n-1 \rangle$, but on *n* -1, corresponding to the maximum fraction, *N*-1, because the average is exactly the double of the maximum:

$$\langle n-1 \rangle = \frac{2}{\lambda}. \tag{6.13}$$

This fact confirms the idea that the excess alkane, with *N* carbon atoms, should be involved in building of wax networks [20] and its melting should weaken this structure.

6.4. General rheological model for shear thinning fluids applied to alkanes and crude oils

The model adopted for both the crude oil and alkanes for shear thinning behavior is the same described in detail and proposed by Al-Zahrani [21]: a three parameters equation of *power-law* type,

$$\eta(\dot{\gamma}) = B\left[\left(\frac{\dot{\gamma}+A}{\dot{\gamma}A}\right)^p - \frac{1}{\dot{\gamma}^p}\right]^{\frac{1}{p}}. \tag{6.14}$$

where $\dot{\gamma}$ is the shear rate, *A* has dimensions of shear rate and *B* of stress, the ratio *B/A* is the viscosity at shear rates tending to infinity and *p* is an exponent, which is related to molecular weight. In the Table 6.1 the values of *A*, *B* and *p* are reported for both the considered oil and an *n*-heptadecane/*n*-eicosane mixture. The specimens of the

considered crude oil are from a sample of the Cantarell reservoir. It is noteworthy that the same model works adequately for mixtures of alkanes and the considered oil. The same cone-plate geometry was used for all the tests with an angle of 0.04 radians and a plate radius of 50 mm.

Table 6.1. Values of *A* and *B* for crude oil and the C17/C20 mixture.

	A (s^{-1})	*B* (dyne cm^{-2})	*p*
Crude oil	$3.98 * 10^{-2}$	29	4.2
C17 / C20 mixture	37.51	1.12	18

Previous research demonstrated that a Weissenberg number [21- 25] scales the shear rate at different temperature for the crude oil considered as well as mixtures of alkanes.

This Weissenberg number was so defined:

$$We = k'\dot{\gamma} = k_0 \exp(\varepsilon / RT)\dot{\gamma} = \frac{\dot{\gamma}}{\dot{\gamma}_c} = \dot{\gamma}', \tag{6.15}$$

where *k'* and k_0 are constants with dimensions of time, and ε is the activation energy. Moreover, $\dot{\gamma}_c$ and η_c are defined as the critical shear rate and the critical viscosity respectively, i.e. shear rate and viscosity, which correspond to the crossing point of the straight line extrapolated by the linear shear thinning region with the straight line extrapolated by the Newtonian region. On the other hand, the viscosity is scaled by the inverse of critical viscosity η_c:

$$\eta' = h'\eta = h_0 \exp(-\varepsilon / RT)\eta = \frac{\eta}{\eta_c} = \eta', \tag{6.16}$$

Since Eqs. 6.15 and 6.16 have a very similar form to Eqs. 6.1 and 6.2., the activation energy ε can be interpreted in this form:

$$\varepsilon = z^* \Delta\mu \tag{6.17}$$

Nevertheless, in this form ε is not a constant, implying also that h_0 and k_0 are not constant as well. The main theoretical difficulty in using Eq. 6.16 in the context of the Adam-Gibbs-like theory is due to the uncertainties associated to k_0 and h_0. However, this obstacle can be overcome by utilizing the model of Eq. 6.14 for a specific temperature as a starting and reference point.

At the selected temperature, e. g., T_1 = 293 K, we can use Eq. 6.15 and obtain $\dot{\gamma}'$ through $\dot{\gamma}_c$. From this equation, $\dot{\gamma}'$ defines the dimensionless shear rate at different temperature. At the temperature T_2, the following equations are valid:

$$\dot{\gamma}' = A_{T_2} \exp(z^* \Delta\mu / RT_2)\dot{\gamma}_{T_2} = \frac{\dot{\gamma}_{T_1}}{\dot{\gamma}_{cT_1}}, \tag{6.18}$$

$$\dot{\gamma}_{T_2} = \dot{\gamma}_{T_1}\left(\frac{A'_{T_2}}{\dot{\gamma}_{cT_1}}\right)\exp(-z^* \Delta\mu / RT_2). \tag{6.19}$$

This implies that $A'_{T_2}/\dot{\gamma}_{cT_1}$ is the parameter used to fit experimental viscosity curves.

The viscosity at the temperature T_2 can be evaluated in the following way:

$$\eta_{T_2} = \eta_{T_1}\left(\frac{\sigma_{cT_1} A_{T_2}}{\eta_{cT_1}}\right)\exp(z^* \Delta\mu / RT_2) = \eta_{T_1}\left(\dot{\gamma}_{cT_1} A_{T_2}\right)\exp(z^* \Delta\mu / RT_2). \tag{6.20}$$

Here σ_{cT_1} is the critical shear stress at T_1. In this case the parameter is $\dot{\gamma}_{cT_1} A_{T_2}$, and it is noteworthy to observe that:

$$\dot{\gamma}_{cT_1} A_{T_2} = \left(\frac{A'_{T_2}}{\dot{\gamma}_{cT_1}}\right)^{-1}; \tag{6.21}$$

which implies that

$$\eta_{T_2}\dot{\gamma}_{T_2} = \eta_{T_1}\dot{\gamma}_{T_1} \tag{6.22}$$

and closes the loop leading us to the well known equation for the viscosity function:

$$\eta(\dot{\gamma}) = \frac{\sigma(\dot{\gamma})}{\dot{\gamma}}. \tag{6.23}$$

Finally, we remind that:

$$h_0 = \frac{1}{A_T \sigma_{cT}}, \tag{6.24.a}$$

$$k_0 = A_T \ . \tag{6.24.b}$$

In Eqs. 6.24.a and 6.24.b, the idea that both k_0 and h_0 are not constant is expressed. The strategy displayed by Eqs. 6.15 – 6.21 permits the calculation of the viscosity curves of the mentioned oil and the mixture of alkanes.

6.5. Application of the model to a mixture of *n*-heptadecane and *n*-eicosane

In an artificial binary mixture of alkanes the molar fractions are known and it is not necessary to suppose the kind of distribution, as in the general case of a crude oil sample.

In this case, the molar fractions of heptadecane and eicosane were:

$$\begin{aligned} X(17) &= 0.84 \\ X(20) &= 1 - X(17) = 0.16 \end{aligned} \ . \tag{6.25}$$

If the assertions of Section 6.3 are valid, which imply that the behavior of the component with maximum molar fraction prevails, the melting temperature of the *n*-heptadecane, taken as 295.9 K and calculated by Eq. 6.12, has the value of θ_o in Eq. 6.10. In this case, the average n is 17.6 not far from the maximum 17, but would imply a melting temperature of 305.8 K, utilizing Eq. 6.12.

Differential Scanning Calorimetry (DSC) was carried out using a calorimeter of TA instruments, Model 2910. The DSC curves of the mixture, of pure heptadecane

(C17), and of pure eicosane (C20) are shown in Fig. 6.5. The melting temperature of the rotator phase of C17 is 295.4K (295.9 K, calculated by Eq. 6.12) and the melting

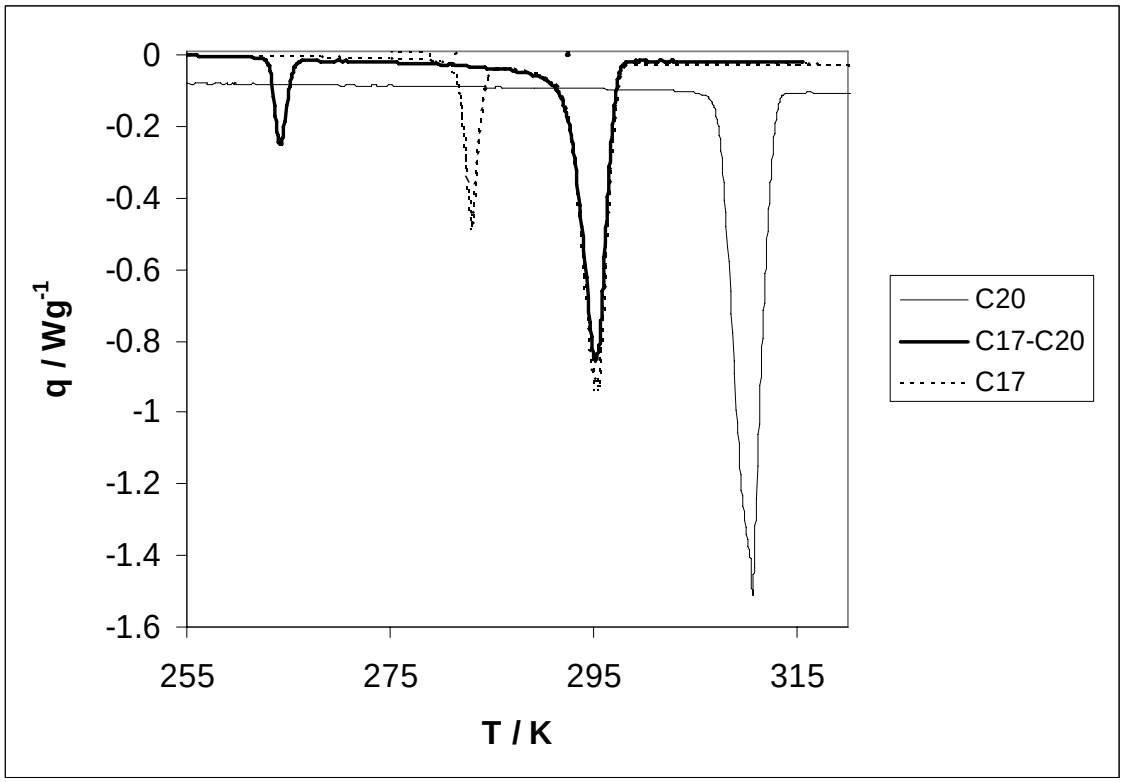

Figure 6.5. DSC curves for C20, C17-C20 mixture and C17 (positive sign is assigned to exothermic values).

point for the triclinic phase of C20 is 310.6 K, as extrapolated from these data. Otherwise, the value calculated from Eq. 12.6 is 310.3 K for C20. The experimental data and the Eq. 6.12 model show good agreement. The transition temperature for the mixture is 295.5 K, very closed to the melting point of the pure C17. In the mixture, the peak of the solid-solid phase transition present in pure C17 is shifted from 283 K to 264K (Fig. 6.5). The melting heat is 73.3 kJ mol^{-1} for C20, 43.9 kJ mol^{-1} for C17, and 38.7 KJ mol^{-1} for the mixture. These results confirm that the transition temperature of the mixture is very close to that of C17 [26].

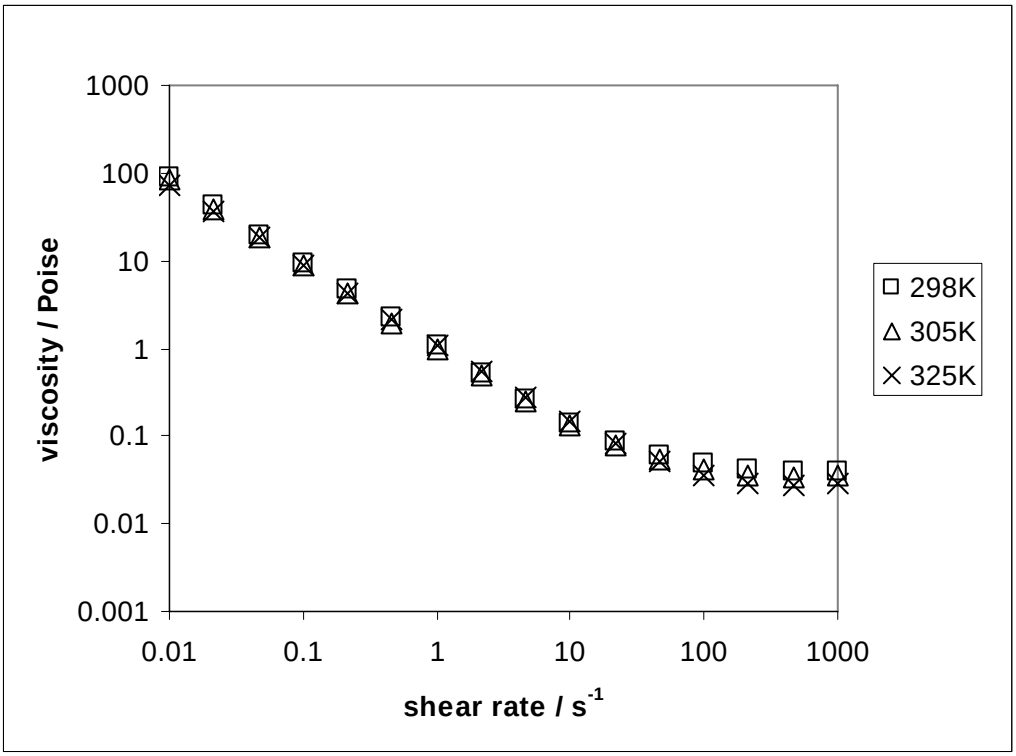

Figure 6.6. Viscosity curves of the C17/C20 mixture at different temperature: 298 K, 305 K and 325 K.

In Fig. 6.6, the viscosities curves of the mixture are shown at three different temperatures [22]. It is possible to reproduce these curves applying the considerations of Section 4.6, supposing that the experimental results are determined by the prevailing C17 behavior, as settled by Eq. 6.10. The results are exposed in Fig. 6.7a. The agreement between model predictions and experimental results is good, as shown in Fig. 6.7b, at 305 K. In order to fit the experimental curves, the parameter A_T has to vary with temperature. However, the effect of temperature on the viscosity curves is low, due to the combination of low z^* and the low variation of the relaxation time A_T of this mixture (between 1 - 8 s) in the considered range of temperature 298 K – 325 K.

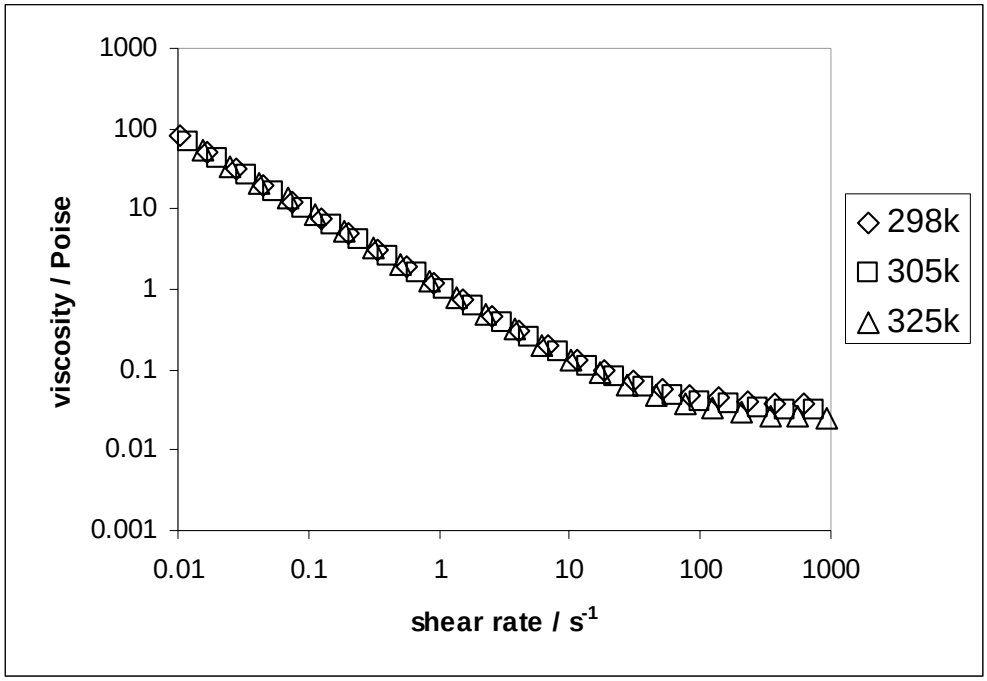

Figure 6.7a. Model predictions of the viscosity curves of the C17/C20 mixture at different temperature: 298 K, 305 K and 325 K.

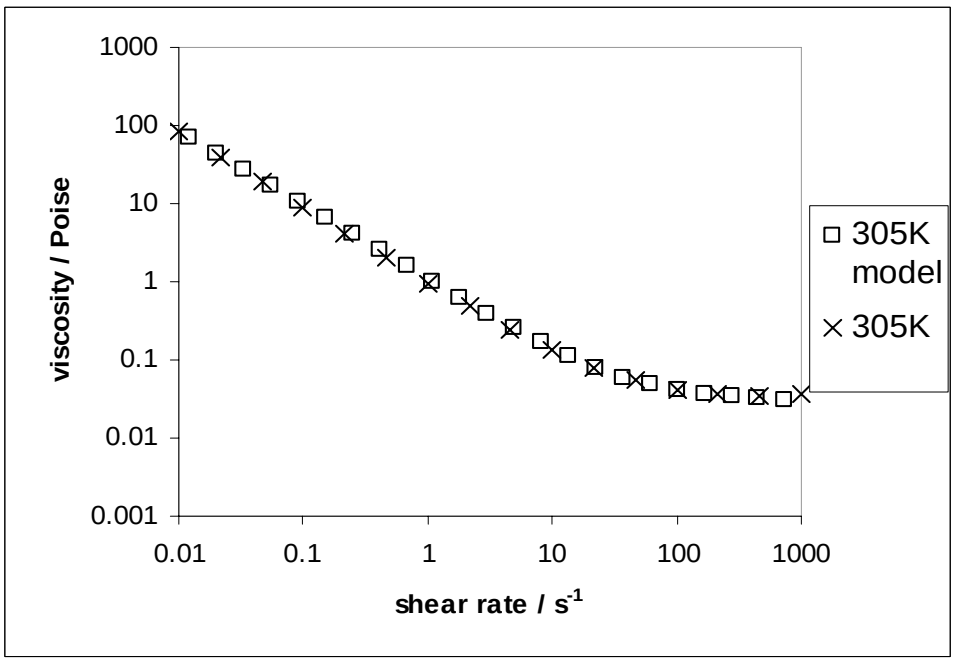

Figure 6.7b. Comparison between the viscosity obtained by model prediction at 305 K, and the experimental viscosity of the C17/C20 mixture at the same temperature.

Indeed, the viscosity at 464 s^{-1} passes from 3.9 $\cdot 10^{-2}$ Poise at 298 K to 2.6 $\cdot 10^{-2}$ Poise at 325 K (Fig. 6.6). Moreover, the viscosity curves tend to be very similar at low shear rates. At high shear rates, where the effect of the temperature should be stronger; however, the decay of the viscosity in not very pronounced (Fig. 6.6).

6.6. Application of the model to the crude oil sample

The DSC analysis of the crude oil sample has not shown a specific transition of the first order that can be associated to any kind of phase change of paraffins (Fig. 6.8), phenomenon that sometimes is observed within the range of temperature of 290 K - 320 K [18]. The viscosity curves are reported in Fig. 6.9. In this case, the effect of the temperature is stronger than in the alkanes' case, as it can be inferred by the huge decay of viscosity at the shear rate of 2.15 s^{-1}: from 860 Poise at 293 K to 29 Poise at 333K .

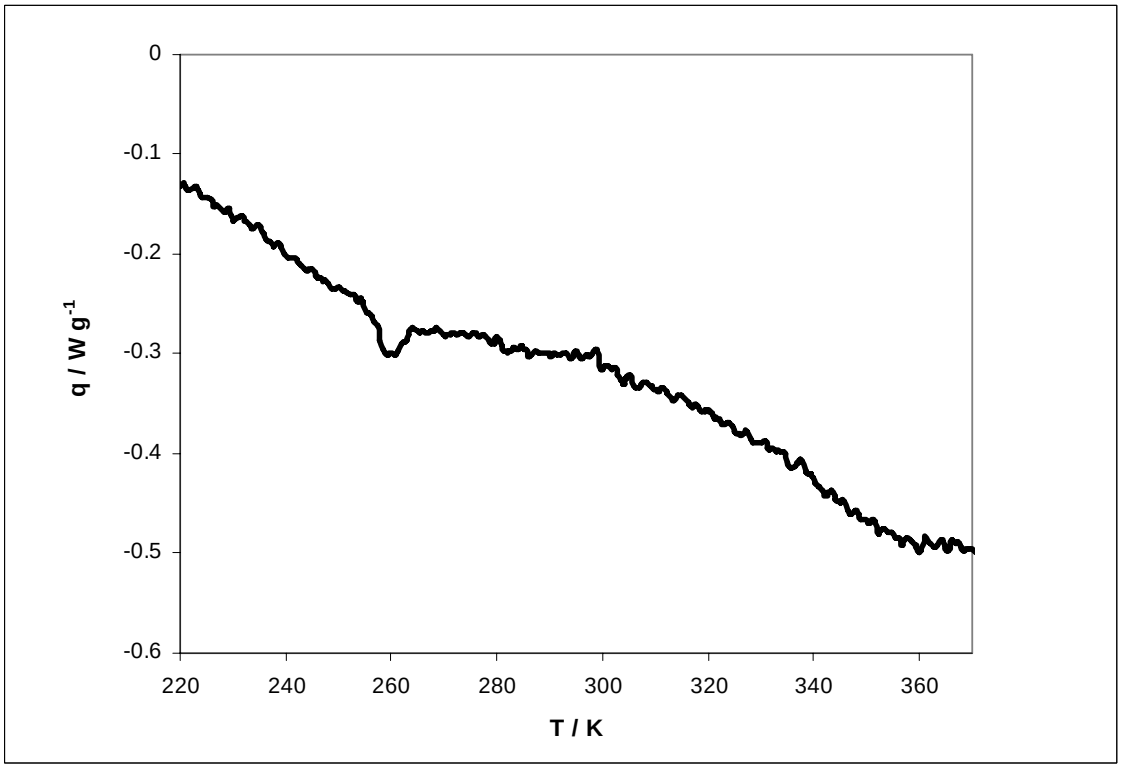

Figure 6.8. Crude oil DSC curve.

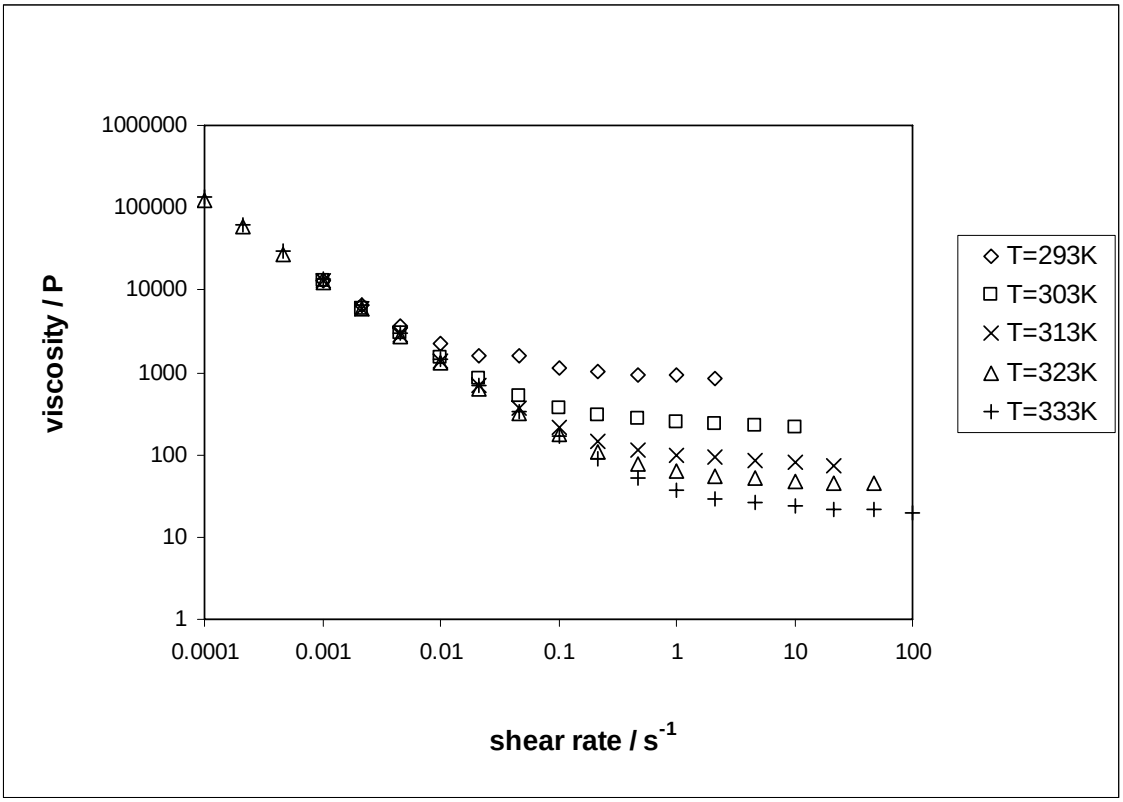

Figure 6.9. Crude oil viscosity curves in the temperature range 293 K- 333 K.

In Fig. 6.10, the results of the model exposed, taking the maximum $N = 20$ (Eq. 6.9), are shown. The choice of $N = 20$ is based onto two evidences. The Thermal Gravimetric Analysis (TGA) of crude oil, carried out by means of a TGA 2950 of TA instruments in N_2 flux, (Fig. 6.11) reveals a region between 340 K and 640 K where aliphatic compounds are the principal cause of weight loss. The derivative curves over-exposed of crude oil, C11 and C20 reveal that C20 is placed approximately in the middle of the aliphatic weight loss occurring between 300 K - 650 K (see Figs. 6.11 – 6.12), as the maximum N should stay in a Poisson-like distribution, and the average to the right, approximately at C40. The variation of A_T is very pronounced (Fig. 6.13), revealing a transition next to 311 K ($1000/T = 3.2$ K^{-1}), similar to the transition of C20 from the triclinic phase to the liquid phase. Since a transition was not observed by DSC, the rheological data were studied in order to find a signal of a possible transition; for these reasons both shear and normal stresses' analysis were considered. From the thermodynamic point of view, stress can be considered as the derivative of the Helmoltz free energy F respect to volume V at constant T. A relaxation time τ is obtained directly by the first coefficient of normal stresses, at the shear rate of 0.2 s^{-1}, which exhibits a significant variation at about 313 K (Fig. 6.14) and can be compared with A_T. In Fig. 6.14, τ is normalized by τ at 293 K.

$$\tau = \frac{2\eta}{\psi_1}. \tag{6.26}$$

In Eq. 6.26, the relaxation time τ is expressed; η is the viscosity and ψ_1 the first coefficient of normal stresses. The shear stress, at the critical shear rate, has a transition at about 312 K (Fig. 6.15), in accordance with the prediction of the model.

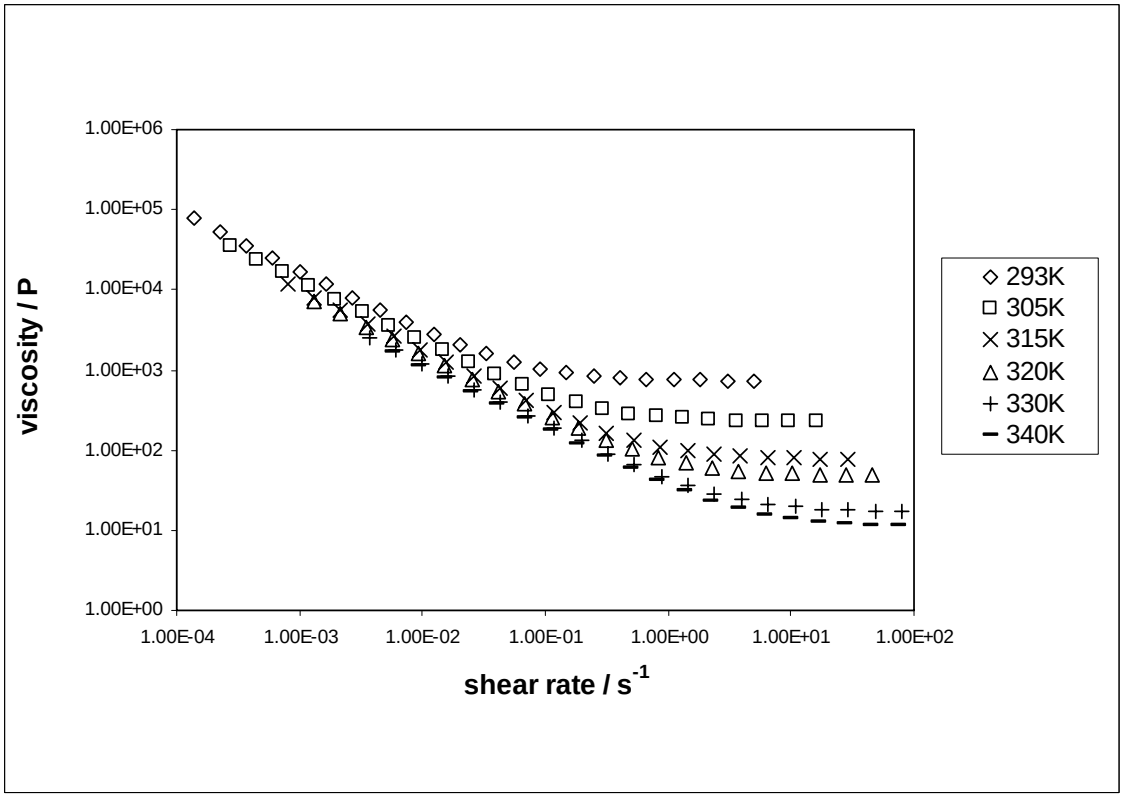

Figure 6.10. Model prediction of the crude oil curves in the temperature range 293 K- 340 K.

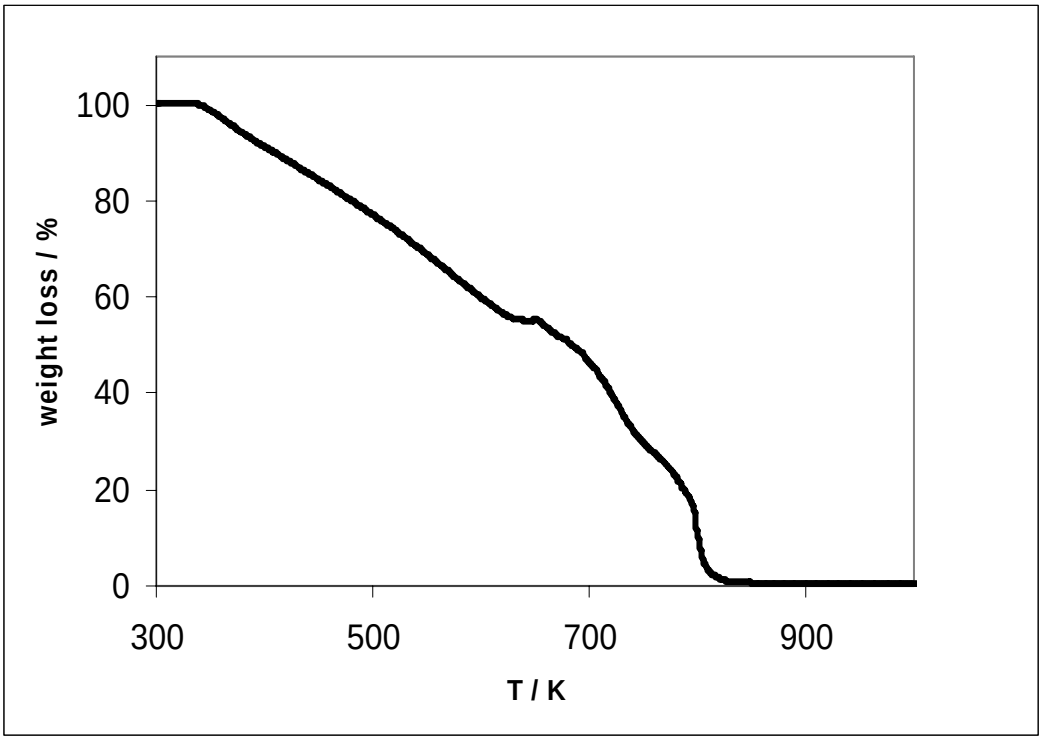

Figure 6.11. TGA weight loss % for the crude oil sample in the range of 300 K-1000 K, executed under N_2 flux.

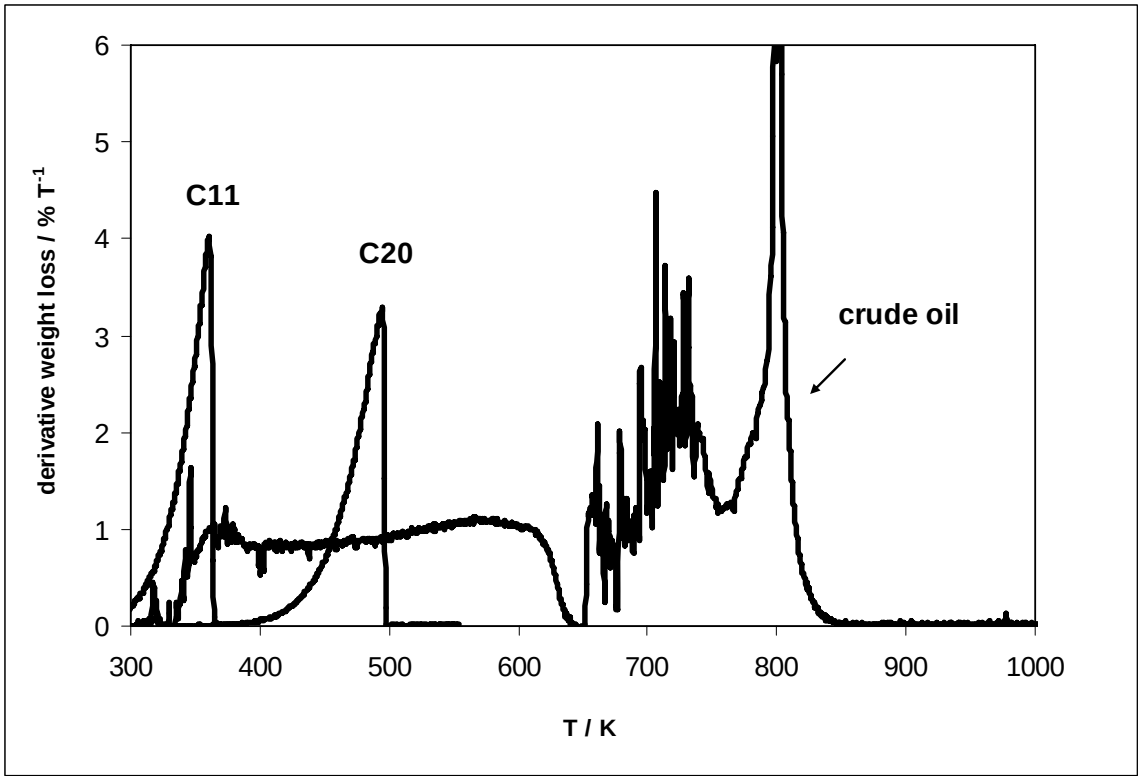

Figure 6.12. Derivatives of the TGA curves of the crude oil sample, C11 and C20.

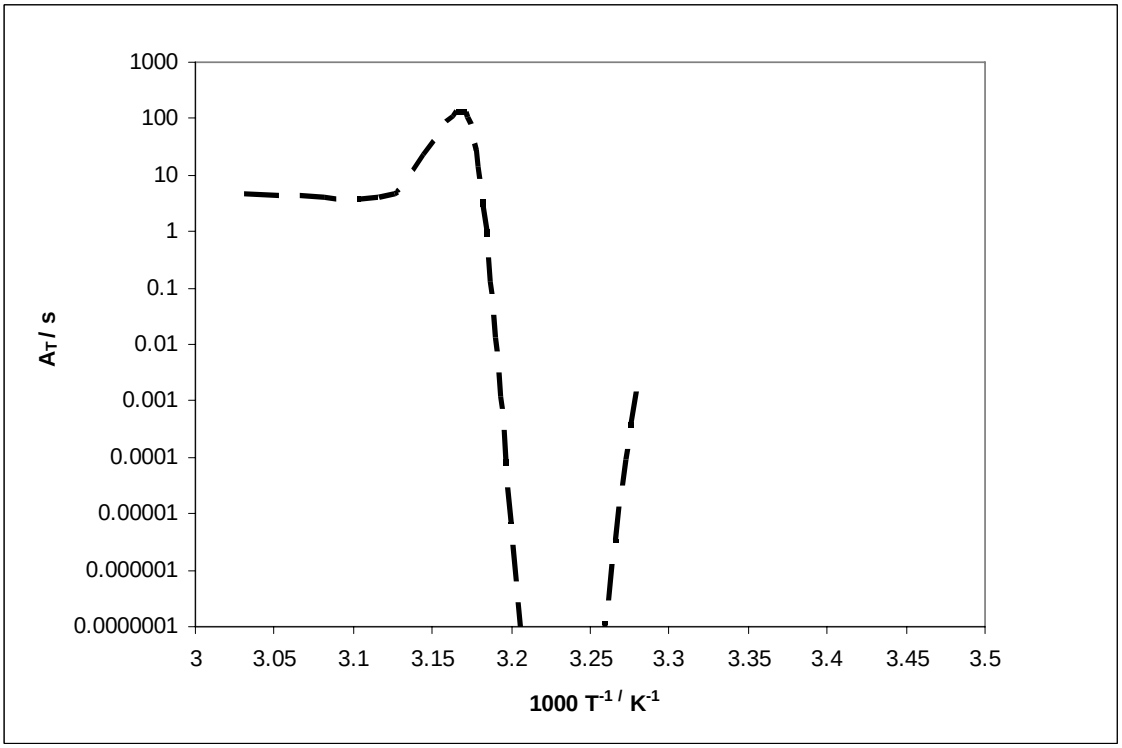

Figure 6.13. A_T variation as obtained by the model.

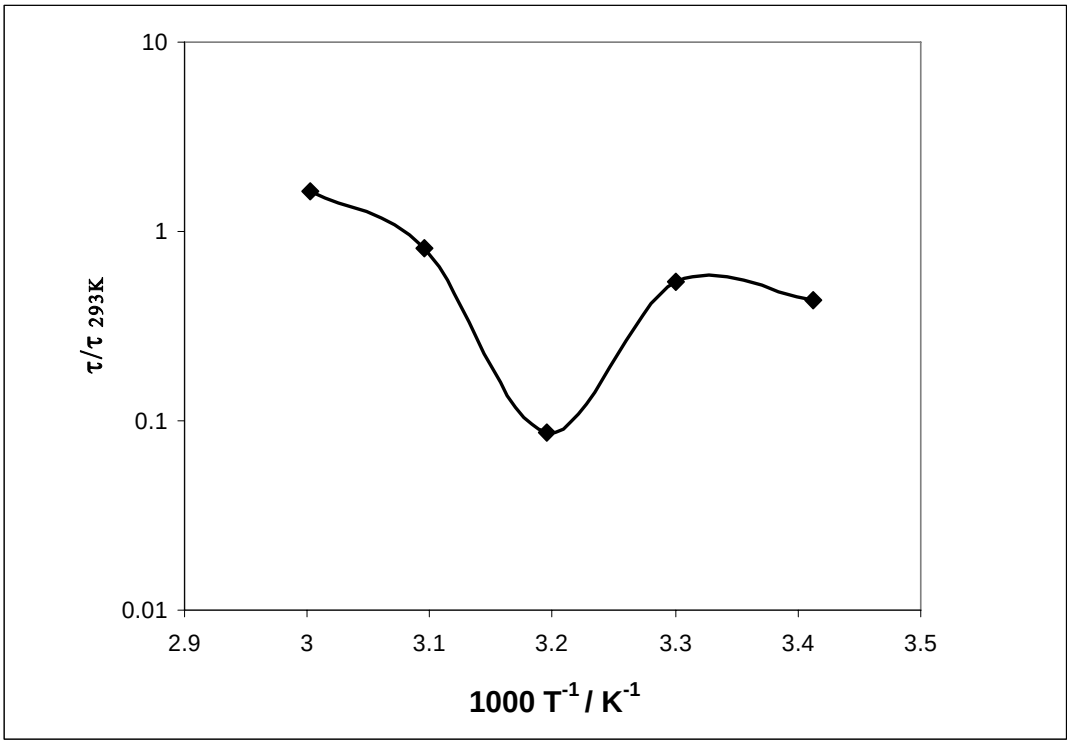

Figure 6.14. Relaxation time τ normalized to τ at 293 K and referred to the shear rate of 0.2 s^{-1}. This relaxation time is calculated through the first coefficient of normal stresses ψ_1.

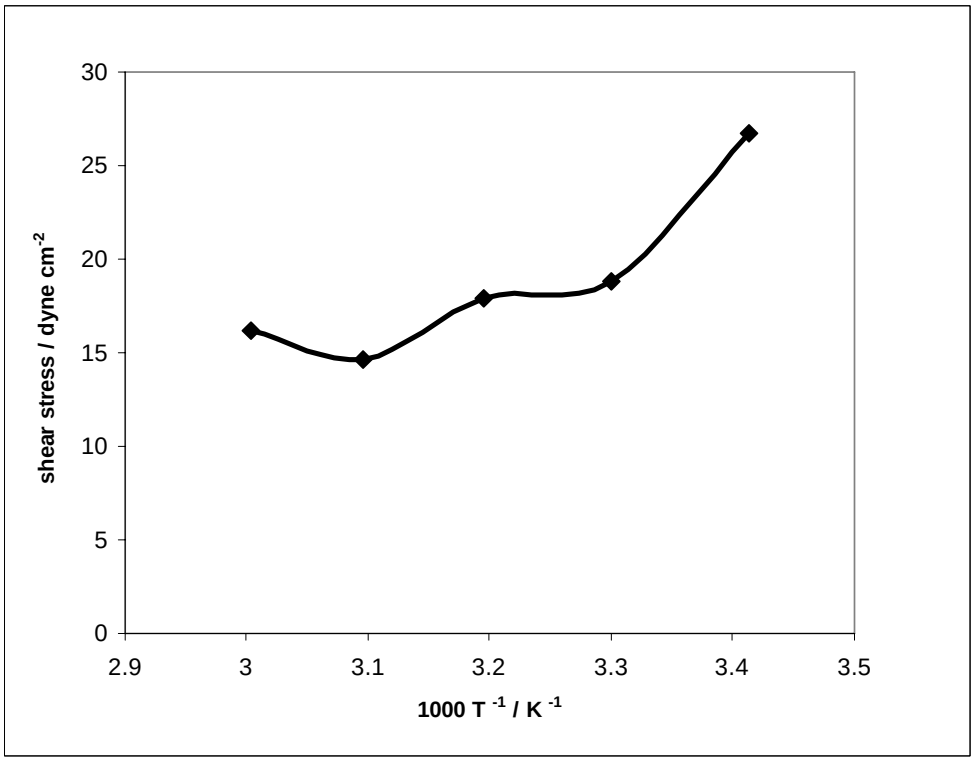

Figure 6.15. Shear stress at the critical shear rate $\dot{\gamma}_c$ defined in Section 4.

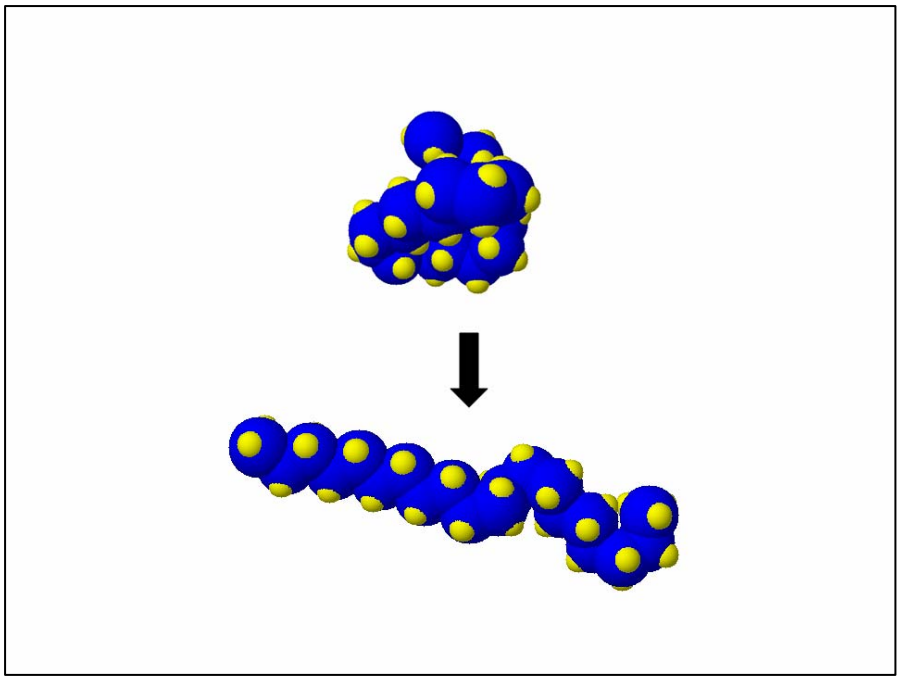

Figure 6.16. Two different conformations of C20. The upper conformation is "ball shaped" and the lower one is "snake-like". An energy barrier, which involves the rotation barrier of C-C bonds, must be overcome to pass from one to another one.

6.7. Discussion

Changes in the conformational organization of the mesostructure of the fluid induced by flow [27] cause the appearance of the activation energy defined in the said adaptation of the Adam-Gibbs theory (Eqs. 6.1. – 6.11.b). The Adam-Gibbs-like model can provide a plausible explanation for the Arrhenius factor found in waxy crude oil and its very pronounced shear thinning effect. As well, alkanes seem to determinate the main features of viscosity properties of the crude oil sample. The higher absolute value of the viscosity of crude oil (Fig. 6.9) depends on the suspension nature of the fluid made up waxy particles dispersed in. Aliphatic components, among them alkanes, surround these dispersed particles composed of wax, asphaltenes and an outer shell of resins. An example of a different conformation change observed in alkane chains is shown in Fig. 6.16 for *n*-eicosane. Polymer-phase-type of changes implicate reorganization of large regions that are interconnected and tangled. On the other hand, elemental segments

requiring changes in their conformation, by means of rotations and torsions, involve an energy barrier associated to $\Delta\mu$. The cooperative region z^* varies with temperature and chain length, i. e., with the number of carbon atoms n. Longer chains have larger z^*, and when the transition temperature is approached, z^* increases dramatically, with the cooperative region becoming of the size of the whole solid. It is noteworthy to mention that the cooperative region size depends on the maximum $\boldsymbol{N}$ and not on the average $\langle n \rangle$. The size of z^* determines the activation energy, which is not a true constant.

The relaxation time $k(T)$ increases with z*, while A_T can be interpreted as the extrapolation of the limit case of $k(T)$ at high T. Nevertheless, it is sensitive to the presence of suspended particles, which also affect the relaxation time. This is the reason for abrupt change of A_T for crude oil, which follows the aliphatic transition at about 310 K (Fig. 6.13). The phase transition of the C17-C20 mixture can be observed in the DSC, data and it is found to be close the C17 phase transition, T = 295.5 K (Fig. 6.5). On the other side, no clear transition is observed in crude oil in the DSC data (Fig. 6.8) near the expected region (~310 K). Two possible reasons can be put forward: firstly, the transition is too small or broad to be detected; and secondly, it is like a second order transition. A second order transition implies an aliphatic network more similar to a gel than to a solid. Some transitions observed for alkane binary mixtures are shifted largely (from 283 K to 264 K in our case), although others, dominated by the excess alkane, are kept most unvaried. However, the rotator phase seems to be more stable and dominated by the excess alkane C17. The shifted and lowered peak of the solid-solid transition (Fig. 6.8) is due to the fact that effects due to these phases are weakened by the presence of the even alkane (C20) [26].

The application of the present adaptation of the Adam-Gibbs theory to viscosity functions is described in Section 6.4. The experimental viscosity curves of Fig. 6.6 for

the alkanes' mixture and Fig. 6.8 for the crude oil can be reproduced taking into account the activation energy expressed by the Adam-Gibbs theory. In this model, the central role is played by the shear thinning model of Eq. 6.14, which describes both alkane blends and the considered oil. The two parameters A, B and can be made dimensionless by means of the Weissenberg number of Eq. 6.15 and by η' of Eq. 6.16, respectively. The parameter p is not often reproducible, indicating that its variation not only depends on molecular weight but also on other factors such as the state of the sample before test [13]. It could be made dimensionless through the average $\langle n \rangle$.

Summing up, temperature effects manifest through N, and the effect of shear forces through $\langle n \rangle$.

6.8. Conclusions

These results show that the crude oil (from the Cantarell Reservoir in Mexico), with a high content of aliphatic compounds, and the blends of alkanes obey to an identical system of phenomenological rheological equations (Eqs. 6.14 – 6.22). This means that the rheological properties of crude oil are determined overall by alkane-like compounds such as paraffins and compounds with a relevant alkylic chain.

The Adam-Gibbs theory [12] can provide a framework to express the relaxation time variation observed in large mesostructures of hydrocarbons compounds, as well as the associated and variable activation energy. Combining this characteristic time with shear rate, a Weissenberg number (Eq. 6.15) [22] is obtained, capable of scaling both alkane and crude oil viscosities.

The cooperative region size z^* (Eq. 6.11.b), which varies depending on the number of carbon atoms of the excess alkanes, can also explain the different activation energies measured in different blends. These analogies allow us to bypass the

complexity of evaluating crude oil samples of different composition and to correlate the rheological properties of crude oil to those of simpler and easily reproducible laboratory samples, such as alkane mixtures [22]. The rheological differences between oil and alkanes depend essentially on the cooperative changes induced by flow and temperature. Although, the Adam-Gibbs theory provides a common framework to the mechanisms which cause the appearance of the activation energy, there are substantial differences [1-4].

Based upon the variation of both the viscosity (Fig. 6.9) and the relaxation time A_T with temperature (Fig. 6.12), the extent of changes is deeper in crude oil, than in alkanes' mixtures. This is due mainly to the colloidal nature of crude oil which includes a large amount of suspended particles. With increment of temperature, the modification of the interactions of these particles with the fluid causes a transition from a gel-like to a colloid-like state [28]. This kind of transitions cannot be clearly detected by DSC (Fig. 6.8). However, as expected by the Adam-Gibbs theory, above the transition temperature, the effect of the activation energy $z^*\Delta\mu$ is faded.

6.9. References

[1] Speight JG. In *The Chemistry and Technology of Petroleum*, 2nd Ed. Marcel Dekker, New York, 1991.

[2] Sjoblom J, Aske N, Auflem IH, Brandal Ø, Havre TE, Sæther Ø, Westvik A, Johnsen EE & Kallevik H. "Our current understanding of water-in-crude oil emulsions. Recent characterization techniques and high pressure performance", *Adv. Colloid Interface Sci*. 2003, **100-102**, 399.

[3] Gruse WA & Stevens DR. In *The Chemical Technology of Petroleum*, McGraw-Hill, New York, 1960.

[4] Koots JA & Speight JG. "Relation of petroleum resins to asphaltenes" ,*Fuel* 1975, **54**/3, 179.

[5] Onogi S, Matsumoto T & Warashina Y. "Rheological properties of dispersions of spherical particles in polymer solutions", *J. Rheology* 1973, **17**, 175.

[6] Sengun MZ & Probstein RF. "Bimodal model of suspension viscoelasticity, *J. Rheology* 1997, **41**(4), 811.

[7] Werner A, Behar F, de Hemptinne JC & Behar E. "Viscosity and phase behavior of petroleum fluids with high asphaltenes contents", *Fluid Phase Equilibria* 1998, **147**, 343.

[8] Al-Besharah JM, Salman OA & Akashah SA. "Viscosity of crude oil blends", *Ind. Eng. Chem. Res*. 1987, **26**, 2445.

[9] Schorling P-C, Kessel DG & Rahimian I. "Influence of the crude oil resin/asphaltene ratio on the stability of oil/water emulsions", *Colloids and Surfaces A* 1999, **152**, 95.

[10] El-Gamal IM & Gad EAM. "Low temperature rheological behavior of Umbarka waxy crude and influence of flow improver", *Colloids and Surfaces A: Physicochem Engineering Aspects* 1998, **131**, 181.

[11] Ferry JD. Chapter 10. "Molecular Theory for Undiluted Amorphous Polymers and Concentrated Solutions; Networks and Entanglements". In: Ferry JD. *Viscoelastic Properties of Polymers*, 3d Ed., John Wiley & Sons, Inc. New York; 1980, p. 224-263.

[12] Hodge IM. "Adam-Gibbs formulation of henthalpy relaxation near the glass transition, *J. Res. Nat. Inst. Stand. Technol*. 1997, **102**, 195.

[13] Bohlin L. "A theory of flow as a cooperative phenomenon"**,** *Journal of Colloid and Interface Science*. 1980, **74**/2, 423.

[14] Ferry JD. Chapter 11. "Dependence of Viscoelastic Behavior on Temperature and Pressure". In: Ferry JD. *Viscoelastic Properties of Polymers*, 3d Ed., John Wiley & Sons, Inc. New York; 1980, p. 264-315.

[15] Ferry JD. Chapter 9. "Dilute Solutions: Molecular Theory and Comparison with Experiments". In: Ferry JD. *Viscoelastic Properties of Polymers*, 3d Ed., John Wiley & Sons, Inc. New York; 1980, p. 177-223.

[16] Van Miltenburg JC. "Fitting the heat capacity of liquid *n*-alkanes: new measurements of *n*-heptadecane and *n*-octadecane", *Thermochimica Acta* 2000, **343**, 57.

[17] Smith GD & Jaffe RL. "A quantum chemistry study of conformational energies and rotational energy barriers in n-alkanes", *J. Phys. Chem*. 1996, **100**(48), 18718.

[18] Musser BJ & Kilpatrick PK. "Molecular characterization of wax isolated from a variety of crude oils", *Energy & Fuels* 1998, **12**, 715.

[19] Burch KJ & Whithead EG Jr. "Melting-point models of alkanes", *Journal of Chemical and Engineering Data* 2004, **49**, 858.

[20] Kioupis LI & Maginn EJ. "Rheology, dynamics and structure of hydrocarbon blends. A molecular dynamics study of n-hexane/n-hexadecane mixtures", *Chemical Engineering Journal* 1999, **74**, 129.

[21] Al-Zahrani SM. "A generalized rheological model for shear thinning fluids", *Journal of Petroleum Science and Engineering* 1997**, 17**, 211.

[22] Dante RC, Geffroy-Aguilar E & Chávez AE. "Viscoelastic models for Mexican heavy crude oil and comparison with a mixture of heptadecane and eicosane. Part I", *Fuel* 2006, **85**, 559.

[23] Miadonye A, Puttagunta VR & Singh B. "Prediction of the viscosity of crude Oil fractions from a single measurement", *Chem. Eng. Comm*. 1993, **122**, 195.

[24] Al-Zahrani SM & Al-Fariss TF. "A general model for the viscosity of waxy oils", *Chemical Engineering and Processing* 1998, **37**, 433.

[25] Pal R. "Scaling of relative viscosity of emulsions", *J. Rheology* 1997, **41**, 141.

[26] Rajabalee F, Metvaud V, Oonk HAJ, Modieig D & Waldner P. "Perfect families of mixed crystals: the ordered crystalline forms of n-alkanes", *Phys. Chem. Chem. Phys*. 2000, **2**, 1345.

[27] Pricl S & Fermeglia M. "Virtual rheological experiments. on linear alkane chains con®ned between titanium walls", *Rheol. Acta* 2001, **40**, 104.

[28] Lapasin R, Visintin RFG, D'Antona P & Lockhart T. "Proprietà lineari e non lineari di greggi cerosi". *Atti VIII Convegno della Società Italiana di Reologia*, Sant'Angelo di Ischia, Italy, 2004.

Chapter 7.
Viscoelastic models for Mexican heavy crude oil and comparison with a mixture of heptadecane and eicosane

Abstract

The knowledge of the viscoelastic properties of crude oils can be interpreted in terms of a distribution of relaxation times. A square relaxation spectrum applied to the Maxwell model is in accordance with experimental results obtained for a crude oil specimen from the Cantarell reservoir in south-east Mexico. In analogy with the Weissenberg number proposed in Chapter 6 for steady viscosity, a similar dimensionless number is also proposed to scale the G' and G'' at different temperature.

The viscoelastic properties of the mixture of *n*-heptadecane and *n*-eicosane are very poor in comparison of those of crude oil, and the trends of G' and G'' are ascribable to typical characteristics of linear alkanes. In general, aging of crude oil causes a decrement of tan δ quicker with temperature increment. Moreover, two years of aging cause a huge increment of G'.

7.1. Introduction

The basic problem in evaluating the oscillatory viscoelastic behavior of crude petroleum is its complexity of composition. The general composition of crude oil frequently depends not only upon the source of crude but also upon the age of the source. Nevertheless, the crude oil aging at room temperature can cause changes in the oscillatory viscoelastic behavior. Therefore, there are several parameters to take into account. As a result, there is a wide variation of viscoelastic properties, depending upon the proportions of the different constituents [1-4] and show also a strong dependence with temperature. In order to better understand the dependence of the oscillatory

viscoelastic behavior as a function of temperature it is necessary to propose a model for the microstructure of the fluid. That is, from a meso-structural point of view, crude oils can be classified in the general field of suspensions. Their steady flow rheology frequently shows a shear thinning behavior in steady shear strain conditions as well as normal stresses [5]. The consequence of such behavior within the dynamic-oscillatory-behavior should be similar, and due to the same structural changes of conformation. This very complex behavior depends partially on a Newtonian contribution of the non-colloidal-fluid, combined with the non-Newtonian contribution due to the colloidal particles [6-10].

The Weissenberg number can be used successfully to scale viscosities at different temperature of both crude oil and alkanes as shown in Chapters 5 and 6. This number was developed through the Adam-Gibbs theory, adapted to the phenomena observed in steady shear flow [11], by correlating the Arrhenius factor, with the conformational changes in the aliphatic chains. The Arrhenius factor is a portion of the characteristic time of the Weissenberg number as shown in Chapter 6. In this case, thermodynamics provides the bridge between the macroscopic rheological behavior and the microscopic changes of molecules' conformation.

A dimensionless frequency ω', formally equivalent to the Weissenberg number is used to scale G' and G'', but now it takes the following form

$$\omega' = k\omega, \tag{7.1}$$

where ω is the frequency and k a constant, Eq. 7.1 corresponds to Eq. 5.10 defined for steady shear flow. In this Chapter, it is specifically considered the case of the same crude oil samples of the Mexican reservoir of Cantarell. A mention will be dedicated to a blend of *n*-heptadecane (C17) and *n*-eicosane (C20) in order to show that the storage and loss moduli, *G'* and *G''*, in this case, are very different in trend and magnitude from

those of crude oil, in spite of the similarity that occurs in steady shear flow. This is attributed to the colloidal particles of crude oil, a very different situation from the nearly homogeneous linear alkanes' blends.

7.2. Methods, equipments and materials

7.2.1. Adam-Gibbs theory and viscoelasticity of crude oil

The Adam-Gibbs theory was first used to explain the viscoelastic properties of polymers about the glass transition temperature range [11]. This theory relates the temperature dependence of the relaxation processes to the temperature dependence of the characteristic volume where cooperative rearrangements take place without affecting neighboring regions [11-13]. This region of cooperative rearrangements is large enough to allow a structural transition into a new configuration; hence, it is determined by the chain microstructure configuration (size conformation), and to the first order approximation, is equal to the sample size, at the temperature of solidification of the substance. The concepts and models, provided by this theory, were adapted to the condition, in which, from a certain grade of order and packing among oligomers' chains in the shear thinning region, a transition occurs to a newly disordered Newtonian region at high shear rates.

In the previous Chapters, it is demonstrated that a Weissenberg number [14] can scale the shear rate at different temperature for the crude oil considered and mixtures of alkanes. If it is assumed that k is the same characteristic time expressed in Eq. 6.2, the following dimensionless frequency is given:

$$\omega' = A_T \exp(z^* \Delta\mu / RT)\omega_T = \frac{\omega_T}{\dot{\gamma}_{cT}}, \qquad (7.2)$$

where $\dot{\gamma}_{cT}$ is the critical viscosity, z^* is the size of the cooperative region and $\Delta\mu$ is the activation energy, taken equal to 13 kJ mol^{-1} which corresponds to the approximated

value for the rotational barrier around a C-C bond (see Chapter 6, Section 6.2) [15], from a stable conformation to another (*GT* transitions). If Eq. 7.2 was valid in order to achieve a dimensionless frequency, also, for the oscillatory shear flow, the temperature dependent phenomena would be due to the aliphatic fraction, to which alkanes belong, in agreement with the results obtained in steady shear flow.

In a similar way, e.g. G'' is scaled as:

$$G_r'' = G''_T \, \eta_{cT}^{-1} A_T^{-1} \exp(-z^* \Delta\mu / RT) = \frac{G''}{\sigma_{cT}} \tag{7.3}$$

where G_r'' is the dimensionless loss modulus, η_{cT} and σ_{cT} are the critical viscosity and shear stress at the temperature *T*, respectively. The critical shear stress σ_{cT} is determined by means of the critical shear viscosity and the critical shear rate, as shown in Eq. 7.3. These critical values correspond to the onset viscosity and shear rate, at the transition from the shear thinning region to the Newtonian region. They were determined in a previous work, described in the Chapter 5 [14]. Their values are reported in Table 7.1. A similar reasoning can be done for G'. There are several methods to obtain master curves of oscillatory functions. In this Chapter, the described dimensionless variables were chosen because they allowed us to have a direct linkage with the Adam-Gibbs-like theory [11], as it was defined for steady shear flow in Chapter 6. Nevertheless, the WLF equation [13] could be used instead of Adam-Gibbs equations, and lead to similar results, when it is modified with an activation energy term, which depends upon temperature as in Adam-Gibbs theory.

Table 7.1 Critical shear rates and critical viscosities determined by intersection of the two linear regions.

$\dot{\gamma}_{cT}$ (s^{-1})	η_{cT} (Poise)	T(K)
0.025	*1069.1*	*293*
0.059	*319.2*	*303*
0.141	*127.1*	*313*

7.2.2. Distribution of relaxation times: the effect of particle dispersion

The relaxation time λ concerns with those properties which are related to either particles or polymers dispersions. A spectrum of relaxation times λ_i addresses the fact that different particle sizes have associated different relaxation times, thus adequate modeling properties which are related to particles dispersion. On the other hand, the utilization of one relaxation time in a Maxwell model will not reproduce the behavior of G' and G'', here presented. However, even the utilization of a simple spectrum with a square shaped distribution of relaxation times can reproduce the main characteristics of G' and G''.

For a Maxwell model, the storage and loss moduli in Maxwell's model are given for one relaxation time by:

$$G'(\omega) = \frac{G\omega^2\lambda^2}{1+\omega^2\lambda^2}, \tag{7.4}$$

$$G''(\omega) = \frac{G\omega\lambda}{1+\omega^2\lambda^2}, \tag{7.5}$$

where ω is the frequency, and G is the elastic modulus. As said above, this model implies that there is only one relaxation time λ, but crude-oil and several other mixtures

or dispersions are best modelled by assuming several relaxation times or, better, by a distribution of relaxation times. In this scenario, the moduli are given by:

$$G'(\omega) = \int_{-\infty}^{\infty} \frac{\omega^2 \lambda^2 \mathrm{H}(\lambda)}{1+\omega^2\lambda^2} d\ln\lambda\,, \tag{7.6}$$

$$G''(\omega) = \int_{-\infty}^{\infty} \frac{\omega\lambda \mathrm{H}(\lambda)}{1+\omega^2\lambda^2} d\ln\lambda\,, \tag{7.7}$$

where H(λ) is the relaxation spectrum function, with a limiting relaxation time $\lambda_{0,}$ in our case a square distribution was utilized. In the case of this relaxation spectrum, the loss and storage moduli result to be:

$$G'(\omega) = \frac{G_0}{2}\ln(1+\omega^2{\lambda_0}^2)\,, \tag{7.8}$$

$$G''(\omega) = G_0 \tan^{-1}(\omega\lambda_0)\,, \tag{7.9}$$

where G_0 is the elastic modulus measured at λ_0. This part on fundaments of viscoelastic models is described in detail in Chapter 4.

Experimental tests, executed two years later on the same crude oil sample, show the effects of slow agglomeration and oxidative phenomena.

7.2.3. Equipments and materials

The specimens of crude oil are from the Cantarell reservoir in south-east Mexico, they have an aliphatic fraction corresponding to about the 40 % in weight. They were tested at different temperatures (293-323 K) without addition of any kind of substances. The linear alkanes used for a brief comparison have numbers of carbon atoms of C17 and C20. The mixtures of alkanes were prepared mixing them by mechanical agitation above their melting points until the formation of solutions. The mixtures have a molar fraction of C20 of 0.17. The rheological tests were carried out by the strain controlled rheometer ARES, described in detail in Chapter 3. The cone-plate geometry was used

for all tests with an angle of 0.04 radians and plate radii of 50 mm, or 25 mm. The measurement were carried out in linear region with strains not exceeding 1%.

7.3. Experimental part

The sweep frequency test results are shown in Figs.7.1a and 7.1b for G' and G'', and their results are shown together in Fig. 7.1c, in order to evidence the crossing points between G' and G''. It is noteworthy to point out that the crossing point is shifted to higher frequencies with increasing temperature. After a maximum observed at about 37 rad s^{-1}, G' decreases slightly at 293 K. And at 313 K G' it does not reach a maximum in the observed range of frequencies. G' has values between 1 dyne cm^{-2} (low frequencies) and 10^5 dyne cm^{-2} (high frequencies). The trend of G'' is similar to that of G', but at 293 K, after the sharp maximum, it decays. At 303 K, G'' decreases after the maximum, although it occurs at slightly higher frequencies than the 293 K case. On the other hand, at 313 K, G'' does not reach the maximum in the frequency range of measure. The values of G'' stay in the interval within 100 dyne cm^{-2} (low frequencies) and $3 \cdot 10^4$ dyne cm^{-2}. The scaled results with the dimensionless variables defined in Eqs. 7.2 and 7.3 are shown in Figs. 7.2a and 7.2b. Scaling causes the superimposition of the different curves. Other data are significant, such as the tan δ evolution with time at different temperature but at the fixed frequency of 10 rad s^{-1}; tan δ always decreases with time but mostly with temperature increment (Fig. 7.3). However, it is mostly undetermined at 323 K, due to the low values of G', at the limit of the sensibility of the equipment. For the mixture of *n*-heptadecane and *n*-eicosane, the tentative to obtain G' and G'' reveals the poor viscoelasticity of the mixture (Fig. 7.4) with values of G' and G'' not exceeding 10^2 dyne cm^{-2} at 295 K (molar fraction 0.17 of *n*-eicosane) in comparison of crude oil, at 303 K. It is noteworthy the divergence of G' and G'', and that G' seems to be constant at high frequencies.

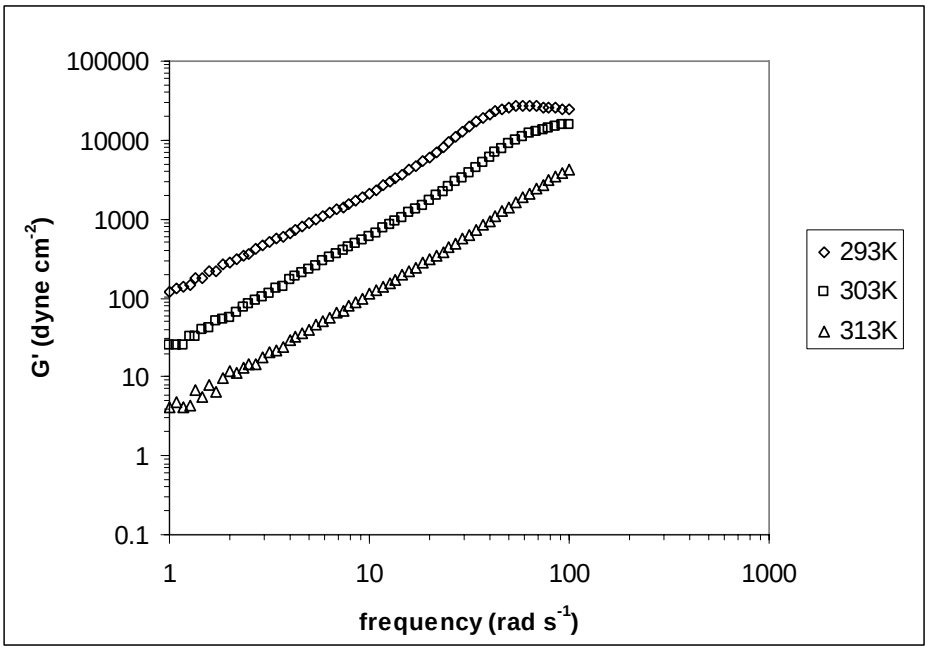

Figure 7.1a. G' curves at three levels of temperature.

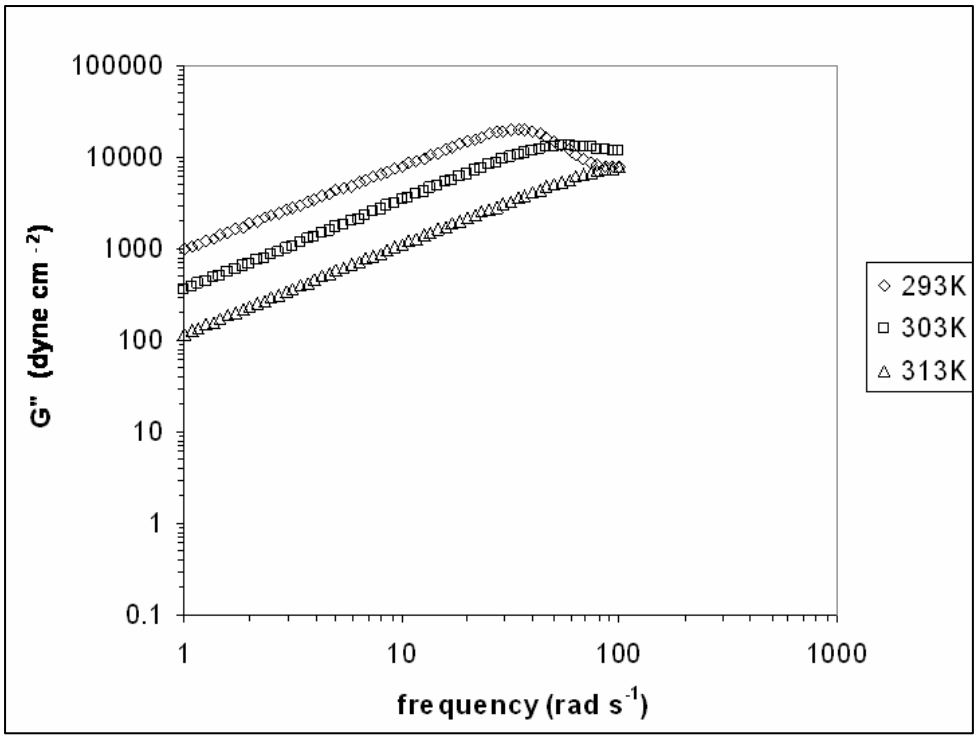

Figure 7.1b. G'' curves at three different temperature levels.

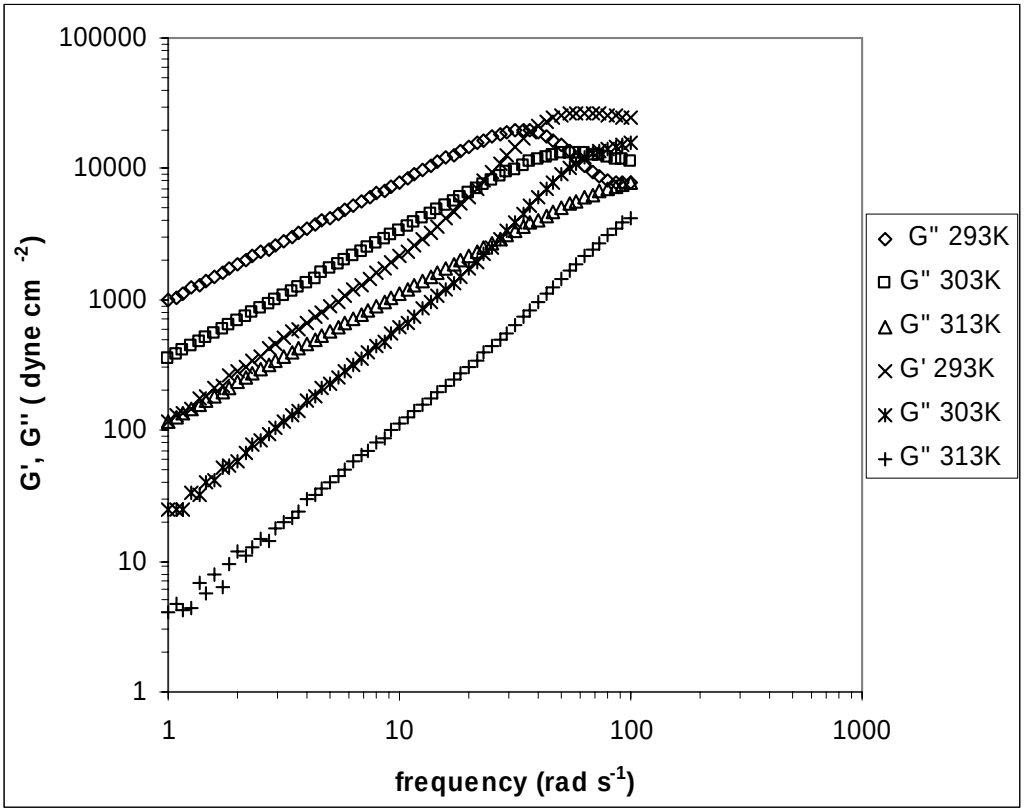

Figure 7.1c. G' and G'' curves at three different temperature levels.

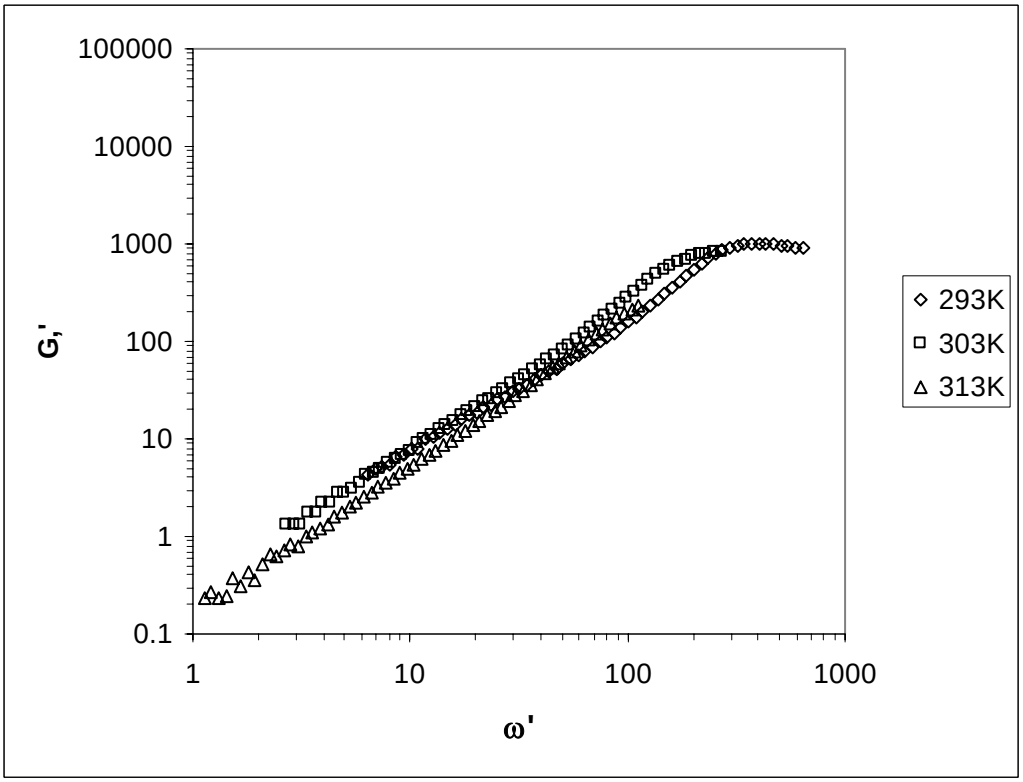

Figure 7.2a. Dimensionless G', at different temperature levels.

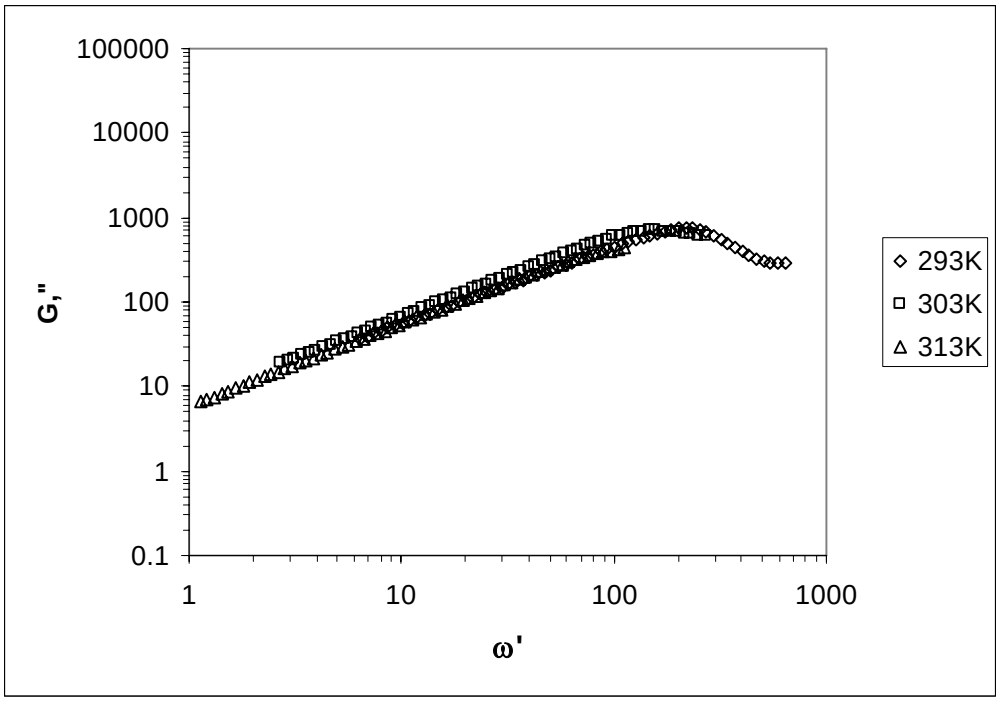

Figure 7.2b. Dimensionless G'', at different temperature levels.

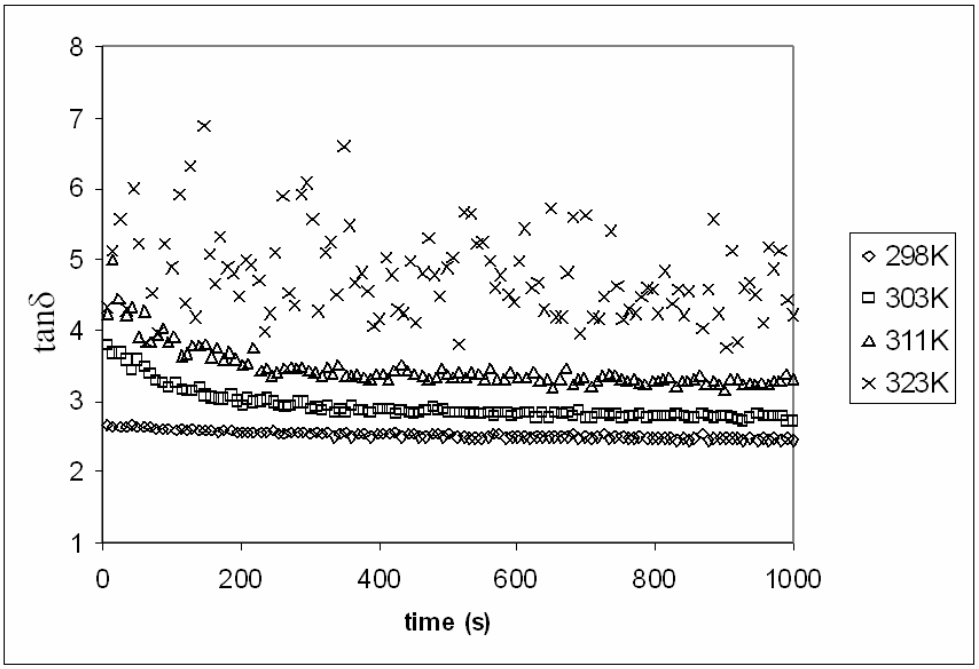

Figure 7.3. tanδ at four temperature levels.

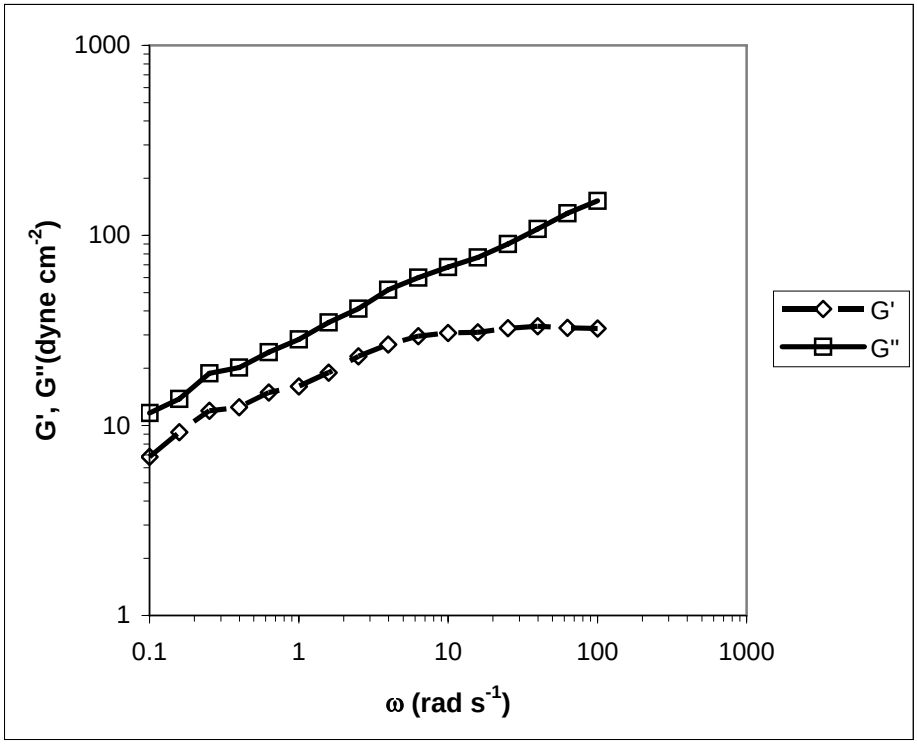

Figure 7.4. G' and G'' for the mixture of *n*-heptadecane and *n*-eicosane at 295 K.

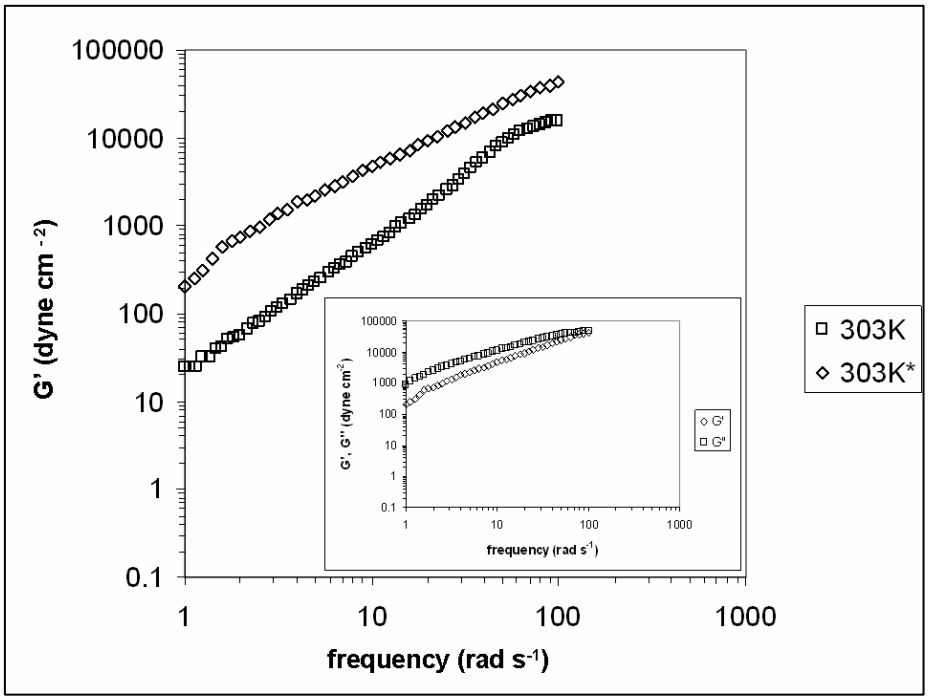

Figure 7.5. Comparison of G' of the sample aged at room temperature * for two years with G' of the fresh sample at 303 K. In the inserted box G' and G'' of the two years aged sample are shown.

Other measures were carried out on the sample of crude oil after two years of aging at room temperature, which show higher G' for the test of the aged sample (Fig. 7.5). At the frequency of 1 rad s^{-1}, the aged sample has G' = 207.15 dyne cm^{-2}, while two years before had 24 dyne cm^{-2}. This difference decreases at high frequencies. In the inserted box of Fig. 7.5, $G'$and G'' of the aged sample are shown. It is possible to notice that the difference between $G'$and G'' is not so marked as in the fresh sample, and that crossing is shifted to higher frequencies than the fresh sample at the same temperature.

7.4. Model results

The application of a spectrum of relaxation times was carried out with λ_0 used as a fit parameter and taken 0.1 s for 293K, 0.02 s for 303 K and 0.016 s for 313 K; while G_0 was calculated using the critical viscosity η_c. These choices show a high degree of coherence with the experimental results, as demonstrated by the relaxation times, calculated by means of the following equation:

$$\lambda = \frac{G'}{\omega G''}. \tag{7.10}$$

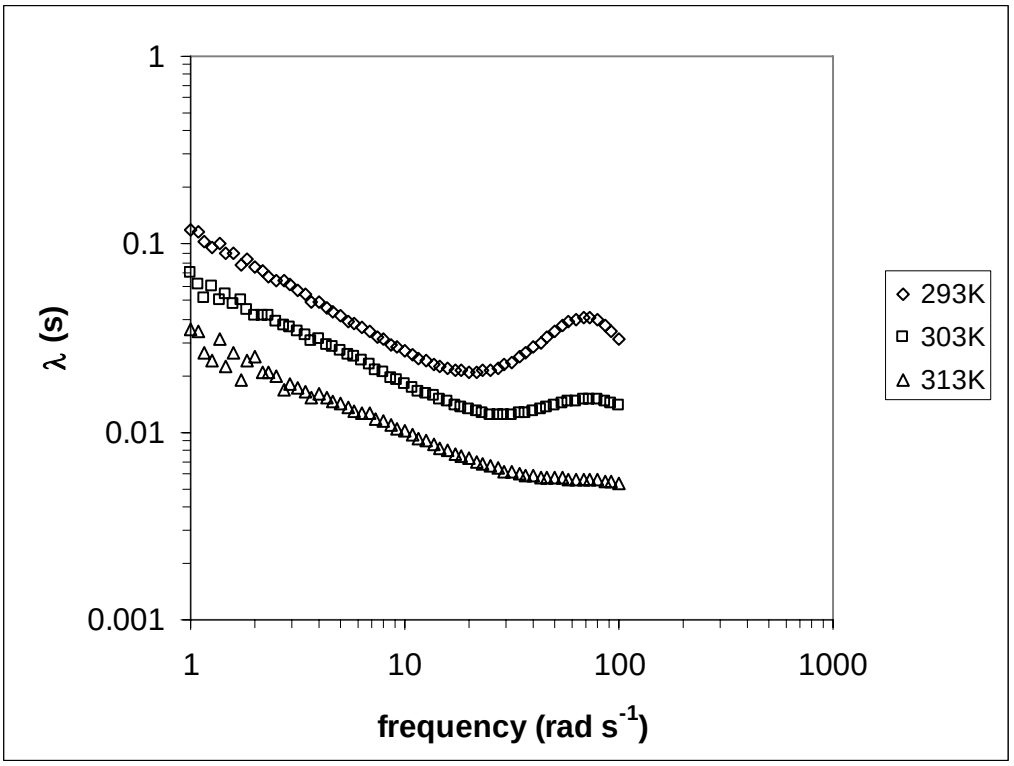

Figure 7.6. Relaxation times as determined by Eq. 7.10 at three temperature levels.

The graphic of λ values, which are expressed as function of the frequency ω, at 293, 303 and 313 K, obtained by Eq. 7.10, is shown in Fig. 7.6. From this graphic, it can be noticed that the values at low frequency are closed to 0.1 s at 293 K (the value used as λ_0).

The model curves of G' and G'' are shown in Figs. 7.7 and 7.8, respectively. The model fails especially at 293 K, while at 313 K the best agreement is achieved. Nevertheless, the choice of just one relaxation time leads to a sharp failure especially for G'', as shown in Fig. 7.9, at 293 K, with λ taken as fit parameter and with the assigned value of 0.027 s.

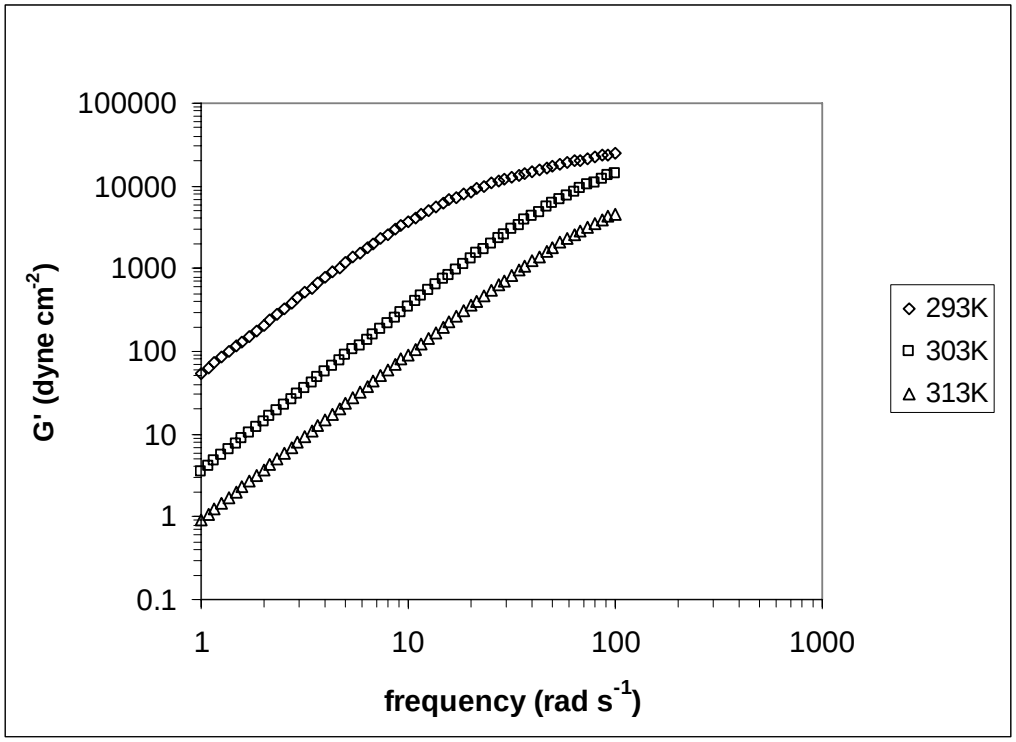

Figure 7.7. G' obtained by means of the relaxation spectrum applied to the Maxwell model.

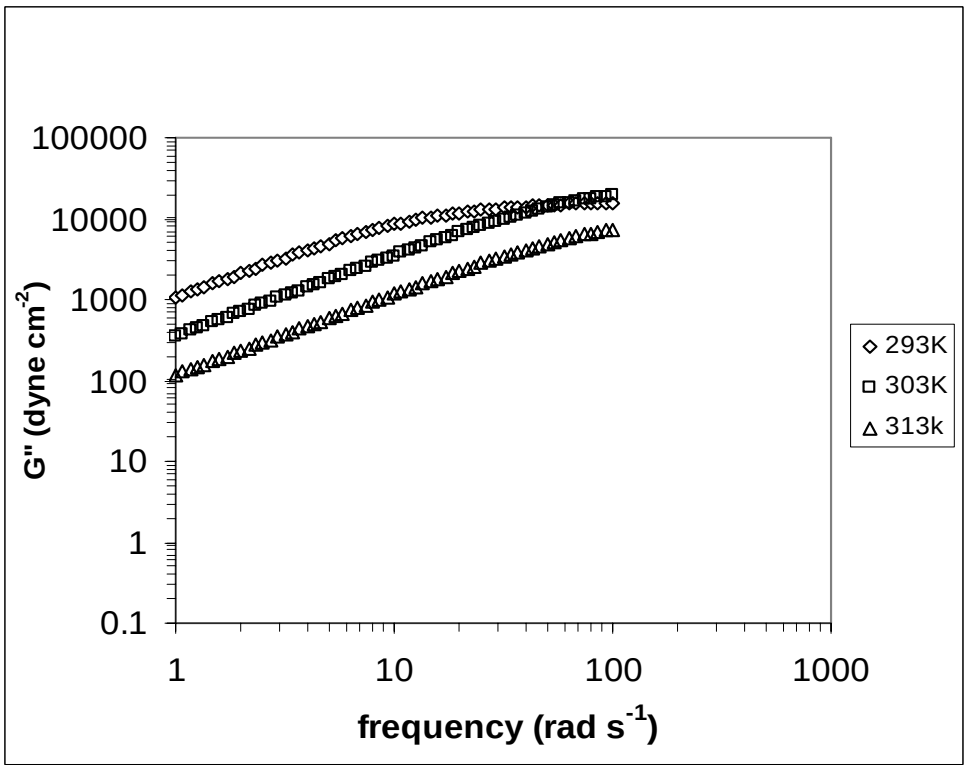

Figure 7.8. G'' obtained by means of the relaxation spectrum applied to the Maxwell model.

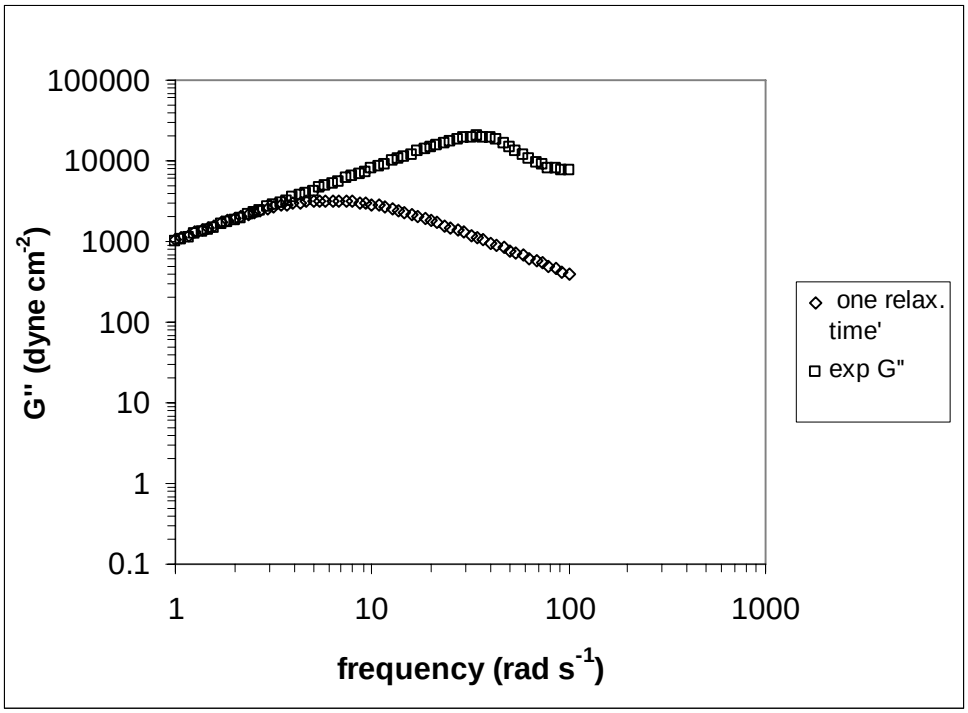

Figure 7.9. Comparison between experimental results of G'' and those of the model based in one relaxation time at 293 K.

7.5. Discussion

The chosen scaling (Figs. 7.2a and 7.2b) implies that the modification of the curves due to temperature is mainly governed by the same activation energy of steady shear flow [7, 8]. This energy barrier should be overcome to reach a flow-organized structure. The value of G' of the sample aged for two years at room temperature is about 10 fold G' of the fresh sample at low frequencies (Fig. 7.5). On the other hand, the curve of the relaxation time versus frequency at 303 K, after two years of aging at room temperature (Fig. 7.10), resembles those curves at higher temperature, in its shape but not for its values, such as that at 313 K of the fresh sample (compare the curve of Fig.7.10 with the curve at 313 K of Fig. 7.6). Since a suspension based on larger particles has a structure more sensible to lower frequencies, in the aged sample, large particles were

formed either by aggregation of small ones or by cross-linking due to oxidative phenomena.

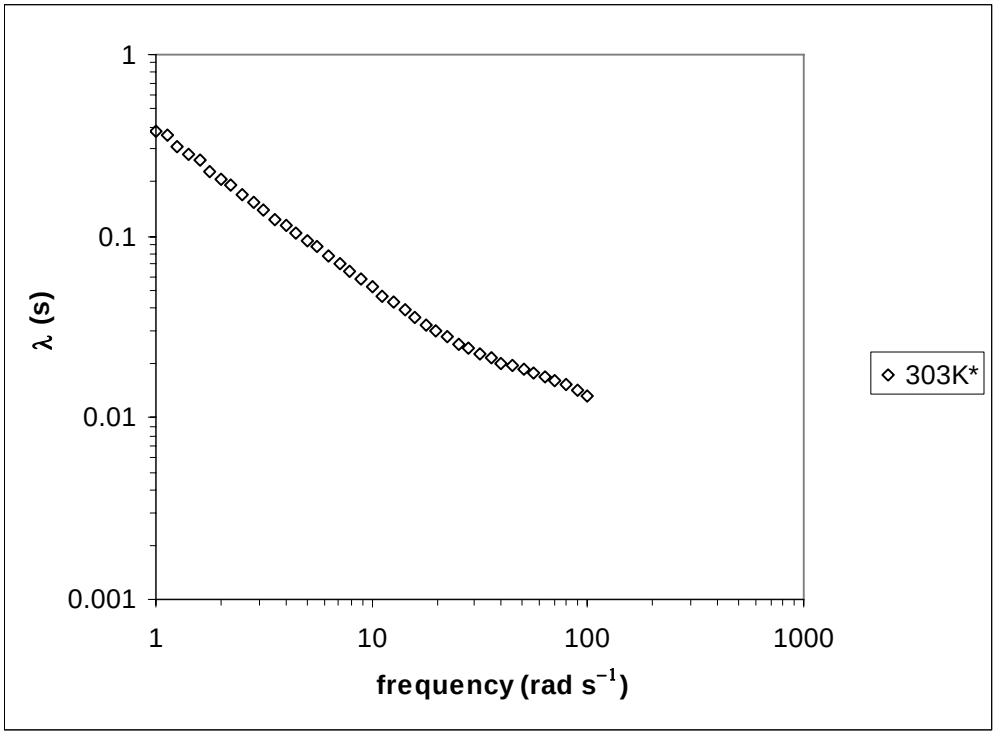

Figure 7.10. Relaxation times at 303 K, as determined by Eq.10 after two years of aging at room temperature.

The graphic of Fig. 7.3 shows that tanδ decreases with time, at first quickly and finally slowly. This is another phenomenon related to gelification of the sample [16], which is accelerated with temperature increment; however, over 323 K is difficult to identify a clear trend. This fact can be confirmed also by the huge increment of G' in comparison with G'' for the sample aged for two years (see Fig. 7.5). In the transition zone, the two curves are nearly parallel.

The choice of a relaxation spectrum is more adequate that the choice of one relaxation time as can be seen from the comparison of the results exposed in Figs. 7.7 and 7.8 with the example of Fig. 7.9. However, the model with the relaxation spectrum fits better the experimental results at higher temperatures, because the system seems to

approach more the square distribution, as it can be observed in Fig. 7.6. A minimum is present in the curves of λ obtained through Eq. 7.10, but it fades with temperature increase. This minimum corresponds to the value of λ at which G' and G'' are equal. This value is usually used for a viscoelastic model with one relaxation time. The fade and disappearance of this minimum mean that the properties of the suspension are moving towards a system where a distribution of relaxation times is dominant.

The square distribution of relaxation times is a rough approximation, but allows us to demonstrate that a relaxation spectrum must be considered to describe crude oil viscoelasticity, as in the case either of melted polymers or polymer suspensions.

Although, alkanes' mixtures can simulate the viscous characteristics of the Mexican crude oil specimen within certain experimental conditions [10], they give poor support to describe viscoelastic properties of crude oil. They have low loss and storage moduli in comparison with those of oil, in the linear regime (see Fig. 7.4). Furthermore, at high frequencies G' and G'' diverge, and G' seems to reach a constant value. This behavior is characteristic of axis-symmetric molecules [17]. Alkanes can approach such a situation in the so called rotator phase, in which they can only rotate around the main axis of the all *trans* molecule [18, 19]. For high frequencies, the molecule orientation cannot keep pace with the alternating shear rate and less energy is dissipated, so *G'* reaches a value characteristic of high-frequency regime.

7.6. Conclusions

The utilization even of the proposed simplified relaxation spectrum provides a good agreement of oscillatory experimental results with a generalized Maxwell model for the crude oil specimen. It is noteworthy that the square-like relaxation spectrum is typical of glassy samples [20]. In general, aging causes an increment of *G'* (decrement of tan δ), which tends to be faster with increasing temperature. Two years of aging at room

temperature cause a huge increment in G' probably due to slow oxidative and aggregation phenomena. The master curves obtained through the relaxation times of molecular processes *k(T)* might would allow us to forecast the behavior of the sample out of the measure range of frequency, at a given temperature. The effect of temperature on G' and G'' is essentially due to the same mechanisms described in Chapters 5 and 6; in other words, it is due to the changes of configuration of the aliphatic fraction, induced by the shear flow and favored by the temperature increment.

The viscoelastic behavior of the C17/C20 mixture is far from simulating crude oil properties either for the magnitude of both G' and G'' or for their trends. Its storage and loss moduli seem to be determined by specific characteristics of linear alkanes, such as axis-symmetry.

7.7 References

[1] Speight JG. In *The Chemistry and Technology of Petroleum*, 2nd Ed., Marcel Dekker; New York, 1991.

[2] Sjoblom J, Aske N, Auflem IH, Brandal Ø, Havre TE. Sæther Ø, Westvik A, Johnsen EE & Kallevik H. "Our current understanding of water-in-crude oil emulsions. Recent characterization techniques and high pressure performance", *Adv. Colloid Interface Sci*. 2003, **100-102**.

[3] Gruse WA & Stevens D. In *The Chemical Technology of Petroleum*, McGraw-Hill; New York, 1960.

[4] Koots JA. & Speight JG. "Relation of petroleum resins to asphaltenes", *Fuel* 1975, **54**, 179.

[5] Onogi S, Matsumoto T & Warashina Y. "Rheological properties of dispersions of spherical particles in polymer solutions", *J. Rheology* 1973, **17**, 175.

[6] Sengun MZ & Probstein RF. "Bimodal model of suspension viscoelasticity**"**, *J. Rheology* 1997, **41**(4), 811.

[7] Werner A, Behar F, de Hemptinne JC & Behar E. "Viscosity and phase behavior of petroleum fluids with high asphaltenes contents", *Fluid Phase Equilibria* 1998, **147**, 343.

[8] Al-Besharah JM, Salman OA & Akashah SA. "Viscosity of crude oil blends", *Ind. Eng. Chem. Res*. 1987, **26**, 2445.

[9] Schorling P-C, Kessel DG & Rahimian I. "Influence of the crude oil resin/asphaltene ratio on the stability of oil/water emulsions", *Colloids and Surfaces A*. 1999, **152**, 95.

[10] El-Gamal IM & Gad EAM. “Low temperature rheological behavior of Umbarka waxy crude and influence of flow improver”, *Colloids and Surfaces A: Physicochem. Engineering Aspects* 1998, **131**, 181.

[11] Hodge IM. “Adam-Gibbs formulation of henthalpy relaxation near the glass transition”, *J. Res. Nat. Inst. Stand. Technol.* 1997, **102**, 195.

[12] Bohlin L. “A theory of flow as a cooperative phenomenon”, *Journal of Colloid and Interface Science* 1980, **74**/2, 423.

[13] Ferry JD. Chapter 11. “Dependence of Viscoelastic Behavior on Temperature and Pressure”. In: Ferry JD. *Viscoelastic Properties of Polymers*, 3d Ed., John Wiley & Sons, Inc. New York; 1980, p. 264-315.

[14] Dante RC, Geffroy-Aguilar E & Chávez AE. “Viscoelastic models for Mexican heavy crude oil and comparison with a mixture of heptadecane and eicosane. Part I”, *Fuel* 2006, **85**/4**,** 559.

[15] Smith GD & Jaffe RL. “A quantum chemistry study of conformational energies and rotational energy barriers in n-alkanes”, *J. Phys. Chem*. 1996, **100**(48), 18718.

[16] Lapasin R, Visintin RFG, D’Antona P & Lockhart T. “Proprietà lineari e non lineari di greggi cerosi”, *Atti VIII Convegno della Società Italiana di Reologia,* Sant’Angelo di Ischia*,* Italy, 2004.

[17] Ferry JD. Chapter 9. “Dilute Solutions: Molecular Theory and Comparison with Experiments”. In: Ferry JD. *Viscoelastic Properties of Polymers*, 3d Ed., John Wiley & Sons, Inc. New York; 1980, p. 177-223.

[18] Chazhengina SY, Kotelnikova E N, Filippova IV & Filatov SK. **“**Phase transitions of *n*-alkanes as rotator crystals”, *Journal of Molecular Structure* 2003, **647**, 1-3, 243.

[19] Rajabalee F, Metivaud V, Oonk HAJ, Mondieig D & Waldner P. “Perfect families of mixed crystals: the ordered crystalline forms of n-alkanes”, *Phys. Chem. Chem. Phys*. 2000, **2**, 1345.

[20] Ferry JD. Chapter 3. Exact Interrelations among the Viscoelastic Functions. In: Ferry JD. *Viscoelastic Properties of Polymers*, 3d Ed., John Wiley & Sons, Inc. New York; 1980, p. 56-79.

Chapter 8.

Rheological aspects of *n*-eicosane, *n*-heptadecane, and their mixtures with reference to crude oil

Abstract

Alkanes are among the main components of crude oil, and heptadecane and eicosane often are among those alkanes of average molar fraction. Their rheological behavior is directly related to the micro-phases these compounds can form. Their shear steady viscosity follows the pattern of a shear thinning region and a subsequent plateau, although the shear rate, in which the regime change occurs, is shifted to higher shear rate with increasing temperature. This fact is attributed to the activation energy necessary to align the molecules along the flow direction. Mixtures rich in eicosane or pure eicosane exhibit a viscosity increment with temperature at low shear rates; this unusual behavior can be explained through the formation of ordered structures similar to those of liquid crystals at low temperature near the melting point.

8.1. Introduction

Crude oil rheology frequently shows a shear thinning behavior in steady shear strain conditions as well as normal stresses, as described in previous chapters [1-6]. This very complex behavior depends partially on the aliphatic fraction. This Chapter focuses on steady shear viscosity of heptadecane and eicosane, which are included frequently among the compounds of the aliphatic fraction of crude oil, with the average number of carbon atoms. They are part of both the paraffinic fraction and the colloidal or suspended fractions of crude oil, since, depending on temperature, they can be in liquid or solid phase, or the so called rotator phase [7]. Therefore, the comprehension and the knowledge of their rheological properties can clarify and enlighten also aspects of crude

oil rheology. The normal alkanes exhibit a rich polymorphic nature, which depends on the parity of the number n of carbon atoms in the molecule, the value of n, temperature and pressure. Pairs of *n*-alkanes with a small difference in chain length (Δn =1 or Δn = 2) readly mix in the solid state, i.e. show mixed crystal formation. It is generally observed that forms which make their appearance for pure *n*-alkanes from a certain value of *n* on, are stabilized in binary systems at considerably lower values of n. From this remark, it may be clear that the termperature *vs.* composition phase diagram of a binary system may have a complex appearance. In the solid phase, even alkanes, such as eicosane, have a triclinic T_p form up to a number of carbon atoms of 26, while odd alkanes, such as heptadecane, present a dimorphism, crystallizing either as an orthorhombic form O_i.or in the so called rotator phase R_I [7].

Their thermodynamic phase changes obtained by means of Differential Scanning Calorimetry (DSC) techniques are briefly presented and commented. The DSC results of crude oil are presented for comparison. The rheology of crude oil is widely discussed in several papers and readers are reminded to these works [8-10], as well as, to the previous chapters of this work. The complexity of crude oil cannot be reduced completely to the physics and rheology of linear alkanes, but they can works adequately, at least, for viscous properties and to explain and model some non-Newtonian properties, such as normal stresses [8].

8.2. Methodology and experiments

The rheological tests were carried out by the same rheometer ARES described in detail Chapter 3. The same cone-plate geometry was used for all tests with an angle of 0.04 radians and a plate radius of 50 mm. By means of a calorimeter of TA instruments, Model 2910, DSC measurements were carried out to determine the phase changes of pure alkanes *n*-heptadecane (C17), *n*-eicosane (C20) and their mixtures.

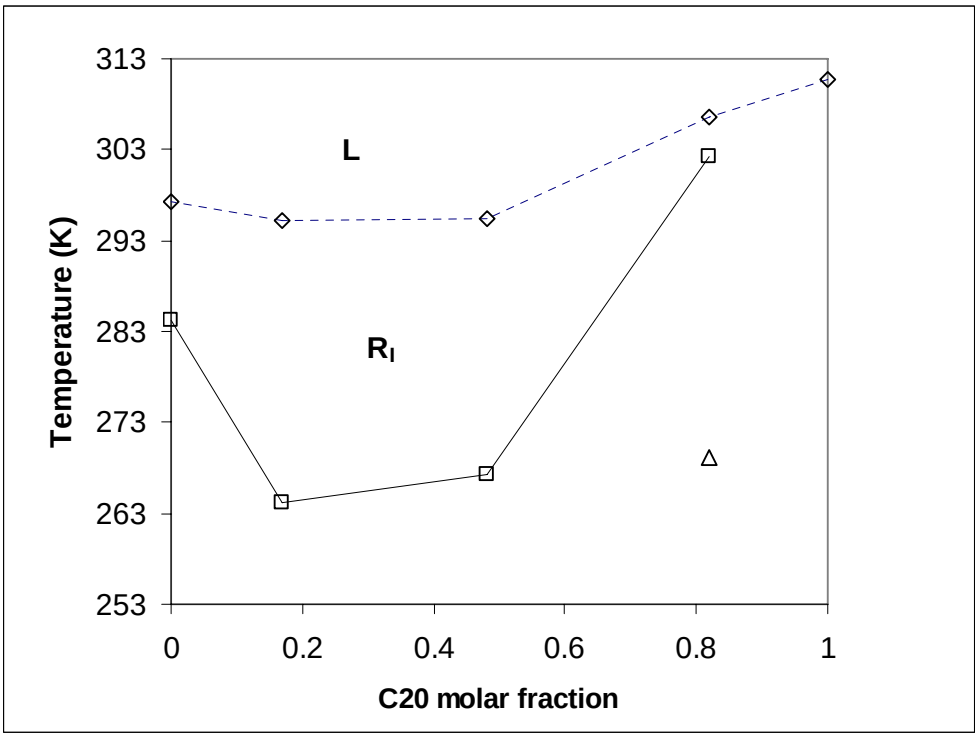

Figure 8.1. Phase change diagram for mixtures of n-eicosane C20 and n-heptadecane C17. L: is the liquid phase, R_I is the rotator phase. Beneath the square symbols (□) there are the different forms of solid phases, they are not specified for the shortage of points. The triangle symbol (Δ) represents another solid-solid phase transition which occurs at high eicosane molar fractions.

8.3. DSC Experimental results

The DSC results are resumed in the phase diagram (Fig. 8.1), where some phase changes of C20, C17 and their mixtures are shown. In Fig. 8.1, the dimorphism of the odd C17 is present in the mixtures of alkanes. The transition to the liquid phase occurs at higher temperatures, and involves all the degrees of freedom for the molecules. According to other measurements [7], at the left of the diagram of Fig. 8.1, the solid phase transitions to the rotator phase should occur from an orthorhombic phase O_i, moving to the left, from a monoclinic form, and then from the orthorhombic O_p, which are all typical forms of odd alkanes. At the right of the diagram, the transition to the

rotator phase should be from a triclinic form T_p, typical of even alkanes. The point marked with a triangle may represent a phase change from the triclinic form typical of even alkanes to the orthorhombic forms, typical of odd alkanes. The rotator phase R_I dominates between the C20 molar fraction of 0.2 – 0.6 and the temperature range of 263 K – 298 K. Nevertheless, in such alkanes cannot be excluded that also the defined upper liquid phase shows a certain grade of order.

8.4. Rheological results

The steady shear viscosity for C17at four different temperature levels above the melting point of 297 K is shown in Fig. 8.2; these four curves are very close to each other. The shear thinning region is very large and only, at high shear rates, above100 s^{-1}, the Newtonian regions begin, which are slightly shifted to higher shear rates with higher temperature. For the case of C20, although test temperatures are higher than the melting points (about 311 K), a dispersion of curves is observed clearly, instead of a group of close curves as in the former case. The rheological measurements show two groups of viscosity: one for higher temperatures 345 K - 355 K, and characterized by higher viscosities with a stronger shear thinning behavior, than the group of viscosities in the range of 315 K-335 K (Fig. 8.3). However, at the end of the shear thinning region, the remaining Newtonian viscosity of the lower temperature group is higher than that of the higher temperature group. The change of slope, occurring at the beginning of a Newtonian plateau, requires higher shear rates incrementing the temperature, in a more marked manner than the case of C17. The viscosities values are similar in the both cases, but in general, at low shear rates, the viscosities of C20 are higher than those of C17.

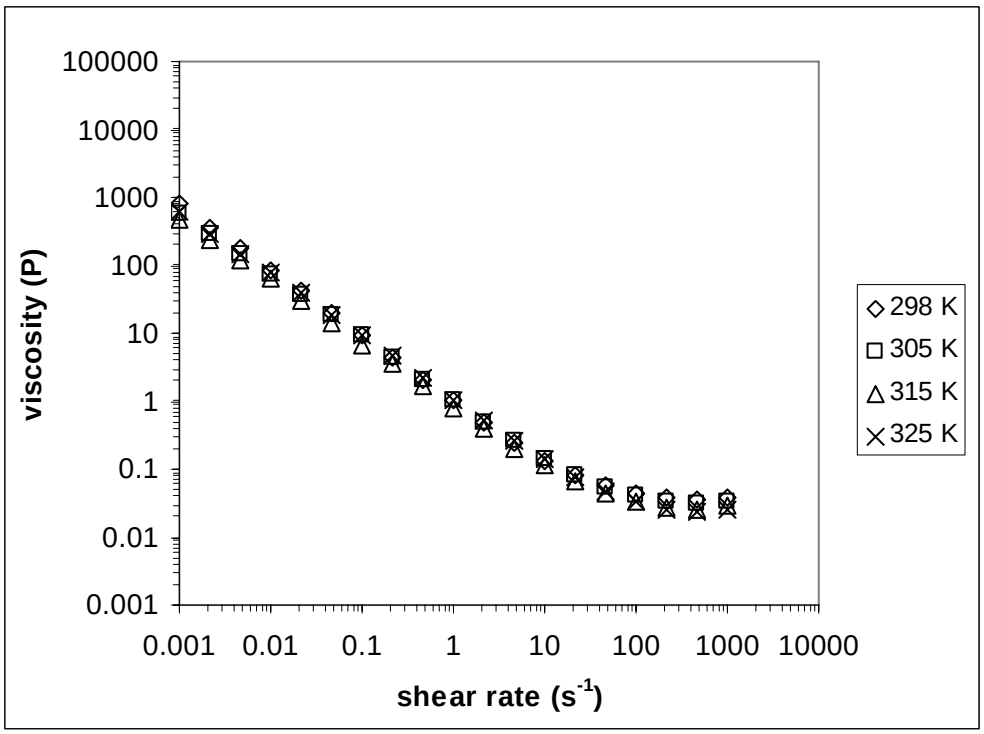

Figure 8.2. Steady shear viscosity for n-heptadecane C17, at different temperatures.

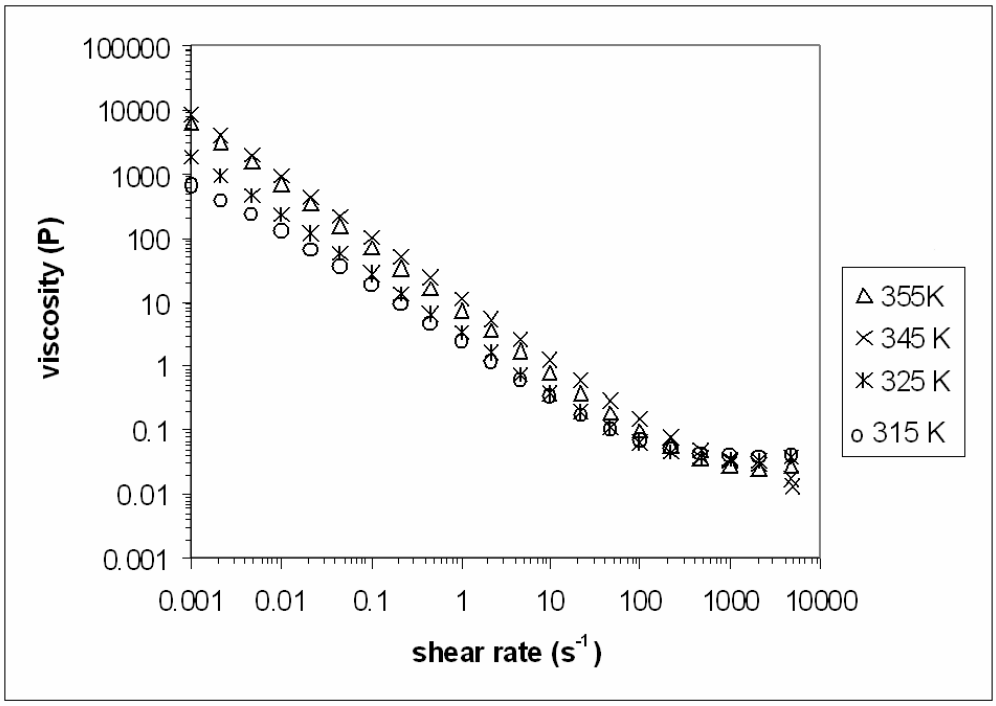

Figure 8.3. n-eicosane steady viscosity at different temperatures.

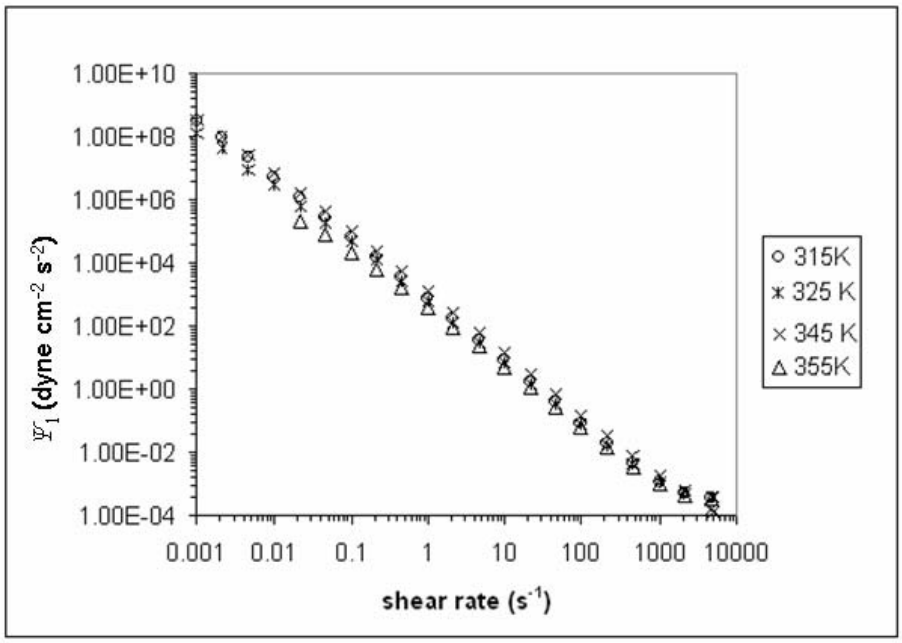

Figure 8.4. n-eicosane first coefficient of normal stresses Ψ_1, at different temperatures.

For the first coefficient of normal stresses Ψ_1 curves of C20, shown in Fig. 8.4, these tend to follow a tighter group behavior than that observed for the viscosities' curves. Also, the shear thinning region is longer than in the case of the viscosity curves, and no Newtonian plateau is observed, but only a slight change of slope. It is noteworthy to mention that Ψ_1 curve, at 355 K and low shear rates, has values lower than the other Ψ_1 curves, at higher temperature levels and low shear rates.

The mixture of molar fraction of 0.82 presents rheological characteristics similar to those of pure eicosane (see Fig. 8.5); although, in general, viscosities are lower, but there is not a clear correspondence between the viscosity level and temperature.

In the case of the mixture of molar fraction of 0.17 (Fig. 8.6), the viscosity curves are very similar in shape and magnitude to those of pure heptadecane, but they are split at high shear rates in an evident manner.

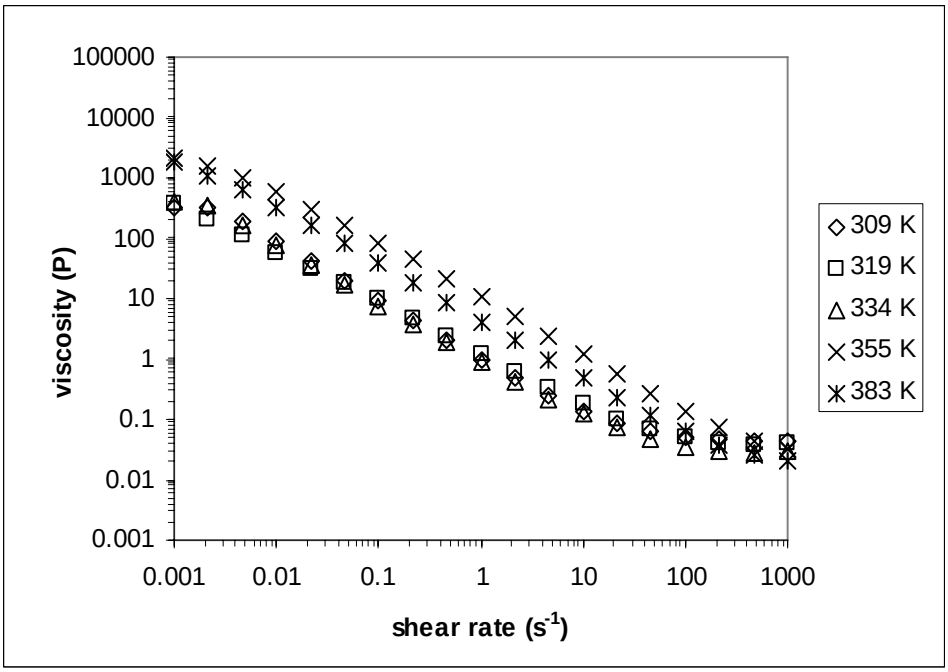

Figure 8.5. Steady viscosity of the mixures of n-eicosane C20 and n-heptadecane C17, the C20 molar fraction is 0.82.

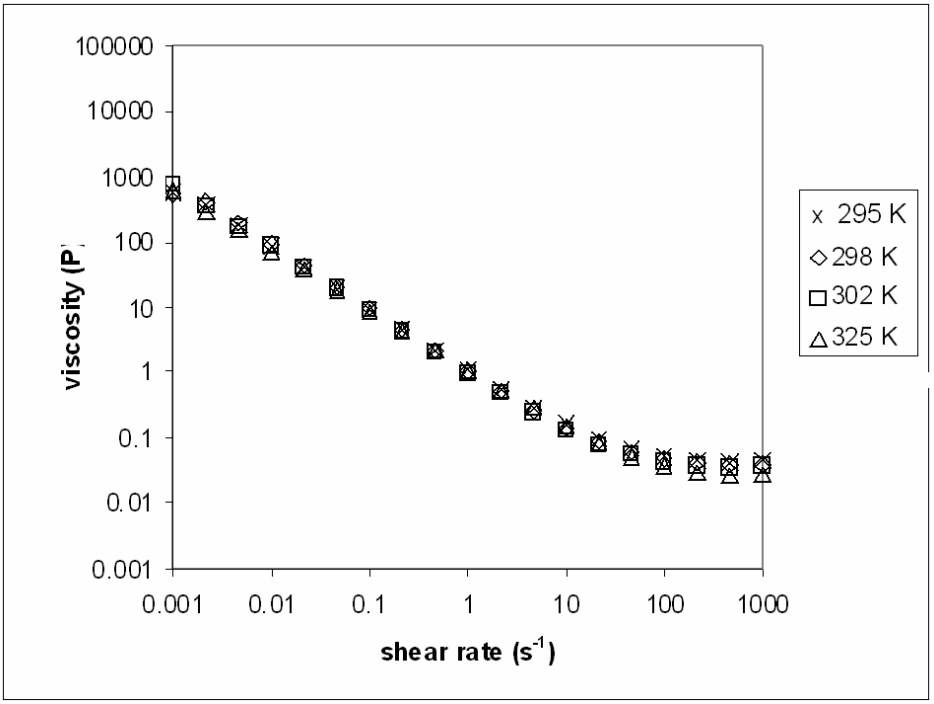

Figure 8.6. Steady viscosity of the mixures of n-eicosane C20 and n-heptadecane C17, the C20 molar fraction is 0.17.

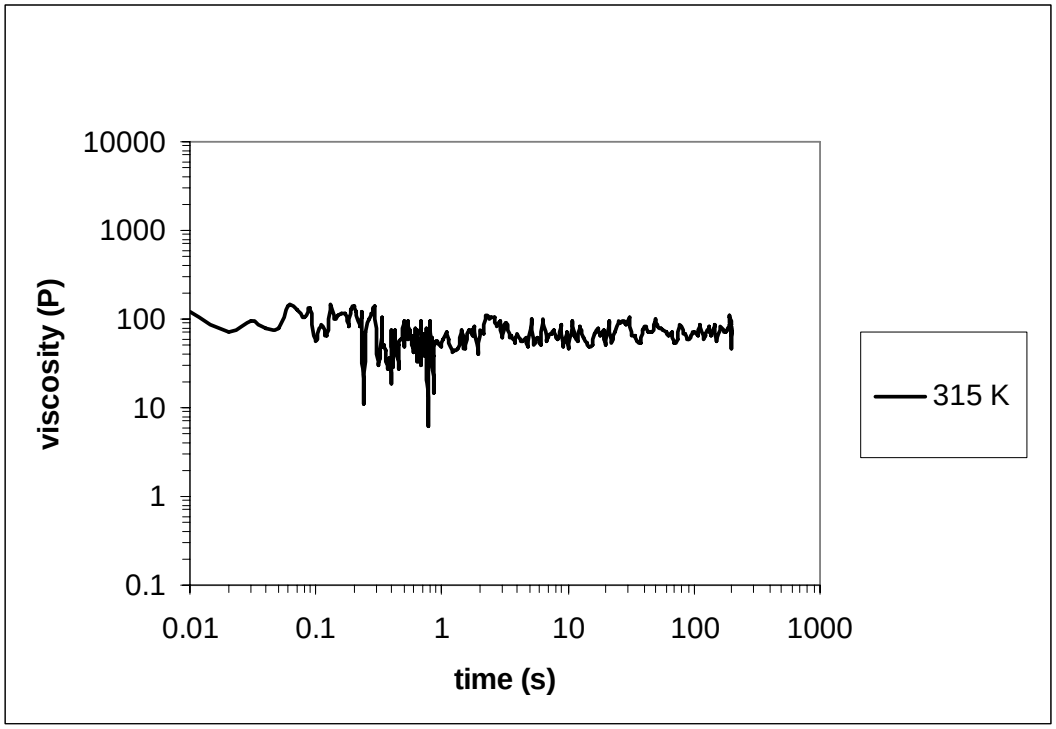

Figure 8.7. Transient viscosity for n-eicosane C20 at the shear rate of 10^{-2} s^{-1} and at the temperature of 315 K. The time interval between a measure and following one is 0.01 s.

Finally, it is noteworthy to indicate that the transient viscosities of C20 at 315 K and C17 at 305 K have a completely different evolution. Indeed, C20 (Fig. 8.7) reaches the steady state quicker and with fewer oscillations than C17 (Fig. 8.8). The transients' tests were carried out at the same shear rate of 10^{-2} s^{-1} for both alkanes, and at a temperature about 4 K more than its melting point for C20, while at about 4 K and 11 K more than its melting point for C17, respectively.

8.5. Discussion

The mixtures of C17 and C20 inherit part of the properties of both alkanes, e. g., the rotator phase is quite dominant in the mixtures (Fig. 8.1), while the transition point from the solid form to the rotator phase rises with incrementing fractions of C20. Above the melting temperature, the alkane in excess quantity seems to dominate the rheological

properties. The viscosities of pure C20 and that of the mixture with molar fraction 0.82 exhibits a shift of the viscosity shear thinning region at different temperatures. There are two blocks, one in the range 315 K – 335 K, and another for 345 K – 355 K range (Fig. 8.3). What is usually expected is a behavior more similar to that of C17, where the viscosities decrease with a temperature increment (Fig. 8.2), but the observed behavior is exactly the opposite. Nevertheless, even for C17 this behavior is not clearly marked.

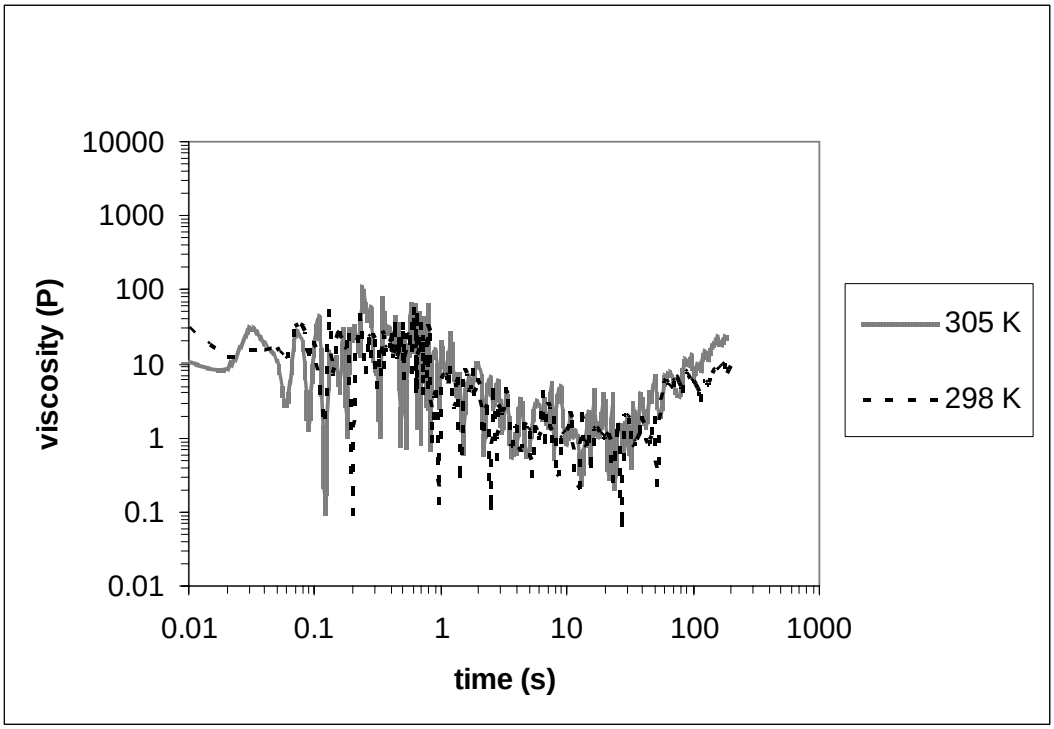

Figure 8.8. n-heptadecane C17 transient viscosities at 298 K, 305 K, both curves were executed at the fixed shear rate of 10^{-2} s^{-1}. The time interval between a measure and following one is 0.01 s.

This surprising behavior, which is reproducible, can be attributed to a residual structure formation of the solid phase in alkanes with a remarkable characteristic length scale. This residual structure should vary depending on the time passed after the melting point, but, in this case, high viscosities will be expected at temperatures near the melting point of C20 (311 K), such as 315 K. For lower temperatures, a reasonable behavior

would be in favor of the self-organization (orientation) of the chains along the flow direction easily. On the other hand, high temperatures promote a higher degree of disorder, but alkane chains can sustain as well more complex conformations with increasing viscosity.

By increasing the test temperature, and after the shear thinning region, the viscosities tend to coincide, although the beginning of the Newtonian plateau is shifted slightly to higher shear rates. This shift with temperature is also observed, although in a weaker manner for both the heptadecane (Fig. 8.2) and the alkanes' mixtures (Fig. 8.6). The latter behavior is assigned an activation energy associated to cooperative regions transformations [8-10].

A thickening behavior has also been observed for increasing temperature. Several published papers works report this anomalous behavior for the linear alkanes' heat capacity, just above the melting point [11]. That is, there is an excess enthalpy that disappears within a span of about 30 K above the melting point. This excess enthalpy corresponds to the entropy needed to randomize the liquid, and it may correspond to the ordering in liquid crystalline state. The effect may be compared to the ordering in the liquid crystalline state [11]. This effect is still present in the mixture with abundance of C20 (Fig. 8.5). Although, the "temperature thickening" is not regular: e. g., at 383 K the viscosity curve is lower than that of 355 K, because increasing the temperature too much means overcoming the temperature range in which the alkanes can manifest ordering in the liquid phase. The mixture poor in C20 (Fig. 8.6) reflects more the properties of C17. The comparison of the transient viscosities of C20 and C17 supports this idea.

The eicosane first coefficient of normal stresses $\Psi_{1,}$ at different temperatures, is very similar (Fig. 8.4). Although, the curves are closer than viscosity curves (Fig.8.3), there is not clear temperature dependence.

The transient test was carried out at 315 K and at the shear rate of 10^{-2} s^{-1} for C20, i. e., at about 4 K more than melting point temperature. The transient tests for C17 were carried out at the shear rate of 10^{-2} s^{-1}, at 298 K and 305 K, i. e., about 4 K and 11 K more than the melting point, respectively. The viscosity of C20 reaches the steady state quicker and with fewer oscillations (Fig. 8.7) than C17 (Fig. 8.8). These oscillations may represent the characteristic initial rotations of entangled chain polymers induced by shear stresses, before these align preferentially along the flow directions. The minor extent of this phenomenon for C20 sample indicates that, in this case, the grade of order in the flow direction is reached readily, probably due to the existence of domains with a certain order before flow field actually begins.

8.6. Conclusions

The viscosity of eicosane and its mixtures with high content of eicosane manifest a temperature thickening behavior, which can be attributed to a certain initial grade of ordering of the chains in the liquid phase, in a similar way to that of liquid crystals. This behavior is not clearly identified in heptadecane, and in mixtures with few eicosane is not detected. The end of the shear thinning region is in any case shifted at higher shear rates as a consequence of the presence of activation energies. These phenomena are superimposed to that of the “temperature thickening”.

8.7. References

[1] Speight JG. In *The chemistry and technology of petroleum*, 2nd Ed., Marcel Dekker; New York, 1991.

[2] Sjoblom J, Aske N, Auflem IH, Brandal Ø, Havre TE, Sæther Ø, Westvik A, Johnsen EE & Kallevik H. "Our current understanding of water-in-crude oil emulsions. Recent characterization techniques and high pressure performance", *Adv. Colloid Interface Sci*. 2003, **100-102**, 399.

[3] Gruse WA & Stevens DR. In *The Chemical Technology of Petroleum*, McGraw-Hill; New York, 1960.

[4] Koots JA & Speight JG. "Relation of petroleum resins to asphaltenes", *Fuel* 1975, **54** (3), 179.

[5] Onogi S, Matsumoto T & Warashina Y. "Rheological properties of dispersions of spherical particles in polymer solutions", *J. Rheology* 1973, **17**, 175.

[6] Sengun MZ & Probstein RF. "Bimodal model of suspension viscoelasticity", *J. Rheology* 1997, **41**(4), 811.

[7] Rajabalee F, Metivaud V, Oonk HAJ, Mondieig D & Waldner P. "Perfect families of mixed crystals: the ordered crystalline forms of n-alkanes", *Phys. Chem. Chem. Phys.* 2000, **2**, 1345.

[8] Dante RC, Geffroy-Aguilar E. & Chávez A.E. "Viscoelastic models for Mexican heavy crude oil and comparison with a mixture of heptadecane and eicosane. Part I", *Fuel* 2006, **85**/4**,** 559.

[9] Al-Zahrani SM. "A generalized rheological model for shear thinning fluids", *Journal of Petroleum Science and Engineering 1997*, **17**, 211.

[10] Al-Zahrani SM & Al-Fariss TF. "A general model for the viscosity of waxy oils", *Chemical Engineering and Processing*, **37**, 433.

[11] Van Miltenburg JC. “Fitting the heat capacity of liquid *n*-alkanes: new measurements of *n*-heptadecane and *n*-octadecane”, *Thermochimica Acta* 2000, **343**, 57.

Chapter 9.

General Conclusions

Rheology of crude oils was always a difficult matter due to the complexity and variability of the systems depending on the origin feedstcks etc. A method to bypass the obstacle consists into developing simple systems based on well known systems, such as linear alkanes' blends, which can explain the main rheological characteristics of some classes of petroleum such as Mexican crude oil types. This implied to find models that can describe both systems. The shear thinning model proposed by Al-Zahrani, suitable for waxy oils and suspensions, seemed to have the adequate flexibility to describe both systems without exceeding in the number of parameters [1, 2]. The hypothesis of this work was that crude oil viscous properties are dominated by aliphatics, mainly alkanes and alkylic long branches; while, the elastic properties are due to the colloidal nature of petroleum. In fact, the colloidal nature of petroleum is due mainly to the asphaltenes and waxes suspended in the aliphatic matrix.

Blends of linear alkanes such as *n*-eicosane and *n*-heptadecane manifest some of the viscous behavior of crude oil. Indeed, it is noteworthy to stand out that a pronounced shear thinning behavior and shear normal stresses are present in both systems and they can be correlated to changes of both alkanes' and alkylic branch conformations. Alkanes, and especially paraffins, share with crude oil their non-Newtonian behavior. The effect of temperature on the crude oil viscosities consists in a lowering of viscosities at high shear rates and in the shift of the critical viscosities (at the end of the shear thinning region) to higher shear rates. This behavior can be explained through the presence of activation energy.

The utilization of Oldroyd contravariant derivatives provides a suitable tool to describe viscoelasticity and transient behavior of both systems [3], avoiding to base the

viscoelastic model on molecular characteristics difficult to manage in the case of oils, and allowing us to use the framework of Maxwell type models. The White-Metzner approximation [4] allowed us to unify the shear thinning model of Al-Zahrani with the Maxwell type model. Moreover, by means of this approximation, the first coefficient of normal stresses becomes dependent on shear rate, in accordance with experiments which show a shear thinning behavior also for the first coefficient of normal stresses. However, molecular mechanisms get into the model through the deepening of the investigation of the activation energies often observed in oils and high alkanes.

The Adam-Gibbs theory, adapted to the alkanes, provides an interpretation of the activation energies found in crude oils viscosity functions [5]. In brief, Adam-Gibbs theory assumes that phase transformations of polymers are cooperative phenomena that involve regions whose size depends on the configurational entropy of the system, and this approach has been used to model the viscosity of polymers. The size of this region is characterized by the number z^*, which is a multiple of the unit segment of the polymer or oligomer. The size of the cooperative region approaches the whole sample volume, when temperature approaches the transition temperature towards either a solid state or a more compact packing arrangement of molecules. More changes of conformations are needed to reach a determined structure or to destroy it; bigger is the size of the cooperative region. The activation energy is given by the product of z^* with $\Delta\mu$, (see Chapter 6) which corresponds to the approximated value of the rotational barrier around a C-C bond, from a stable conformation to another one (*GT* transitions). The characteristic time obtained through this model is assumed to be the same observed in the viscosity function of crude oil and alkanes' blends. This activation energy interpretation permits to relate macroscopic properties (viscosity) to microscopic properties, e. g., the changes of conformations in long and flexible molecules such as alkanes and alkylic chains (see Fig. 6.16). The study on linear alkanes' blends lead to

these conclusions: temperature effects manifest through the excess alkane with the N carbon atoms, and the effect of shear forces through the average number of carbon atoms $\langle n \rangle$.

Dimensionless numbers permit to obtain master curves and lead the behaviors of apparently different systems into the same physical drawing. These dimensionless numbers associated to shear rate are very required in suspension rheology, and they often represent a balance between work and some energy barrier, such as the energy to overcome attractive forces among particles in suspension [6, 7]. These successful attempts guessed the possibility to interpret the dimensionless shear rate found for crude oil in terms of a specific Weissenberg number. The developed Weissenberg number, based on this activation energy and the characteristic time of the cooperative phenomena involved in crude oil flows, adequately scales curves of both oils and alkanes of long chains (17 and 20 carbon atoms); moreover, the model is flexible and of general validity (see Eqs. 6.15 - 6.20). In the case of oscillatory measurements, since alkanes have poor viscoelastic properties, the model only is utilized for crude oil, where the effect of the excess alkane N persists. It means that the same activation energy cause the shift of G' and G'' to higher frequencies, while the shape of the moduli' functions is controlled by the suspended particle. The properties of oscillatory shear strain are mostly dominated by the colloidal nature of crude oil, as the introduction of a relaxation time spectrum demonstrates. A simple square shaped relaxation time distribution can give a better fitting of the experimental data of G' and G''. A relaxation time spectrum is essentially given by the distribution of the suspended particles. Aging of the samples alters in a large manner the relaxation times, indicating that a slow agglomeration, mainly due to cross-linking oxidative phenomena, occurred.

On the other hand, a factor must be taken into account and that is the rheology of pure linear alkanes is complicated by the fact that they can maintain a certain grade

of order also after melting. This can cause an increment of viscosities with temperature increment. Nevertheless, this effect tends to vanish in alkanes' blends. When the excess alkane is *n*-heptadecane, the "ordering effect" is no more present at high shear rates.

A mathematical and physical model of crude oil rheology has been achieved [8]. Doubtless, one of the principal achievements of this work is the specific Weissenberg number developed for crude oils and alkanes, as well as the interpretation of the activation energy, which was provided through an adaptation of the Adam-Gibbs theory to the specific case of alkanes and crude oil. Therefore, alkanes not only provide a physical model for crude oil, which within certain limits is a rough sketch of crude oils, but also an explanation to the viscosity decay at high shear rates with temperature. The phase changes, in which alkanes are involved, can be the main cause of this decay as interpreted through the relaxation times defined through the Adam-Gibbs theory adapted to alkanes.

This framework is considered to be the base for further studies focused on the rheology of oil-in-water suspensions, which has as fundaments the comprehension of oil rhelogy *in primis*. In case of water-in-oil emulsions, i.e. where the continuous phase is oil, the equations developed throughout the text will be useful to manage the complex rheology of this non-Newtonian fluid and to create adequate models to describe their flow behavior.

9.1. Acknowledgements

- I am grateful to Miguel Ángel Canseco Martínez for assistance with the calorimetric measurements, and to Gerardo Guevara Flores for technical support.
- This project received support through CONACyT, project NC-204, assigned to Dr. Enrique Geffroy-Aguilar, and through PAPIIT, Universidad Nacional Autónoma de México.

9.2. References

[1] Al-Zahrani SM. “A generalized rheological model for shear thinning fluids”, *Journal of Petroleum Science and Engineering* 1997, **17**, 211.

[2] Al-Zahrani SM & Al-Fariss TF. “A general model for the viscosity of waxy oils”, *Chemical Engineering and Processing* 1998, **37**, 433.

[3] Oldroyd JG. “On the formulation of rheological equations of state”, *Proc. R. Soc. Lon.* 1950, **A 200**, 523.

[4] White JL & Metzner AB. “Development of constitutive equations for polymer solutions and melts”, *J. Appl. Polym. Sci.* 1963, **7**, 1867.

[5] Bohlin L. “A theory of flow as a cooperative phenomenon”, *Journal of Colloid and Interface Science* 1980, **74**/2, 423.

[6] Jansen KMB, Pearson JRA & Mackley MR. “Viscosity of surfactant stabilized emulsions”, *J. Rheology* 2001, **45**(6), 1341.

[7] Pal R. “Scaling of relative viscosity of emulsions”, *J. Rheology* 1997, **41**, 141.

[8] Dante RC, Geffroy-Aguilar E & Chávez AE. “Viscoelastic models for Mexican heavy crude oil and comparison with a mixture of heptadecane and eicosane. Part I”, *Fuel* 2006, **85**/4**,** 559.